Charge Transport through Self-Assembled Monolayers with Eutectic Gallium-Indium Top Contacts
Fracasso, Davide

Charge Transport through Self-Assembled Monolayers with Eutectic Gallium-Indium Top Contacts

Davide Fracasso

Charge Transport through Self-Assembled Monolayers with Eutectic Gallium-Indium Top Contacts

Davide Fracasso

Ph.D. Thesis
University of Groningen
The Netherlands

7 February 2014

university of groningen

faculty of mathematics and natural sciences

university of
groningen

Charge Transport through Self-Assembled Monolayers
with Eutectic Gallium-Indium Top Contacts

PhD Thesis

to obtain the degree of PhD at the
University of Groningen
on the authority of the
Rector Magnificus, Prof. E. Sterken
and in accordance with
the decision by the Collage of Deans.

This thesis will be defended in public on

Friday 7 February 2014 at 11.00 hours

by

Davide Fracasso

born on 3 May 1984
in Arzignano, Vicenza, Italy

Supervisors: Prof. J. C. Hummelen

Prof. R. C. Chiechi

Assessment Committee: Prof. M. D. Dickey

Prof. G. C. Solomon

Prof. A. Herrmann

Dedicated to my dear Grandmother. Riposa in pace Nonna

"You must be shapeless, formless, like water. When you pour water in a cup, it becomes the cup. When you pour water in a bottle, it becomes the bottle. When you pour water in a teapot, it becomes the teapot. Water can drip and it can crash. Become like water my friend."

Bruce Lee

Contents

1

Liquid Metal Junctions in Molecular Electronics

1.1 Introduction-Scientific background

Since 1960 with the work of Herward and Angello[1] stating that "The trend in electronics circuit construction is toward microminiaturization and molecular electronics" the efforts of Industry and Academia have been toward the minimization of the electronic components. The increasing need for complexity in integrated circuits was predicted by Gordon E. Moore in 1965, who predicted an exponential increase of the number of transistors, *i.e.*, Moore's Law.[2] Silicon based technology has a lower dimension limit and it's clear that in the near future there will be a need for small, less consuming and faster electronic computer components. Molecular Electronics nowadays is often considered the best candidate to scale down electronic components, and in this sense Aviram and Ratner back in 1974 proposed, for the first time, a molecular-scale electronic device that could act as a molecular diode, in which a single molecule performs an electronic function.[3] Dimension is not the only development required; operation speed, reliability, stability, and more importantly production cost and scalability. Up to now there is no clear evidence that Molecular Electronics (ME) will compete with or follow up silicon based technology. The most appealing aspect of ME is the low cost of production. Organic electronics is a field that originated back in 1862 when Henry Letheby produced a partly conductive material by anodic oxidation of aniline in sulfuric acid. The material was probably polyaniline. In 1954, researchers at Bell Laboratories

and elsewhere reported charge-transfer complexes. [4,5] In particular, high conductivity of 0.12 S/cm was reported in a perylene-iodine complex in 1954. [6] This finding indicated that organic compounds could carry current. In 1972, researchers found metallic conductivity in the charge-transfer complex TTF-TCNQ. After this point research on conducting polymers flourished especially after the 1977 discovery that polyacetylene can be doped with halogens to produce materials with insulating, semiconducting, or highly conducting properties. [7,8] For this work, Alan J. Heeger, Alan G. MacDiarmid, and Hideki Shirakawa were jointly awarded the Nobel Prize in Chemistry in 2000.

In general, efforts to incorporate molecules and polymers into electronic devices have been motivated by six major considerations[9]: (i) molecules (1-2 nm) are smaller than the smallest features in semiconductors (presently approximately 22 nm; with well-defined engineering development, less than 10 nm estimated for 2015) [10] and might therefore facilitate the packing of more computational power onto a smaller footprint, (ii) the electronic properties of molecules and polymers are tunable by organic synthesis; these procedures can, in principle, have very low cost, (iii) under certain conditions, molecules self-assemble into ordered monolayers (SAMs) or Langmuir-Blodgett monolayers, multilayers on surfaces, and into ordered arrays in solution, (iv) films of molecules and polymers can be deposited over large area and on flexible substrates, (v) the electronic and optical properties of many molecules can be controlled via modulation of temperature, electric and magnetic fields and other environmental parameters, and (vi) assemblies of molecules perform complex, high-efficiency electronic and optoelectronic charge and energy transport functions in nature (*e.g.*, electron transport, photosynthesis, coupling of one- and two-electron processes in metabolism). For SAMs the costs are low since only small quantities are required to cover large areas, making self-assembled monolayers a very inexpensive primary product. For example, with only 1 g of dodecanethiol molecules $(HS-C_{12}H_{25})$, a densely packed SAM on gold can be formed over an area of $\sim 600 m^2$.

The first report of electrical measurement on SAMs belongs to Mann and Kuhn[11] who studied tunneling current through fatty acid monolayers of different length on Al electrodes with mercury used as top electrode. Molecular-scale electronics is, so far, a purely academic pursuit suffering from poor reproducibility among measurements of the same systems gathered using different techniques, a set of daunting experimental issues concerning the connection of fragile molecules to macroscopic leads, and an in-

complete theoretical basis. ME now suffers from both a well-deserved lack of credibility and an identity crisis "Can we understand the molecule in molecular electronics?"[12] and "Is the point of molecular-scale electronics to gain a detailed mechanistic understanding of CT through molecules or to build functional devices?"[13]. On one hand the performance of systems suited to evaluate the electrical properties of individual molecules, such as mechanically controlled break junctions (MCBJ) and scanning tunneling microscopy (STM) experiments under ultra high-vacuum conditions and low temperatures, do not easily translate to the performance in practical devices. On the other hand, there are other techniques, which rely more on the properties of monolayers than single molecules. Such techniques can be use in bottom-up technology, among which I would like to mention conductive probe atomic force microscopy (CP-AFM)[14], Large Area Molecular Junctions[15], Nanotransfer printing[16], Nanopores[17], Cross wires[18] Arrays of nanoparticles[19], and Liquid Metal Junctions which I explore more in detail in this chapter, and which comprise mercury drop junctions (Hg-drop)[20] and Eutectic Gallium Indium (EGaIn - a metal alloy of Ga 75.5% and In 24.5% by weight and has a melting point m.p=15.7°C[21].

It's not the goal of this thesis to review ME techniques and compare pros & cons, however, later on in this chapter we will explore Liquid Metal Junctions in detail with emphasis on EGaIn. Fundamental studies of charge transfer (CT) through organic molecules–especially at the interfaces between organics and metals or semiconductors– that define the field of ME today are necessary for continued innovation in organic electronics. Self-assembled monolayers (SAMs) are an important tool in creating metal or semiconductor–molecule junctions that can be characterized electrically using one or more of the techniques mentioned above. SAMs of alkane(di)thiols are well known to form densely packed and well-ordered domains on metals, like gold and silver[22], and for this reason alkane(di)thiols are a perfect benchmark for any experimental testbed in ME. Charge transport studies on alkane-based SAMs have been ongoing for more than 30 years, but unfortunately the electrical properties are not yet fully understood. The large spread in conduction/resistance values of molecules in the literature reflect the different geometries and technical details of the techniques used[23]; a close correlation to theory is more often complicated.[24–27]

1.2 Molecular Junctions

Before delving into liquid metal junctions and the mechanism of the CT a brief description of what a "Molecular Junction" (MJ) is required. We make a distinction between two types of junctions, Metal-Insulator-Metal (MIM) with thin film/multilayers sandwiched between two metal electrodes and Metal-Molecule-Metal (MMM) where usually a SAM is fabricated on the bottom electrode and later a top electrode is placed on the top of the supporting molecular layer. Another important distinction which can be used to address the different techniques is between *top-down* and *bottom-up*. *Top-down* and *bottom-up* are generally used in nanotechnology to define two approaches for the manufacture of products. Bottom-up approaches seek to have smaller (usually molecular) components built up into more complex assemblies, while top-down approaches seek to create nanoscale devices by using larger, externally controlled ones to direct their assembly. The top-down approach often uses the traditional workshop or microfabrication methods where externally controlled tools are used to cut, mill, and shape materials into the desired shape and order. Micropatterning techniques, such as photolithography and inkjet printing belong to this category. Bottom-up approaches, in contrast, use the chemical properties of molecules to cause single-molecule components to (a) *self-organize* or *self-assemble* into some useful structures, or (b) rely on positional assembly. In ME these two strategies are used to form MJs: defining the smallest dimension using the molecules (*i.e.*, bottom-up) or preforming a molecule-sized gap and populating it with the molecules (*i.e.*, top-down). The former strategy utilizes a top-contact that is placed on top of preformed SAM, whereas the latter is almost exclusively used for single-molecule measurements, which are not easily comparable to SAM-based measurements comprising micrometer-sized areas of molecules. Two notable exceptions are CP-AFM in which a conductive AFM tip is brought into contact with a SAM, and STM break-junctions (STM-BJs), in which molecules are plucked from a monolayer of dithiolates using a Au STM tip. They are, however, clearly *top-down*, and whereas CP-AFM may be considered a SAM-based (or few-molecule) measurement, STM-BJs are single-molecule measurements. With CP-AFM and STM-BJs the probe is rigid rather than conformal and can be pushed through the SAM, and thus the molecules are not defining the smallest dimension. Techniques such as Hg-drop, EGaIn, and Large Area Molecular Junctions can be defined as *bottom-up*. Despite the techniques chosen, every

MJ can be divided into three major components, see Figure 1.1: the electrodes, the molecule(s), and the two interfaces. In the following sections we will explore in detail the properties and effects of electrodes, molecules, and interfaces for SAM-based MJ.
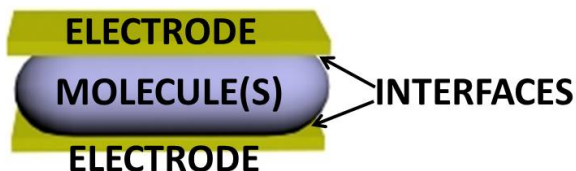
Figure 1.1: Schematic representation of a molecular junction. One or more molecules are sandwiched between two electrodes.

1.2.1 The Electrodes

With the exception of single molecule techniques like MCBJ and STM-BJ, all other types of MJ don't have both electrodes fabricated simultaneously. Generally after the first electrode is fabricated a SAMs is formed onto it, and subsequently the second electrode is formed. The bottom electrode can be either a metal or a semiconductor. Common metal substrates used in ME are: Au, Ag, Pt, Pd, Cu. Depending on the nature of the bottom electrode the molecule can assemble with different packing density and tilt angle[22]. The combination of the metal type, the roughness of the surface and the chemical bonding type of molecules head group with the bottom electrode determine the assembly and largely the CT properties. An important distinction is between molecular monolayers formed via *self-organization* (*e.g.*, through irreversible bonding to SiO_2 substrates) and *self-assembly* (*e.g.*, through thiolates on gold to form SAMs), give rise to disparate properties.[22,28,29] For instance, self-organized monolayers cannot self-repair or undergo dynamic exchange with molecules from solution, but are not subject to thermal or electrochemical desorption. The top-electrode is perhaps the most critical and key step of the MJ formation. Direct evaporation of metals onto a SAM results likely in penetration of "hot" atom through the molecule monolayers, introducing short circuits.[30–32] As a consequence direct evaporation onto SAMs result in very low yields of working devices and unreliable results. A key factor in ME often underestimated is the reproducibility of the process or the technique used. Due to the complexity and di-

versity of the techniques used to measure the electrical properties of organic molecules, it is more often complicated if not impossible to duplicate or compare results from different laboratories. Furthermore reproducibility is not only a credibility factor associated to the measurement technique but an essential fact to give credit to the whole ME community. Differing degrees of both intramolecular disorder within the organic film and defect at the metal-organic interfaces (due to impurities on the electrodes) are two major cause of irreproducibility of electrical measurements, or more generally speaking measurement on such modified surfaces. In molecular-scale electronic devices where the organic layer is ∼ 1-5 nm the performance could be driven by defects and impurities, which are always present. For this, and many more reasons, characterization of the surface before and after functionalization is extremely important to correctly interpret the physical properties of the molecule(s) investigated. Most of the defects that occur at the metal-organic interfaces of a SAM could dominate (if not strongly influence) the current through the monolayer. One example is the electromigration that metal atoms can undergo when bias is applied; this results in highly conductive filament between the electrodes through which the electrons can travel[30]. For SAMs of n-alkanethiolates, step edges and grain boundaries in the metal surface result in "thin areas" of the SAM, *i.e.*, areas in which the molecular density is less or the molecule don't possess the right standing-up configuration "kinks", resulting in many cases in a poor contact with the top-electrode[22]. This type of defect may result in a reduced length of the through-bond pathway and higher current is observed. Another relevant source of defects is vacancy islands, which form when individual metal atoms dissociate from the plane of the islands over time[33–35]. This process leave behind vacancies of atomic size which tend to anneal into larger vacancy islands[36]. In the case of MJs measured in solvents (such as the case of Hg-drop junctions) solvent molecules could be trapped at the van der Waals interfaces, reducing the coupling to the electrode, and generally speaking increasing the uncertainty at the molecule-top electrode interface. In Figure 1.2 are pictured common defects on a metal substrate. Molecules may "kink" due to the presence of grain boundaries or step edges in the metal film or impurities in the solvents and reagents that deposit on the metal surface during SAM formation. In a recent theoretical study *self-assembly* processes and the dynamics of defects were simulated, finding that domain boundaries are ubiquitous, and are often associated with substrate defects as well as transitions between molecular domains with different SAM chain orientations. Interestingly for the

application of SAMs on gold in nanofabrication and the coproduction of reproducible nanopatterns with few nanometer feature sizes, we find that strong molecule-SAM interactions occur at SAM domain boundaries, competing with molecule–molecule clustering on top of the SAM. Domain boundaries can trap excess molecules, with trapped excess molecules adopting different orientations in different SAM domain boundaries, leading to SAM self-healing and repair in some instances.[37] An ideal defect-free surface over large areas remains a tenet, however a way to minimize the frequency of defects at the electrode-organic interface and within the organic layer is to start with an atomically flat electrode. Ultra-smooth metal substrates, which possessed low root-mean-square (RMS) roughness and large grains, produced with the general method of the template stripping TS[38] have proven to be useful in the study of applications of well-ordered SAMs (especially in application where the film/layer thickness is comparable with the RMS)[14,39–45]. Weiss et al. developed a procedure to obtain ultrasmooth metal surfaces by evaporating metal directly onto a silicon wafer bearing native oxide and transferring the metal to another (semi)rigid substrate, such as glass slide or polydimethylsiloxane (PMDS), by using an optical adhesive or a solder[46]. By doing so it's possible to cleave the metal film from the template and expose the face of the film that had been adjacent to the Si/SiO_2 surface, which is atomically flat, *i.e.*, RMS < 1nm. Figure 1.3A illustrates the procedure to form TS metal substrates. TS substrates could be stored when the metal film is protected by the optical adhesive and the mechanical support from contamination and oxidation. Figure 1.3B shows the low roughness of the Ag^{TS} compared to the as deposited (AS-DEP) Ag. More recently Borukhin et al. demonstrated that a simple annealing, at adequate temperature, of the metal film does reduce surface nanodefects improving even further the quality of the metal film.[47] Standard gold deposition onto silicon wafers requires adhesion layer such as Ti or Cr 1-2 nm because the interaction of gold and the silicon native oxide is weak, and the metal film tends to peel off easily. The adhesion layer however makes it impossible to template the metal film and as a consequence deposited metal film are usually rougher. The great disadvantages of the TS metal film is the compatibility of the optical adhesive with the solvents use to form the SAMs. Usually ethanol is used as a solvent for *n*-alkanethiolates which does not swell the adhesive, however, for some rigid aromatic molecular wires, the solubility in ethanol is very low and halogenated solvents or tetrahydrofuran (THF) are required. The TS film could be separated from the protecting template in two ways: (mTS) me-

chanically by using a razor blade, cleaning the edge of the mechanical support from the excess of adhesive and by applying a small lateral pressure to cleave the rigid support (glass) from the wafer and exposing the fresh TS metal film. The second method is the chemical template stripping (cTS) which consists of immersing the sandwich structure in a solution of thiols, such that the film never comes into contact with O_2. Weiss et al. observed by using Reflectance-Absorbance Infrared (RAIR) that the SAMs formed on the ultrasmooth Ag were more crystalline than those on the as deposited AS-DEP substrates [46]. More crystalline densely packed monolayers have significantly enhanced the reproducibility, stability and yields of working junctions. Weiss et al reported for Hg-drop junctions a great improvement overall for SAMs of n-alkanethiolates on Ag^{TS}; in Figure 1.4 a plot shows a comparison of all the $|J| - V$ curves measured for a junction of Ag^{TS}-SC_{14}//C_{14}S-Hg with AS-DEP Ag substrate, where - indicate the chemical contact, and // the van der Walls interface between the two SAMs. [48]. Another common substrate used to obtain low RMS metal surfaces is gold on mica. Derose et al. have optimized the process to obtain flat, large areas (μm^2) of gold which have been widely used [49]. The gold on mica method does not produce the same topology as the TS method (hundreds of μm^2), but has the advantage that the surface is solvent resistant and can be used whenever the TS substrates are not compatible with the solvent chosen to form the SAM preparation. [50] The choice of both bottom and top electrodes is highly dependent on the purpose of the device or MJ. In some cases a particular metal is used because of it's Fermi level and work function, Φ, other times other reasons limit the choice to a commonly used metal, without any doubt gold is the most used for both top and bottom electrodes.
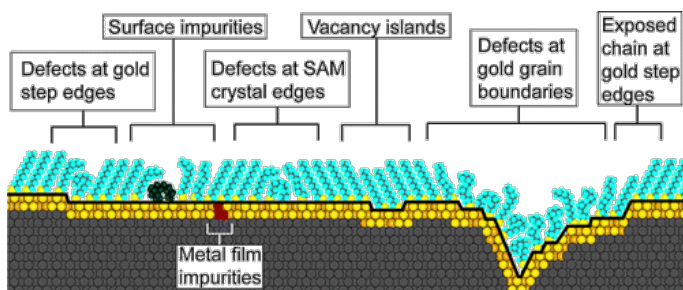
Figure 1.2: Realistic example of surface and SAMs defects. "Reprinted with permission from reference [22]. Copyright 2005 American Chemical Society."
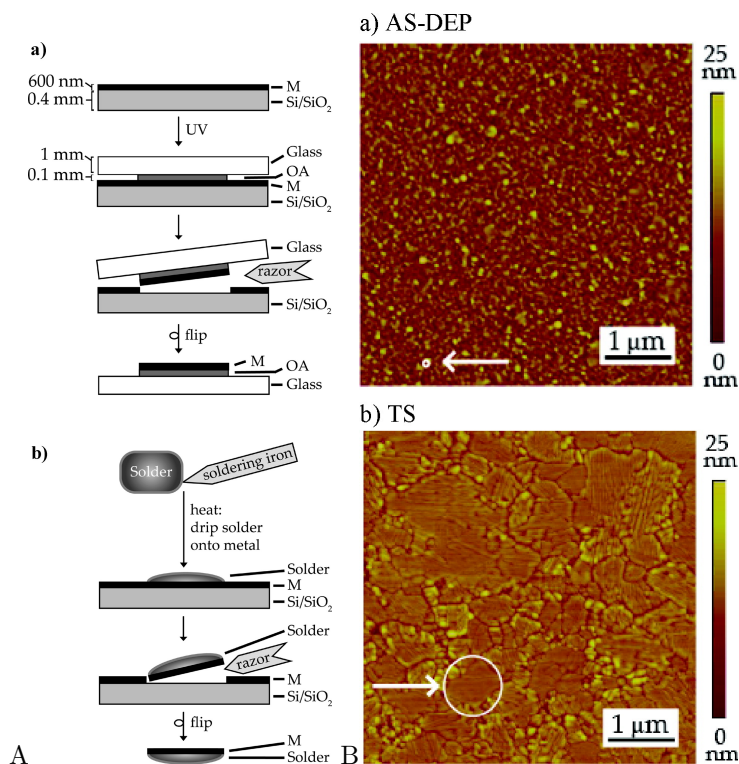
Figure 1.3: *A*: Schematic representation of template stripping process: **a)** with optical adhesive (OA) and **b)** with solder. *B*: Contact mode AFM images of the topography of the **a)** AS-DEP silver film and **b)** Ag^{TS} film. The root-mean-square roughnesses of a $25\mu m^2$ area of the silver films are 5.1 ± 0.4 nm for AS-DEP and 1.2 ± 0.1 nm for TS. The white circles indicate the approximate size of the largest grains in each film and have diameters of **a)** AS-DEP, 80 nm, and **b)** TS, 1μ. "Adapted with permission from reference[48]. Copyright 2007 American Chemical Society."

1.2.2 The Molecules

Compared to silicon technology and semiconductors, molecular systems possess several advantages: they represent confined stable units, can form complex structure, *i.e.*, functional units, have a high degree of freedom in structural variety, and perform subtle conformational changes. In Figure 1.6 a schematic diagram of an ideal Self Assembled Monolayer, SAM, is shown; molecules used either for *self-organization* or *self-assembly*

Ag-SC$_{14}$//C$_{14}$S-Hg Junction
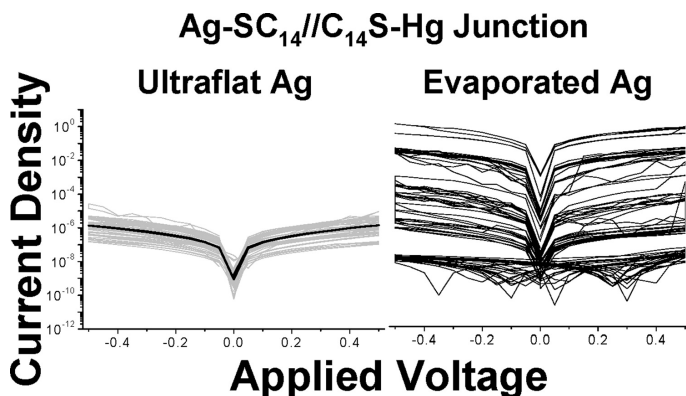
Figure 1.4: Current density J vs applied voltage V traces for 1-mercapto tetradecane on Ag^{TS} and Evaporated Ag. "Reprinted with permission from reference [48]. Copyright 2007 American Chemical Society."

contain a surface-active "head" group, *i.e.*, anchor group, the backbone or spacer, and the functional end group which is meant to interact, strongly or poorly, with the top electrode. The extensive literature on SAMs has established a common, though simple, point of view that SAMs naturally exhibit a high degree of structural order after assembly, that is, they are well-defined phases of organic groups organized in precisely understood lateral organizations on the underlying substrate. A point of fact, however, is that SAMs are dynamic structures that include significant forms of structural complexities, especially when immersed in fluids. A simple single-chain model is sufficient to facilitate comparisons of the organization adopted by different organosulfur compounds with (mostly) linear conformations on different types of substrates, see Figure 1.5. Two parameters describe the variations in the orientation of the organic molecules in the SAM: the angle of tilt for the linear backbone of the molecule away from the surface normal (α) and the angle of rotation about the long axis of the molecule (β). As defined in Figure 1.5, α can assume both positive and negative values; values of β range from 0° to 90°. For SAMs formed from n-alkanethiols on gold, palladium, silver, copper, mercury, platinum, and other materials, the alkane chains adopt a quasi-crystalline structure where the chains are fully extended in a nearly all-trans conformation. The tilts of these chains vary for the various metals: the largest cants, α (with an absolute value near 30°), are found on gold, while the structures most highly oriented along the

10

surface normal direction arise on silver ($\alpha \approx 10°$) and mercury ($\alpha \approx 0°$). The average β for gold lies near $50°$, while for other metals, the data, where available, indicates values generally clustered near $45°$.
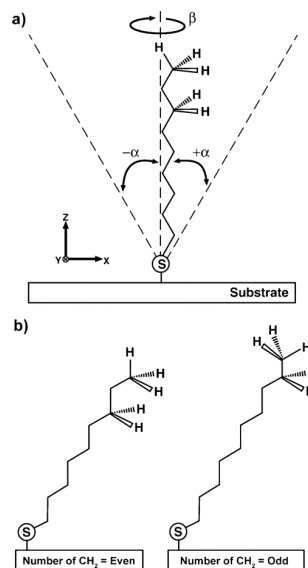
Figure 1.5: **a)** Schematic view of an all-trans conformer of a single, long-chain alkanethiolate ad-sorbed on a surface. The tilt angle (α) is defined with respect to the surface normal direction. The twist angle (α) describes the rotation of the CCC bond plane relative to the plane of the surface normal and the tilted chain. **b)** Schematic views of single, long-chain alkanethiolates (with even and odd numbers of methylene groups) adsorbed on gold. The conserved value of α for each produces different projections of the terminal methyl group on the surface. "Reprinted with permission from reference [22]. Copyright 2005 American Chemical Society."

The early literature on SAMs focused largely on the assemblies formed by the adsorption of organosulfur compounds from solution or vapor phase onto planar metal substrates of gold and silver. These studies used three types of organosulfur compounds such as: alkanethiols $HS(CH_2)_nX$, dialkyl sulfides $X(CH_2)_mS(CH_2)_nX$, and dialkyl disulfides $X(CH_2)_mS-S(CH_2)_nX$, where n and m are the number of methylene units and X represents the terminal functional group (-CH_3, -OH, -COOH etc.). Comprehensive summaries on alkanethiol SAMs are available in several reviews [22,51–53]. As mentioned earlier alkanethiolates have been widely studied because of their excellent self-assembly

properties and low cost. However due to the large energy gap between the highest occupied molecular orbital (HOMO) and lowest unoccupied molecular orbital (LUMO) of about 8-10 eV these molecules are insulating, and consequently a tunneling current is expected (for molecules shorter then 5nm) with exponential decreases with increasing length and temperature dependence. Thus, insulating molecules are intrinsically "less interesting" for ME; more interesting are molecules, which could provide some phenomena such as rectification *i.e.*, diode, high conductance *i.e.*, wire, switching, quantum interference (QI), negative differential resistance (NDR), Kondo effect [54], π-π orbital coupling. T. R. Lee and co-workers intensively studied organosulphur SAM with mono- and pluri-dentate linkers proving that having multiple linkers attach to the surface does increase the overall stability and durability of the monolayer. [55–58] Like the organosulfur many other head group have been used to form SAMs onto metallic surfaces (-CN, -COOH, -Se, -CS_2) and *self-organization* monolayers on semiconductors (alkyl and halogen silanes, alkyne and alkene, phosphates). The combination of chemical and physical properties of the molecules and the substrate rule the assembly process, which can ultimately be tuned by changing temperature (to overcome energy barrier) and concentration. [22]
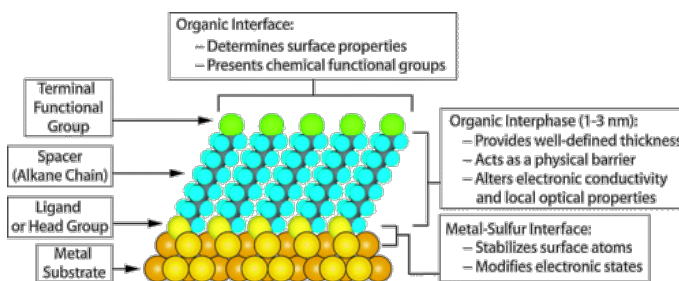
Figure 1.6: Self Assembled Monolayer components. "Reprinted with permission from reference [22]. Copyright 2005 American Chemical Society."

1.2.3 The Interfaces

The interfaces are in most cases in ME crucial for the overall performance of devices and MJ. The first interface is between the molecules and the bottom electrode. The molecules can be either chemisorbed or physisorbed, depending on whether the head

groups have a specific affinity to the substrate or not. I defined in the former section the difference between *self-assembly* and *self-organization*. In most of the cases the molecules are chemisorbed on the surface via head groups or ligands, see Figure 1.6. However an exception to this can be found in supramolecular chemistry where molecules self-assemble on the surface in organized pattern, although they have no specific interactions with the substrate used. In the former case hydrogen bonds and van der Walls interaction are the driving forces and the molecules are laying flat on the surface.

The second interface is between the molecule and the top electrode, which is in most of the junctions the less well defined of the two interfaces. The reason for this uncertainly is related to the inhomogenous topology of the SAMs due to defects in the monolayer and the metal substrate. The difference in contact at the top electrode can lead to few orders of magnitude difference in conduction of the junctions, especially when the molecules contain a functional group able to couple to the top electrode as well as the bottom.[59,60] This is the case of alkanedithiols which are able, at least partially, to couple tightly to both electrodes in certain experimental condition (CP-AFM). In other cases it was found that the interfaces were not playing any remarkable role in the CT[61]. Due to the nearly infinite variables between each system it is complicated to compare results and apply generally the conclusions to other systems. Nevertheless it is clear that to control the overall properties of the MJ it is necessary to have a fine control and a complete understanding of all its components.

1.3 Charge Transport Mechanism

The rate of long-distance (greater than 1nm) CT is dictated by some combination of a strongly distance-dependent tunneling mechanism and weakly distance-dependent incoherent transport.[62,63] The contributions of each of these mechanisms to CT through a metal–insulator–metal (MIM) junction or an organic film are dictated by the energy gap between the work function or energy band of the electrode that injects the charge carrier (electron or hole) and the energy of the orbitals of the insulating organic material. When this energy gap is on the order of $k_b T$, molecular orbitals are energetically accessible to the incoming charge carrier and a short-lived oxidation or reduction of the molecule or polymer occurs. In a molecular junction, this charge is then absorbed by the other electrode; in an organic film, it hops to another molecule until it reaches an interface with a

collecting electrode or recombines with a complementary charge carrier. For MIM junctions where the work functions of the electrodes lie well within the energy gap between the highest occupied and lowest unoccupied molecular orbitals (the HOMO–LUMO gap) of the insulating material, CT proceeds by a non-resonant tunneling process.

1.3.1 Non-resonant coherent super exchange tunneling

The calculation of the coherent, elastic conductance, g, across a molecule sandwiched between two continuous densities of states, and in the presence of a time-dependent voltage, is most often approached through the Landauer formula,[64–69]

$$g = \frac{2e^2}{h} \sum_i T_i \qquad (1.1)$$

where T is the scattering matrix, whose elements give the probability of scattering of the electron in channel i, and $2e^2/h$=$(12.8k\Omega)^{-1}$ is the quantum of conductance. The scattering matrix can be expanded in the Greens function of the molecule[70] or estimated via superexchange formulation, as described below. The form of the scattering matrix directly reflects the mechanism by which the charge moves through the junction, and there are two such mechanisms. The first is direct tunneling, which takes place only if the wave functions of the two electrodes extend far enough into the junction to overlap such that they are directly electronically coupled. The second mechanism of non-resonant CT in molecular junctions (which almost always applies if we are, indeed, speaking of molecular conduction and not just chemical modification of a metal surface) is superexchange: superexchange is an indirect transfer of electrons or holes from donor to acceptor through an energetically well-isolated bridge, during which bridge orbitals are utilized solely as a coupling medium.[71,72] The total probability of transmission of an electron or hole from electrode 1 to electrode 2 via indirect tunneling is the electronic superexchange coupling, $(\tau_{\mathrm{DA}})^2$.[73]

1.3.2 The Barrier model for non-resonant tunneling and the β parameter

The superexchange model accounts for the explicit electronic structure of the molecular bridge and the metal-molecule contact. There are, however, simpler approaches to

calculate the magnitude of the current through a molecular junction; these approaches consider the molecule to be a homogeneous dielectric layer (a single tunneling barrier) between two metal electrodes and are used to describe both direct (overlap of electrode wave functions) and indirect (no direct coupling between electrodes) tunneling. For a rectangular barrier, one can obtain an analytical solution for the coefficient for transmission of an electron. A semiclassical expression is necessary to describe non-rectangular barriers. In both cases, as for superexchange, the transmission probability decays exponentially as the width of the barrier increases. The most popular and used approach for estimating the magnitude of the tunneling current though a barrier of arbitrary shape is the Simmons model for elastic tunneling. [17,74] In this model, a system of two equipotential metals with an insulating layer between them at zero applied bias is in thermal equilibrium such that the Fermi level is uniform throughout the system. If a bias is applied, current can flow. At small applied voltages (V) (where the size of the injection barrier $\gg V$), the current density depends linearly on V. At higher voltages (the intermediate regime), when the barrier is on the same order as the applied voltage, there is a hyperlinear dependence of current density on V. Equation 1.2 gives the dependence of the magnitude of the current density (the current divided by the area of the junction, J) on the length of a potential barrier,

$$J = J_0 e^{-\beta d}; J_0 = j_0 e^{-\alpha d_0} (d, d_0 \geq 0) \tag{1.2}$$

which we have partitioned into a portion whose length (d_0, Å) is constant as we vary the molecular structure of the insulating layer, and a portion whose length (d, Å) changes as we vary the molecular structure of the insulating layer. A plot of $\ln J$ versus d has slope β ($\mathring{A}^{-1}$), which quantifies the decay of the tunneling probability with increasing d and does not depend on the choice of d_0, and intercept $\ln J_0$ (A cm^{-2}), the value of which depends on three factors: (i) j_0, the current that would flow through the junction if the thickness of the insulating layer were zero, (ii) the choice of d_0, and (iii) α, the characteristic decay of the tunneling probability with increasing d_0. The factor $e^{-\alpha d_0}$ is sometimes called the contact resistance because it quantifies the characteristics (height and length) of the tunneling barrier that the electron encounters at interface between the metal and the molecule. [75] An electron may tunnel through the junction via multiple pathways, some that follow the carbon backbone of the molecule and some that involve multiple molecules. For close-packed SAMs of n-alkanethiolates, for example,

15

the magnitude of the tunneling current appears to correlate with the molecular length, *i.e.*, the distance between the electrodes along the molecular axis, and not with the average shortest physical distance between the electrodes. The parameter β has been used as a benchmark for the suitability of a molecule as a wire: the smaller the value of β, the longer the distance over which charge can be transferred without penalty. The β parameter is often used to characterize all types of transport, although from its very definition it only applies to exponentially decaying processes. The range of β values, see Table 1.1 found for identical bridge units measured in solution and through SAMs of organic thiols on the surface of metal electrodes reflects the fact that the most fundamental aspects of transport, including length dependence, are sensitive to the environment in which the measurement is performed. [23,76] The Simmons model, and it's approximation, have been widely used to fit experimental results of various systems and molecules. [48,77–80] Nevertheless this model ignores the electronic structure properties of the molecules and the geometry of the contacts, plus it neglects any intermolecular and electron-electron interactions, which are taken into account by more sophisticated electronic structure theory. [81] The Simmons model therefore does not give any insight into the mechanism of CT. Now that the general concepts of what is a molecular junction and it's component are introduced it's time to look closely to two specific techniques to measure molecular tunneling junctions, Hg drop junction and Eutectic Gallium Indium (EGaIn), which are the only top electrode liquid metals used in ME.

Number of carbon (N)	Contacts	Technique	Number of molecules	β (per carbon)
6, 8, 10	Au−S/S−Au	STM	1	0.99 to 1.09
2, 3, 4, 5, 6, 7, 8	Au−NH$_2$/NH$_2$−Au	STM	1	0.86
6, 8, 10, 12	Au−S/CH$_3$−Au	CP-AFM	100-1000	0.88
4, 6, 8	Au−S/S−Au	CP-AFM	100-1000	1.16
6, 8, 10, 12	Au−S/CH$_3$−Au	CP-AFM	1000	1.01
8, 10, 12	Au−S/S−Au	Nanoparticle AFM	1	0.54
8, 10, 12	Au−S/S−Au	Nanoparticle AFM	1	0.95
9, 10, 11, 12, 15, 16, 18	Au−S/S−Hg	hanging Hg drop junction	2.5×10^{11}	1.06
16, 18, 20, 22, 24	Au−S/S−Hg	hanging Hg drop junction	2.5×10^{11}	1.01
20, 24, 28	Au−S/S−Hg	hanging Hg drop junction	3.7×10^{11}	0.85
8, 12, 16	Au−S/CH$_3$−Au	Nanopores	7300	0.83
8, 10, 12, 14, 16	Au−S/HS−PEDOT	Large Area junction	3.2×10^8 - 3.6×10^{10}	0.66
8, 10, 12, 14, 16	Au−S/CH$_3$−PmPV	Large Area junction	3.2×10^{11} - 3.2×10^{12}	1.13
6, 10, 12	Au−S/CH$_3$−Au/Au−CH$_3$/S−Au	Nanoparticle bridge	100	0.87
17, 18, 19, 20, 21, 22	Al$_2$O$_3$−O$^-$CO/CH$_3$−Au	PALO	9.2×10^{12}	0.85
8, 12, 16	Au−S$_/$CH$_3$−Au	Thermally evaporated	1.5×10^7	1.08

Table 1.1: Comparison of the measured decay coefficient β_N for alkane-based molecules in different molecular junctions and by different research group.

1.4 Hg & Eutectic Gallium Indium: powerful tools to study the electrical properties of Self-Assembled Monolayers

From here on we will focus on the measurement of current-voltage response for mono-layers on metal and semiconductor (silicon) using liquid metal electrodes. We already mentioned the advantages of using ordered-monolayers instead of few/single molecules. Enclosing a molecule inside a well ordered 3D structure allows us to study the CT with the preferential conformation of the molecule on the surface due to different variables, which does not allow tailoring the "position" of the molecule on the surface. However most of single molecule measurement have uncertainty about molecular position and, moreover, it contacts the electrode. SAMs of saturated hydrocarbons[33,53,75,80,82–96] and conjugated oligomers, such as oligophenylenes[97–107], oligophenylenethylenes and carotenes[108,109] have been intensively used as basic building block for MJs. Each type of junction and technique have advantages and disadvantages with respect to fabrication cost, simplicity, reproducibility, and application.

1.5 Hg-drop Junctions

Mercury, Hg, is the only metal that is liquid at standard conditions for temperature and pressure and for this reason was used by humans for many applications. In molecular electronics, Slowinski and Majda first utilized Hg-drop on SAMs in 1996. The Hg-drop is based on liquid mercury electrode(s) suspended on the target organic layer or monolayer.[20,91,94,95,110–113] Different architectures of Hg-drop have been used and we are going to describe one by one in the current chapter. The MIM junction can be describe as follow: Hg-SAM//SAM-M where // represent the van der Waals interface between the SAMs, M the metal of the surface or bottom electrode, and - the interface between the thiol group and the metal *i.e.*, it is chemisorbed. We will describe four types of Hg-drop junctions that differ by substrate (M) used and the measurement apparatus. Figure 1.7 shows the four different junction type which utilized Hg.

Hg-drop junctions reveal several advantages when compared to other conventional techniques to measure CT : i) ease of assembly, simple, inexpensive equipment, no clean
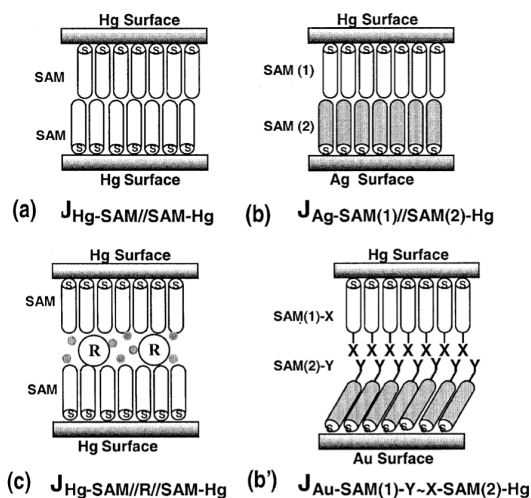
Figure 1.7: Schematic representation of Hg-drop junction type. **(a)** liquid-liquid; **(b)** liquid-solid; **(c)** liquid-redox-liquid; **(b')** particular case of **(b)**. "Reprinted with permission from reference [91]. Copyright 2002 Elsevier."

room or lithography; ii) it gives stable and reproducible results; iii) it is a versatile technique since it can host a large variety of molecules. Furthermore, the Hg-drop electrodes, themselves present several advantages: i) Hg is liquid at room temperature (RT) and, as a liquid, has no surface features or defects, such as step edges, terraces etc., which results in an ideal surface to grow defect-free monolayers; ii) SAMs form within a few seconds on the surface of Hg in the presence of alkanethiols in solution; iii) the Hg-drop can make conformal contact with molecules on a solid surface without applying pressure (beyond the weight of the Hg) on the monolayers. In the following paragraphs I will introduce the different Hg-drop architectures.

1.5.1 Hg-SAM$_1$//SAM$_2$-Hg

Figure 1.7(a) shows the schematic view of the junction: Hg-SAM//SAM-Hg. These are called *liquid-liquid* junctions, and they are formed by bringing carefully two drops of Hg covered by SAM of alkanethiolates into contact in a solution of ethanol that contains the alkanethiol. The SAMs$_{1-2}$ may or may not be the same. A tungsten wire inside a micro syringe is used to connect the conductive Hg drops to the electrometer. Using two liquid

electrodes (with the same work function) has the advantage of avoiding any issues from contamination of a solid metal electrode by mercury vapor, plus the tilt angle α (which is the angle normal to the surface where the direction of the alkane chain is pointing) is close to 0°. The null tilt angle makes Hg-drop junctions ideal to study the length dependence properly since the full length of the molecule is preserved. Nevertheless the *liquid-liquid* Hg junctions present several disadvantages such as: the contact area is difficult to evaluate and change with the potential applied, intercalation is possible at high voltages, and the system simply does not work well with non *n*-alkanethiolates. Using capacitance measurements as a function of the length of the alkanethiols in the SAMs, and impedance spectroscopy, SAMs of alkanethiols have been extensively characterized. [94,111,112,114,115] Capacitance measurements in polar solvents indicated that the junction formed with hexadecane thiol does not include solvent molecules between the two SAMs. It seems that the solvent is included at the interfaces only when no voltage is applied; thus the presence or absence of hydrocarbon solvent between aliphatic SAMs may depend on the total pressure,*i.e.*, potential, across the junction. The total pressure depends on the Hg-drop weight and the electrostatic pressure due to the bias applied.
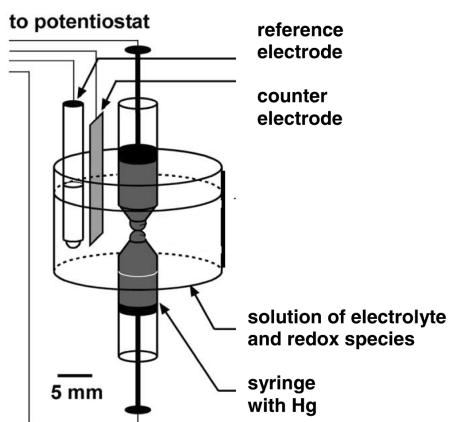
Figure 1.8: Schematic view of liquid-liquid electrochemical cell apparatus. "Reprinted with permission from reference[91]. Copyright 2002 Elsevier."
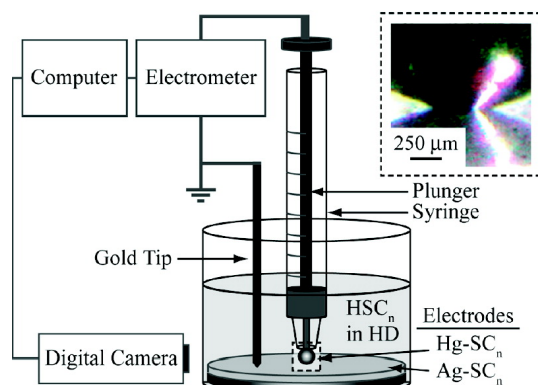
Figure 1.9: Schematic drawing of the apparatus used to measure the tunneling current through Hg-drop junctions. "Reprinted with permission from reference [48]. Copyright 2007 American Chemical Society."

1.5.2 Hg-SAM$_1$//SAM$_2$-M

The *liquid-solid* junction represented in Figures 1.7(b) and 1.9 comprises a Hg drop with a SAM$_1$ and a solid metal surface ($M=$ Ag, Au, Cu, Pd, Pt, Ti, Hg/Au alloy) covered by a second SAM$_2$ where 1 and 2 may differ. The solid flat metal surface makes the fabrication straightforward and in all cases the two SAMs are formed separately. A SAM$_1$ of hexadecanethiol ($HS-C_{15}H_{24}CH_3$) is usually formed on the Hg-drop. The two metal surfaces are then brought carefully together using a micromanipulator in a solution (usually hexadecane) containing the thiol used to form SAM$_2$. The liquid-solid junction is more versatile because the SAM$_2$ on the solid substrate can be characterized prior to junction formation, the supramolecular structure can be tuned by changing the metal substrate, [116] and as a consequence, the tilt angle. The solvent not only "heals" SAM$_2$ when the two electrodes are not in contact, but protects the Hg drop from vibration, and protects the surfaces from contamination. It has been shown that the solvent chosen does not play important role in the conductivity. [91] Furthermore the *liquid-solid* junction makes it possible to form several junctions on different spots on the solid substrates by lateral translation of the metal substrate. By doing so more cycles *i.e.*, sweeps, can be acquired and more substantial statistical analyses can be made. The *liquid-solid*, is definitely more versatile than *liquid-liquid*, allowing the systematic study of different metal substrates and several molecular organizations.

1.5.3 Hg-SAM$_1$-R//R-SAM$_2$-Hg and Hg-SAM$_1$//R//SAM$_2$-Hg

Another Hg junction type, such as the one showed in Figure 1.7(c) and Figure 1.8, contain an R group, where R is a redox molecule trapped at the interface between the two SAMs. The two electrode system (Figure 1.7(a) and (b)) suffer from an ambiguity in the relative position of the Fermi level of the electrodes with respect to the energy levels of the redox molecules sandwiched between them. In an electrochemical cell the macroscopic reference electrode allow potentiostatic control of the energy level of redox sites trapped in the junction, relative to the potentials applied to the metal electrodes. We distinguish two different electrochemical junctions that incorporate redox sites: one where the Hg electrodes are functionalized to covalently bind to redox sites (Hg-SAM$_1$-R//R-SAM$_2$-Hg), and one where the redox sites are incorporated into the inter-electrode gap (Hg-SAM$_1$//R//SAM$_2$-Hg). In both junctions, the potentials of the mercury electrodes are driven in such a way that one electrode acts as the electron donor and the other one as the electron acceptor. The current between the electrodes is measured by keeping constant the potential of one electrode and sweeping the other electrode. In the case of trapped redox sites a SAM of alkanethiolate terminated with carboxylic acid group is commonly used because the $-COOH$ complexes the redox sites (Ru(NH$_3$)$_6$$^{3+}$).

Weiss et al. compared the structural and electrical characteristics of self-assembled monolayers using Hg-drop.[48] Figure 1.10 is a plot of $\log J$ for Hg-drop junctions incorporating SAMs of n-alkanethiolates versus the total number of carbon in the alkyl chain(s) N_c between the electrodes in the junction[48]. A linear least-squares fit to the largest dataset (aggregated dataset) yields to $\beta = 1.1/carbon$ ($0.85\mathring{A}^{-1}$) and $J_0 = 1.0 \times 10^6$ A cm^{-2}. The aggregated dataset contains instead values of J measured at $V = -1.5V$ (in an electrochemical setup). In this case, $\beta = 0.86/methylene$ -CH$_2$- ($0.69\mathring{A}^{-1}$) and $J_0 = 1.7 \times 10^2$ A cm^{-2}. These values were use to validate their method and has an evidence of tunneling through the alkyl chain rather than through-space.

The Hg drop junction was largely used for almost a decade as main *bottom-up* technique in ME despite the toxicity and volatility of mercury. In most of the cases the high affinity of Hg with other metals to form amalgams and its high sensitivity for defects in the monolayer, *i.e.*, tendency to short with thin disordered monolayers, from here the need for a solvent bath to "heal" the junction limited the yield of working junctions and the information that could be extracted from such a molecular system.

Figure 1.10: Log J for Hg-drop junctions incorporating SAMs of *n*-alkanethiolates versus the total number of carbons in the alkyl chain(s) between the electrodes in the junction. The slope of the linear least-squares fit to these data is $\beta/2.3$. Aggregated dataset 1 (the solid diamonds and open squares) includes values of J measured at V=0.4 or 0.5 V (the solid diamonds are data acquired using $\mathrm{Ag}^{\mathrm{TS}}$). For this dataset, β=1.1/methylene group (0.85 $\mathring{A}^{-1}$), and $J_0 = 1.0 \times 10^6$ Acm^{-2}. Aggregated dataset 2 (the solid circles) contains values of J measured at V=-1.5V. For this dataset, β=0.86/methylene group (0.69 $\mathring{A}^{-1}$), and $J_0 = 1.7 \times 10^2$ Acm^{-2}. "Reprinted with permission from reference [48]. Copyright 2007 American Chemical Society."

1.6 Eutectic Gallium Indium EGaIn

Eutectic Gallium Indium EGaIn (EGaIn) was developed in the group of Whitesides at Harvard University by Chiechi et al. [21] who thought to substitute Hg with another liquid metal. Hg is indeed known for its vapor toxicity and tendency to form amalgams with other metals (in particular with gold, in fact mercury was intensively used for extraction of the precious metal until the latter period of the first millennia) which makes it unlikely to be user-friendly and of any use for practical application. EGaIn is a metal alloy of Ga 75.5% and In 24.5% by weight and has a melting point m.p=15.7°C [117]. Although EGaIn is a liquid at room temperature, it does not spontaneously reflow into the shape with the lowest interfacial free energy as do liquids such as Hg and H_2O: as a result, it can be formed into metastable, non spherical "tips". This behavior along with its high conductivity (3.4×10^4S cm^{-1}) [118] and its tendency to make low-contact resistance interfaces with a variety of material [117], makes EGaIn useful for forming electrodes for thin-film devices [119–121], such as liquid metal-based plasmonics. [122] In the first report Chiechi et al. reported measurement of current density (J, A cm^{-2}) versus applied voltage (V, V) through SAMs of n-alkanethiolates on Ag^{ts} Ag$-$SC$_n$H$_{2n+1}$ using EGaIn as top soft-conformal electrode, in a way similar to Hg-drop electrode. An ideal electrode for physical-organic studies of SAMs would i) make conformal, non-damaging contacts, ii) readily form small-area contacts to minimize the influence of defects in the SAM to J, iii) form without specialized equipment. EGaIn looked promising as a substitute for Hg since both allow to measurement under ambient conditions, but Hg is toxic, amalgamates with metals, and require a solvent bath during the measurement. An abstract representation of what we mean as an *ideal electrode* is Figure 1.11.

EGaIn does not flow until it experiences a critical surface stress (0.5 N m^{-1}), at which point it yields, [21]. Since 2008 several scientific reports have been published on the use of EGaIn in ME [21,50,61,80,122–147]. In ambient conditions the surface of EGaIn oxidizes rapidly and spontaneously and it absorbs adventitious contaminants (*e.g.*, water, organic molecules, particles). Figure 1.15 shows the formation of an EGaIn MJ. The EGaIn "tip" is formed by stretching a droplet between a syringe (filled with EGaIn) and a substrate to which the droplet adheres. As we move the syringe away from the sacrificial substrate with the help of a micro manipulator, the droplet elongates into an hourglass shape, Figure 1.15, which eventually snaps and create two sharp tips. The

Figure 1.11: Idealistic top-"electrode"

tips retain their conical shape, due to the Ga_2O_3 skin [21]. The MJ is then formed by bringing into contact the freshly prepared tip with the substrate supporting the SAM. With a camera, from the side, we can estimate the size of the junction after calibration with a microruler. Since the tip has a conical shape we can assume that the contact has a circular shape with $(A=\pi(d/2)^2)$ where d can be measured with the camera. A microscopy study suggests that the effective area of contact is $\sim$25% of the estimated one [148]. One tip is–with the common protocols–used to form approximately 10 junctions in different spots of the sample. Over time the tip can absorb contaminants from the surface and atmosphere, thus it is good practice to change the tip frequently in the same manner as it is formed (*i.e.*, the original droplet on the sacrificial substrate can be reused over a few hours). The two most serious ambiguities of EGaIn junctions lie with the surface of the top electrode: specifically i) the absolute contribution of the oxide and the adventitious contaminants to the resistance of the junction is unclear, and ii) the effect of environmental and user variables (resistance, local thickness, and composition of the oxide) which can all lead to ambiguities in the electrical measurement. Dumke et al. analyzed the surface of Ga_2O_3/EGaIn by ion sputtering and scanning Auger spectroscopy [149]. They conclude that the oxide layer was mostly Ga_2O_3 about $\sim$2nm,

however following studies suggested that the oxide is mainly Ga_2O_3 and the In is more abundant in the interface between the liquid alloy and the oxide, and that the oxide is passivating the surface limiting the growth [21]. The oxide was later found to be about ~0.7nm thick (on average). In the report of Cademartiri et al. the authors deeply investigate the oxide properties, composition, and morphology; they evaluate the influence of the oxide on the transport of charge through the junctions [141]. In their report they consider the various hypotheses based on the previous knowledge and novel experiments concluding that:

1. The oxide skin forms spontaneously on EGaIn in ambient conditions is 0.7 nm thick, and it is composed mostly of Ga_2O_3

2. XPS studies revealed that the oxide composition remains stable, mechanic deformations and curvature does not affect the average thickness and composition of the oxide

3. The transport of charge through the junction is dominated by the SAM. The consistency of $J(V)$ [130,132,134] suggest that the influence of the oxide skin and the adsorbates on the conductivity of the junction is either negligible or similar from junction to junction. This conclusion might be not valid for highly conductive SAMs where the oxide could be indeed limiting the conductivity [50].

4. The adsorbates do not contribute to the magnitude of J within 15min. (However, I strongly believe that few hours of exposure of the tip to air increase the risk of irreversible contamination which would lead in lower contact area or either low current traces)

In conclusion, despite the influence of the oxide creating doubts about EGaIn, different laboratories have successfully demonstrated the capability of such a technique which, in only half a decade, produced several publications and has risen to the attention of the entire ME community. In the following sections I will emphasize the more relevant (up to date) publications regarding EGaIn as top electrode omitting our own publication(s) which are further describe in the following chapters.

1.6.1 EGaIn Microfluidics

The ability to inject metal into microchannels is extremely important for the production of low cost, flexible electronic components such as microscale wires, circuit elements, electrodes, and electromagnets.[150,151] Dickey et al. showed that EGaIn was able to form stable structures in micro channels at room temperature.[21] EGaIn, at least for some applications, may have an advantage over molten solders (used in a set of methodologies called "microsolidics"), which require heating and cooling steps that increase the time needed for the fabrication process, and make it incompatible with heat-sensitive materials such as organics. For most applications requiring a liquid metal, EGaIn is superior to Hg, which readily fills microchannels at RT, but is toxic and forms unstable structures that spontaneously retract from the channels to minimize interfacial free energy. EGaIn possesses the unique ability to remain inside the channels even after pressure/vacuum is removed. This intrinsic stability was found to be due to the oxide skin because by pretreating the channel with HCl, EGaIn does behave like mercury and retracts from the microchannels. In the same manner a "tip" of EGaIn immersed in diluted HCl solution does not retain the shape, and behaves like mercury. The work of Dickey et al. lead to subsequent publications that explore the properties of EGaIn in confined microfluidic junctions.[148] Nijhuis et al. manufactured small arrays of tunneling junctions comprising SAMs of alkanethiolates with ferrocene moieties sandwich between Ag^{TS} and EGaIn confined inside microchannels. These arrays, shown in Figure 1.12, allow temperature dependent measurements, ensure a fine control of the junction area, potentially allow to the measurement of different SAMs without removing the top electrode, and permit reversible assembly and disassembly of the junctions. The authors validate the previous results on ferrocene SAMs[125]. In the early stage of my PhD, I fabricated soft-soft molecular junction in which both electrodes (EGaIn and Au^{TS}) were confined in microfluidic channels. An example of such molecular junction can be seen in Figure 1.13 and Figure 1.14. When measuring the charge transport of such devices we had several problems, in particular the lack of stability of the Au^{TS} film and in some cases the presence of Au was not restricted in the channel, see 1.14, causing undefined junctions. The solution proposed by Nijhuis et al., although more laborious, definitely give rises to higher yields of working junctions, which is the figure of merit.

Figure 1.12: Microfluidics solid state molecular junction comprising ferrocene SAMs with EGaIn trapped into the microchannels and arrays of Ag^{TS} as bottom electrode. "Reprinted with permission from reference [148]. Copyright 2010 American Chemical Society."

Figure 1.13: Schematic view of the molecular junction where both the top and bottom electrodes are confined into microfluidics channels.

Figure 1.14: Picture of an home made PDMS-Au^{TS}-SAM//EGaIn-PDMS device.

1.6.2 EGaIn in Molecular Rectifiers

As mentioned above, EGaIn has been used as top electrode with the classical "tip" shape[124,125,131,133] and in microchannels[148]. Since the first molecular rectifier was proposed from Aviram and Ratner,[3] much effort has been invested in demonstrating their hypothesis.[152–157] The hypothesis underlying this design is based on the relative energies of the highest occupied molecular orbital (HOMO) of the donor unit and the lowest unoccupied molecular orbital (LUMO) of the acceptor: the current observed with one bias voltage (resulting from resonant electron transfer from the LUMO of the acceptor to the HOMO of the donor) would be greater than that of the current for the opposite bias (resulting from nonresonant transfer). In many past works, the rectification observed was not necessary due to the molecule, but the experimental conditions and electrodes. By definition a rectifier is a molecular species or component which changes the ratio of the flow of current, making the current flow preferentially in one direction than to other. Nijhuis et al. intensively studied molecular rectification observed in SAMs of $SC_{11}Fc$[125] where it was found that the ferrocene moiety induces a dramatic increase in the rectification ratios (R $\approx 1.0 \times 10^2$). This result was attributed to the asymmetric potential drop across the SAM and, importantly, the mechanism of charge transport changes from tunneling to hopping at one bias, but not the other.[148] Interestingly the ferrocene SAMs rectify only when the Fc moiety is located asymmetrically in the SAM, which means that the Fc must be close in space to one of the electrodes.

In their case the Fc moiety has a van der Waals contact with the Ga_2O_3/EGaIn top electrode and consequently the HOMO of the Fc can follow the Fermi level of the top electrode,*i.e.*, couple tightly. At sufficient negative bias ($\sim -0.6V$), the HOMO of the Fc can participate in charge transport, and the potential drops mainly across the insulating C_{11} alkyl chain. At positive bias, the HOMO of the Fc cannot participate in charge transport, and the potential drops more or less equally along the entire length of the molecule ($C_{11}Fc$). The measurement of $J(V)$ as a function of temperature indicated that, at negative bias, when the HOMO of the Fc participate in the charge transport, the mechanism changes from tunneling (T independent) to more efficient hopping (T dependent), while at positive bias the HOMO cannot participate and they just observed tunneling[148]. The authors proved that the cause of rectification is indeed the Fc moiety and not the SAM or the asymmetric electrode (Ag^{TS}-Ga_2O_3/EGaIn). When the Fc is omitted, the *n*-alkanethiolates SAM does not give rise to statistically significant rectification: $R \approx 1.0$ to 1.5; in the same way, when the Fc moiety is buried in the SAM, far from the electrodes, the HOMO of the Fc cannot enter into resonance with the Fermi energy level. Nijhuis et al. also demonstrate that adding two Fc moieties further increases the rectification ratio at the expense of the stability of junctions.[131] Nijhuis and coworkers proposed a model illustrated in Figure 1.16. In a more recent work Nerngchamnong et al. demonstrate that on Ag^{TS} an odd number of methylene spacers in the alkyl chain lead to a more densely packed SAMs, and expose the Fc moiety directly to the top electrode, giving rise to higher rectification ratios[146]. The reverse was found for gold, where even number of methylene gives better results for Au^{TS} due to the different intermolecular interactions and the different tilt angles, α. So far the best candidate of their series remain the earlier report $HSC_{11}Fc$ which forms robust and dense SAMs with over 90% working junctions and R $\approx$ 100.

$$R = \frac{|J(-V)|}{|J(+V)|} \tag{1.3}$$

1.6.3 Odd-Even Effects in Self-Assembled Monolayers

SAMs of odd-numbered *n*-alkanethiols differ from corresponding SAMs of even-numbered *n*-alkanethiols with respect to many properties, including structure, surface free energy, kinetics of molecular exchange, tribology, kinetics of electron transfer, electrochemistry,
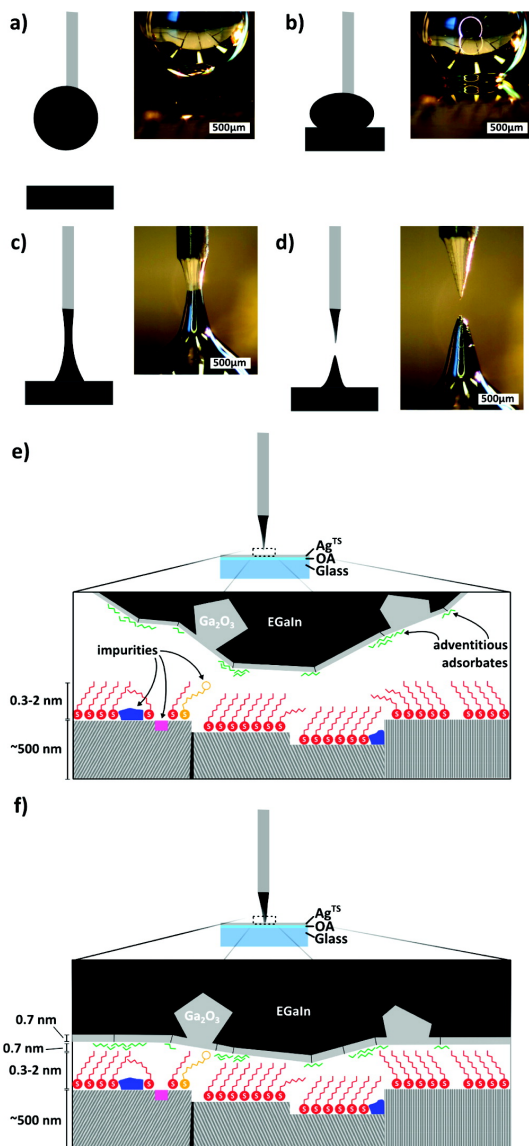
Figure 1.15: Tip formation from **a** to **d**; Figure **e** and **f** junction formation by approaching the tip on the surface. "Reprinted with permission from reference [141]. Copyright 2012 American Chemical Society."
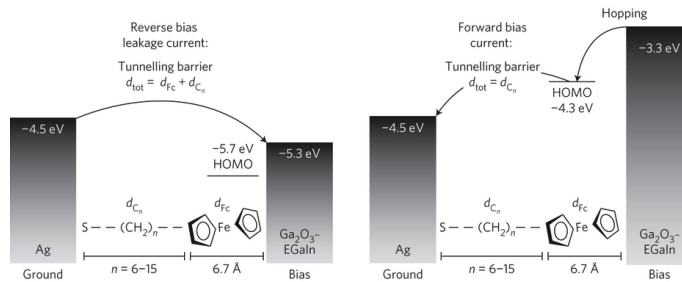
Figure 1.16: Energy level diagrams of the junctions at a bias of $+1$ V and -1 V. At negative bias (or forward bias), when the molecular diode allows current to pass through, the HOMO level centred at the Fc units falls between the energy window of both Fermi levels and can participate in the mechanism of charge transport. The two-step mechanism of charge transport involves tunneling of an electron from the HOMO of the Fc across the alkyl chain to the bottom electrode, followed by hopping of an electron to the Fc unit in a second step. The width of the tunneling barrier, d_{tot}, is determined by the length of the alkyl chain, d_{alkyl}, or $d_{tot}=d_{alkyl}$. At positive bias (or reverse bias), when the diode blocks the current, this HOMO level falls below both Fermi levels and cannot participate in the mechanism of charge transport. Consequently, the whole length of the molecule forms a barrier against tunneling of width $d_{tot}=d_{alkyl}+d_{Fc}$. For ideal diodes, this current would be infinitesimally small and is called "leakage current" in analogy to conventional diodes. "Reprinted with permission from reference [146]. Copyright 2013 Nature Publishing Group, a division of Macmillan Publishers Limited."

reactivity, and packing density [22,158,159]. Odd-even effects have been observed in liquid crystals, molecule-capped quantum dots, and field effect transistors. Thuo et al. compared the charge transport across SAMs of n-alkanethiols containing odd and even number (n from 9 to 18) of methylenes with EGaIn as top electrode. The authors collected statistically significant amounts of data and since J is log-normally distributed (due to random defects) it is possible to fit the distribution of $\log|J|$ with a Gaussian function, see Figure 1.17. The $\mu_{\log}$ Gaussian fit usually differs from the arithmetic average because Gaussian is less sensitive to outliers [21]. Thuo et al. determined the tunneling decay constant β for both odd and even-numbered of alkanethiols. β_{odd}=1.19±0.08 n_{C}^{-1}, and β_{even}=1.05±0.06 n_{C}^{-1} at $-0.5V$ without an actual significant difference between the two. Interestingly the authors evaluate the influence of user experience on these result by having several novice experimentalists acquiring data on these SAMs. The result is a non-significant difference in β values that emphasizes the ease and straightforward technique of EGaIn.

1.6.4 Charge Transport Is Insensitive to Many Functional Groups

Recently Yoon et al. [61] measured a series of modified alkanethiols containing a range of common aliphatic, aromatic, and heteroaromatic organic tail groups. The MJs studied in their work have the following structure: Ag^{ts}-$S(CH_2)_4CONH(CH_2)_2R$//Ga_2O_3//EGaIn; R= functional terminal group which in their studies vary from thiophene, naphthalene, phenyl, cyclohexane and many more, see Figure 1.18. Yoon et al. compared values of tunneling current across these SAMs, which have approximately the same thickness, thus they evaluate what is the actual influence of the R groups alone. Surprisingly the charge transport across these SAMs is insensitive to changes in the organic molecules where length is kept the same. Although subtle and in some cases within the confidence interval, there are differences between the R group. The $J(V)$ value for aromatic moieties **1-7** appears to increases as the volume of R increases, while the $J(V)$ value for aliphatic moieties **8-13** appears to decrease. The authors suggested that, over a range of structures typical of those used in conventional organic chemistry, changing the structure, for a constant thickness of the SAM, has little influence on the rates of tunneling. This conclusion indicates that the rate of charge transport can be modeled by tunneling through a rectangular barrier whose structure at the atomic/molecular level is not important. It's however worth noting that the molecules studied in this work are
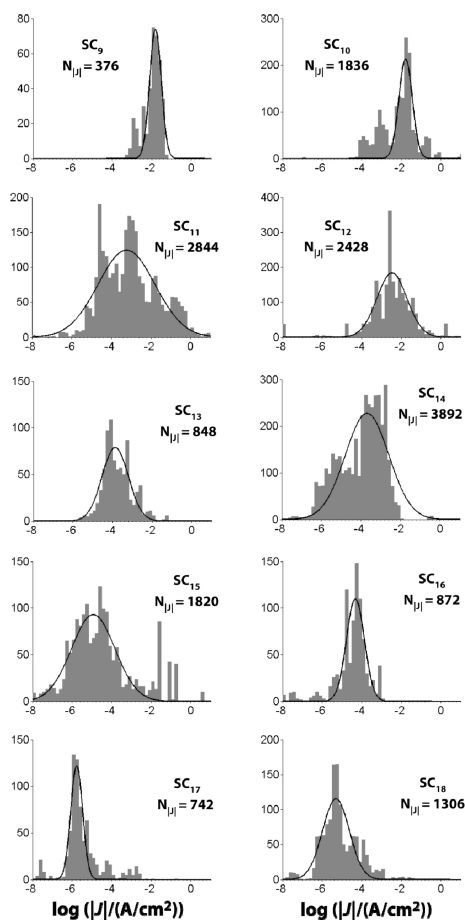
Figure 1.17: Summary of current density, J, data derived from all *n*-alkanethiols. Histograms of $\log |J|$ with a Gaussian fit include all the data collected by different users for *n*-alkanethiols (SC_n, where $n = 9$-18); $N_{|J|}$ is the number of measurements collected for each SAM. A gradual decrease in the current density as chain length increases can be observed from the fitted data. "Reprinted with permission from reference[80]. Copyright 2011 American Chemical Society."

highly insulating despite the nature of the terminal groups, thus the charge transport properties are mostly dictated by the alkyl spacer, which is kept constant. I believe that, in this case, the different kinetics and packing density, *i.e.*, possible defects in the SAMs, are the main reason of variance of J. It is intuitive that bigger bulky group on the surface of the SAMs could not pack as tightly as a methyl, resulting in defects and higher J.
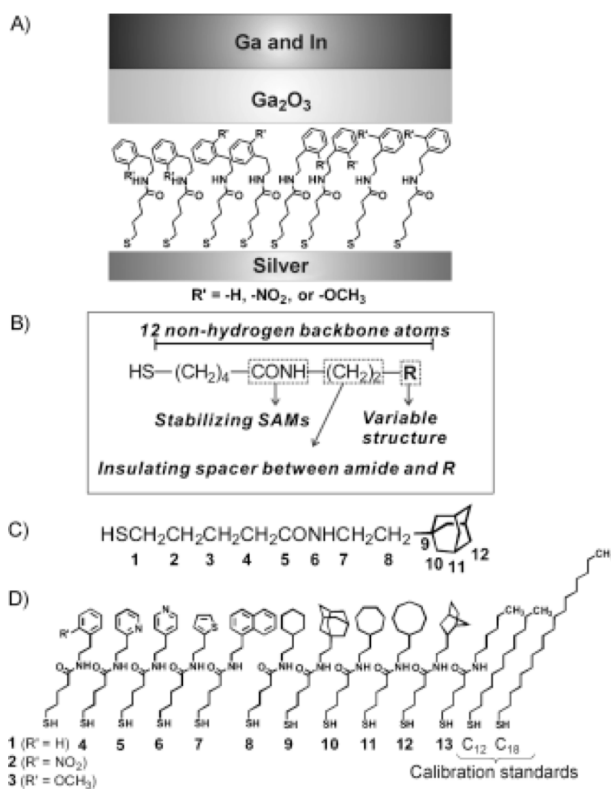
Figure 1.18: **A)** Schematic representation of a tunneling junction consisting of a $\mathrm{Ag^{TS}}$ bottom electrode supporting a SAM, and contacted by a $\mathrm{Ga_2O_3/EGaIn}$ top electrode. **B)** A schematic representation of one junction. **C)** The numbering system based on non-hydrogen atoms in the backbone of the molecules tested. **D)** Molecules used to form SAMs for this study. "Reprinted with permission from reference [160]. Copyright 2012 Wiley."

1.6.5 Effect of Torsional Angle

Samori et al. in a recent publication reported a careful study on biphenylthiol based SAMs. The authors spectroscopically (high-resolution X-ray photoelectron spectroscopy HRXPS and angle-resolved near-edge X-ray absorption fine structure NEXAFS spectroscopy) and electrically characterized them with EGaIn as top electrode. The authors conclude that the charge transport through the SAMs with varying torsion angles chemisorbed on Au surfaces exhibits a good degree of correlation with the packing density and orientational order in the monolayers. The last parameters were mostly governed by molecular conformation, which was specifically adjusted by the site bridging or substitution of/at the individual phenyl rings. The efficiency of the charge tunneling through the SAMs shows a characteristic decay with the increasing separation between the metallic contacts *i.e.*, an increase of the effective SAM thickness. The authors found $\beta = 0.27 \pm 0.08 \mathring{A}^{-1}$.[143]

1.6.6 EGaIn as Top Electrode in Quantum Dots

Weiss and co-workers utilized EGaIn as top electrode in arrays containing Quantum Dots (QD). They studied the effect of quantum dots size in their devices, see Figure 1.19. The authors concluded that the turn-on voltage depended on the size of the QDs next to the PEDOT:PSS.[161] Weiss published the same year a follow up of their previous study, see Figure 1.20. The authors found that size-selective photoexcitation of the arrays of multiple sizes of QDs helped to determine (i) the location of the interface at which photoinduced separation of charge occurred, (ii) whether the energy absorbed by the QDs was redistributed before separation of charge, and (iii) the dependence of the photovoltage on the locations of various sizes of QDs within the junction.[162] More recently Weiss and co-workers managed to enhance the photocurrent density of the cross-linked QD films when the DAE (diarylethylene) ligand is switched from its open, non-conductive form (by illumination with 500-650 nm light), to its closed conductive form (by illumination with 300-400 nm light).

1.6.7 Stretchable Organic Solar Cells

Lipomi et al. designed and fabricated a stretchable organic solar cell by spin-coating the transparent electrode and active layer on a pre-strained elastomeric membrane. Upon
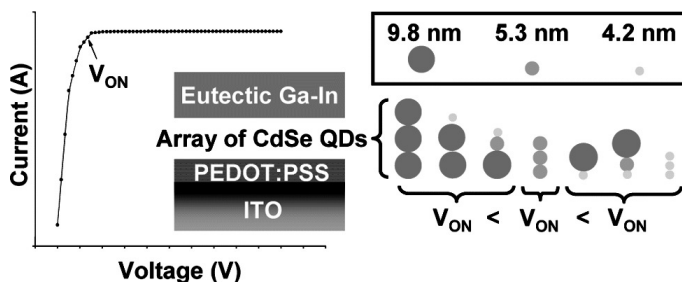
Figure 1.19: The TOC figure summaries the scientific work of Weiss and co-workers. The authors explore the electrical characteristics of junctions composed of three-dimensional arrays of colloidal CdSe quantum dots (QDs) with tin-doped indium oxide (ITO)/poly(3,4-ethylenedioxy-thiophene):poly(styrenesulfonate) (PEDOT:PSS) and EGaIn electrodes. "Reprinted with permission from reference[161]. Copyright 2008 American Chemical Society."
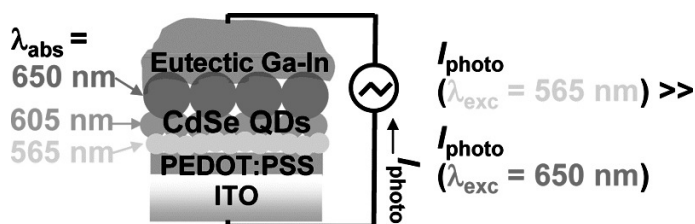
Figure 1.20: The TOC figure summaries the report of Weiss A. Emily and co-workers where they study the generation and flow of photocurrent through junctions containing three-dimensional arrays of colloidal CdSe quantum dots (QDs) of either a single size or multiple sizes. The electrodes were indium tin oxide (ITO) covered with a thin layer of poly(3,4-ethylenedioxy-thiophene):poly(styrenesulfonate) (PEDOT:PSS) and a eutectic alloy of Ga and In (EGaIn). "Reprinted with permission from reference[162]. Copyright 2008 American Chemical Society."

release of the pre-strain, the device buckled. The topographic waves that arose imparted elasticity to the device under tensile strain (up to 27%). The device exhibited similar photovoltaic properties when both stretched and unstretched. The device preparation is shown in Figure 1.21. The EGaIn in this case is used as top electrode. The photovoltaics properties of the OPV are worst then rigid solar cells, *i.e.*, using ITO, however the authors found that the device maintain good efficiencies when stretched.[129] The topic has been reviewed shortly after by Lipomi and Bao.[127]
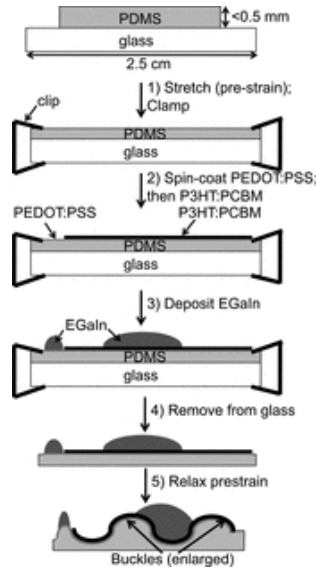
Figure 1.21: Summary of the procedures used to fabricate stretchable organic solar cells. "Reprinted with permission from reference[129]. Copyright 2011 Wiley."

1.6.8 Liquid Metal Microstructure

The ability to pattern materials into arbitrary 3D microstructures is important for electronics, microfluidic networks, tissue engineering scaffolds, photonic band gap structures, and chemical synthesis. Dickey and co-workers demonstrate that it is possible to direct write structures composed of a low-viscosity liquid with metallic conductivity at room temperature. The liquid metal is useful for soft, stretchable, or shape reconfigurable electronics. Some photographs of direct writing with EGaIn are shown in Figure 1.22.[163]
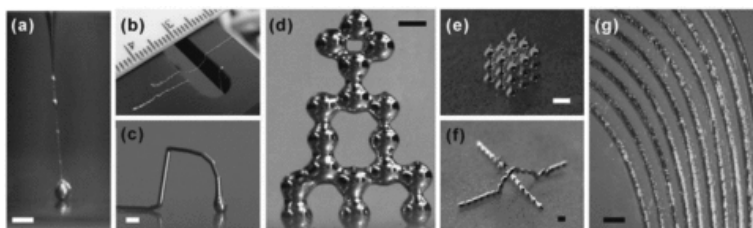
Figure 1.22: Direct writing of liquid metal 3D structures. Photographs of the diverse free standing, liquid metal microstructures that can be direct printed at room temperature. **a)** Liquid metal ejected rapidly from a glass capillary forms a thin wire. **b)** These fibers are strong enough to suspend over a gap despite being composed of liquid. **c)** A free standing liquid metal arch. **d)** A tower of liquid metal droplets. **e)** A 3D cubic array of stacked droplets. **f)** A metal wire and an arch composed of liquid metal droplets. **g)** An array of in-plane lines of free standing liquid metal fabricated by filling a microchannel with the metal and dissolving away the mold. Scale bars represent 500 μm. "Reprinted with permission from reference [163]. Copyright 2013 Wiley."

1.6.9 Soft-Matter Diodes

So et al. presented a soft-matter-based diode composed of hydrogel and EGaIn. The ability to control the thickness, and thus resistivity, of an oxide skin on the metal enables rectification. The authors describe a device with liquid-metal/electrolyte-solution/Pt architecture. The electrically insulating oxide skin on the EGaIn electrode is reduced or oxidized further depending on the direction of the bias, thereby allowing unidirectional ionic current. The forward current of the diode increases as the conductivity of the electrolyte increases, whereas backward current depends on the pH of the medium in contact with the insulating oxide layer on the EGaIn electrode. As a result, the diode shows a higher rectification ratio with more conductive electrolyte at neutral pH. Replacement of the liquid electrolyte solution with a hydrogel improves the structural stability of the soft diode. The rectification performance also improves due to the increased ionic conductivity by the gel. The authors also studied a diode entirely made of soft materials, see Figure 1.23, by replacing the platinum electrode with a second liquid-metal electrode. Contacting each liquid metal with a polyelectrolyte gel featuring different pH values provided asymmetry in the device, which is necessary for rectification. [136]
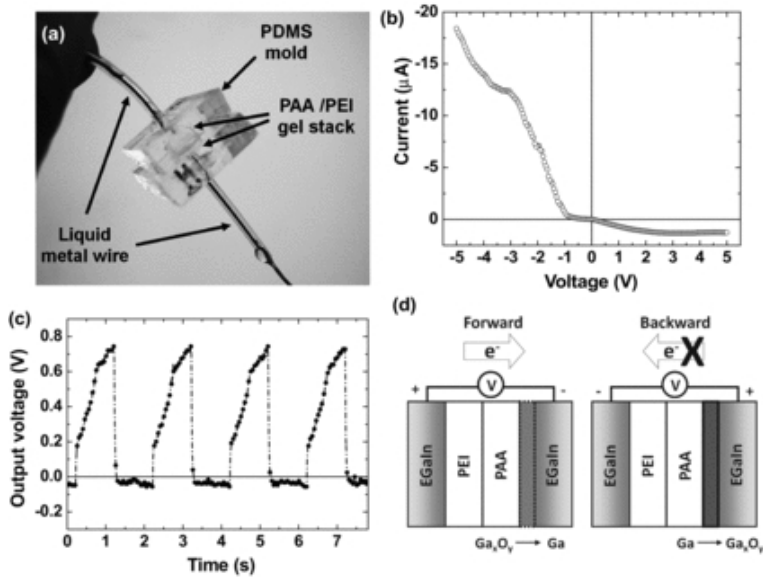
Figure 1.23: **a)** Photograph of a prototype diode composed entirely of soft matter. **b)** Current as a function of applied voltage and **c)** Transient voltage response under AC signal of the soft-matter diode. The EGaIn electrode interfacing the PEI gel is grounded. The output voltage is the voltage applied to the diode under AC bias with amplitude of ± 3 V. **d)** A schematic depiction of the soft-matter diode with asymmetrically configured polyelectrolyte gels under forward and backward biases. "Reprinted with permission from reference[136]. Copyright 2011 Wiley."

1.6.10 Microfluidics Devices

As mentioned before EGaIn can be confined into microchannels and can be used for free standing 3D structures. Dickey and co-workers showed interesting applications where EGaIn is used as strained-controlled diffraction, [145] a pressure responsive resonator, [164] and a reconfigurable circuits formed by liquid metal shaping. [165]

Overall EGaIn was used in several devices, in laboratories across the world. Despite the utility of EGaIn being uncovered only in the last 5 years, many scientific reports have been produced, and I'm certain many more are on their way.

1.7 Thesis Outline

In this thesis, several SAMs based MJ are presented. I used EGaIn as top electrode to make electrical contact with the different monolayers to characterize the electrical properties. In Chapter 2 we looked at the effect of conjugation pattern in dense monolayer or arylethynylene thiolates. Three different SAMs are discuss, anthracene AC (fully conjugated), anthraquinone AQ (cross conjugated), and dihydroanthracene AH (broken conjugated). We observed an excellent agreement between large area charge transport measurement and the single molecule transport calculation, which allowed us to conclude that destructive interference occurs (Quantum Interference) in such device. In Chapter 3 I measure, in a similar manner, two almost equivalent series of molecules which form dense and robust SAMs. Thanks to the information already present in literature about these molecules, we could investigate the electrical properties and correlate the observable transition voltages, V_{trans}, to the calculated HOMO level and to the shift in work function $\Delta\Phi$. The fact that two almost identical series, that differ only by one atom, can be quickly distinguished was up to now far from being obvious. In Chapter 4 I looked at a plausible substitute in ME to thiols as anchoring group to metal surfaces. I found that terminal alkynes can form very good SAMs, which can be measured with EGaIn and have comparable density with n-alkanethiolates. A further comparison between gold and silver as bottom electrode is presented. In Chapter 5 we looked at self-assembly

properties of double-stranded DNA in mixed SAMs. We extensively characterized our monolayers with a combination of Quartz Crystal Microbalance (QCM), IR, AFM and charge transport properties using EGaIn. Not only have we developed a method to make dense solid state junction comprising ds-DNA but we were able to distinguish DNA of different length.

Bibliography

[1] S. W. Herwald and S. J. Angello. Integration of circuit functions into solids. *Science*, 132(1127), 1960.

[2] G. E. Moore. Cramming more components onto integrated circuits. *Electronics*, 38(8), 1965.

[3] A. Aviram and M. A. Ratner. Molecular rectifiers. *Chem. Phys. Lett.*, 29(2):277–283, November 1974.

[4] H. Akamatu, H. Inokuchi, and Y. Matsunaga. Electrical conductivity of the perylene-bromine complex. *Nature*, 173:168–169, January 1954.

[5] Y. Okamoto and W. Brenner. *Organic Semiconductors*. Rheinhold, 1964.

[6] H. Naarmann. *Polymers, Electrically Conducting*. Wiley-VCH, Weinheim, 2002.

[7] H. Shirakawa, E. J. Louis, A. G MacDiarmid, C. K. Chiang, and A. J. Heeger. Synthesis of electrically conducting organic polymers: halogen derivatives of polyacetylene, $(CH)_x$. *J. Chem. Soc. Chem. Commun.*, (16):578, 1977.

[8] C. Chiang, C. Fincher, Y. Park, A. J. Heeger, H. Shirakawa, E. Louis, S. Gau, and A. G. MacDiarmid. Electrical Conductivity in Doped Polyacetylene. *Phys. Rev. Lett.*, 39(17):1098–1101, October 1977.

[9] A. Vilan and D. Cahen. How organic molecules can control electronic devices. *Trends Biotechnol.*, 20(1):22–29, 2002.

[10] en.wikipedia.org/wiki/14nanometer.

[11] B. Mann. Tunneling through Fatty Acid Salt Monolayers. *J. Appl. Phys.*, 42(11):4398, 1971.

[12] S. L. Bernasek. Can We Understand the Molecule in Molecular Electronics? *Angew. Chem.*, 51(39):9737–9738, August 2012.

[13] R. F. Service. MOLECULAR ELECTRONICS: Next-Generation Technology Hits an Early Midlife Crisis. *Science*, 302(5645):556–559, October 2003.

[14] V. B. Engelkes, J. M. Beebe, and C. D. Frisbie. Analysis of the causes of variance in resistance measurements on metal–molecule–metal junctions formed by conducting-probe atomic force microscopy. *J. Phys. Chem. B*, 109(35):16801–16810, 2005.

[15] H. B. Akkerman, P. W. M. Blom, Dago M. de Leeuw, and B. de Boer. Towards molecular electronics with large-area molecular junctions. *Nature*, 441(7089):69–72, May 2006.

[16] A. Carlson, A. M. Bowen, Y. Huang, R. G. Nuzzo, and J. A. Rogers. Transfer Printing Techniques for Materials Assembly and Micro/Nanodevice Fabrication. *Adv. Mater.*, 24(39):5284–5318, 2012.

[17] W. Y. Wang, T. Lee, and M. A. Reed. Mechanism of Electron Conduction in Self-Assembled Alkanethiol Monolayer Devices. *Phys. Rev. B*, 68(3):035416–1–035416–7, 2003.

[18] J. G. Kushmerick, J. Naciri, J. C. Yang, and R. Shashidhar. Conductance Scaling of Molecular Wires in Parallel. *Nano Lett.*, 3(7):897–900, July 2003.

[19] J. Liao, L. Bernard, M. Langer, C. Schönenberger, and M. Calame. Reversible Formation of Molecular Junctions in 2D Nanoparticle Arrays. *Adv. Mater.*, 18(18):2444–2447, September 2006.

[20] K. Slowinski, H. K. Y. Fong, and M. Majda. MercuryMercury Tunneling Junctions. 1. Electron Tunneling Across Symmetric and Asymmetric Alkanethiolate Bilayers. *J. Am. Chem. Soc.*, 121(31):7257–7261, August 1999.

[21] M. D. Dickey, R. C. Chiechi, R. J. Larsen, E. A. Weiss, D. A. Weitz, and G. M. Whitesides. Eutectic Gallium-Indium (EGaIn): A Liquid Metal Alloy for the Formation of Stable Structures in Microchannels at Room Temperature. *Adv. Funct. Mater.*, 18(7):1097–1104, April 2008.

[22] J. C. Love, L. A. Estroff, J. K. Kriebel, R. G. Nuzzo, and G. M. Whitesides. Self-assembled monolayers of thiolates on metals as a form of nanotechnology. *Chem. Rev.*, 105(4):1103–1170, 2005.

[23] A. Salomon, D. Cahen, S. Lindsay, J. Tomfohr, V. B. Engelkes, and C. D. Frisbie. Comparison of electronic transport measurements on organic molecules. *Adv. Mater.*, 15(22):1881–1890, 2003.

[24] F. Chen, J. Hihath, Z. Huang, X. Li, and N. J. Tao. Measurement of Single-Molecule Conductance. *Annu. Rev. Phys. Chem.*, 58(1):535–564, May 2007.

[25] S. M. Lindsay and M. A. Ratner. Molecular Transport Junctions: Clearing Mists. *Adv. Mater.*, 19(1):23–31, January 2007.

[26] N. J. Tao. Electron transport in molecular junctions. *Nature*, 1(3):173–181, December 2006.

[27] G. C. Solomon, A. Gagliardi, A. Pecchia, T. Frauenheim, A. Di Carlo, J. R. Reimers, and N. S. Hush. Understanding the inelastic electron-tunneling spectra of alkanedithiols on gold. *J. Chem. Phys.*, 124(9):094704–094704–10, 2006.

[28] G. M. Whitesides and M. Boncheva. Beyond molecules: Self-assembly of mesoscopic and macroscopic components. *Proc. Nat. Acad. Sci. USA*, 99(8):4769–4774, 2002.

[29] S. Zhang. Fabrication of novel biomaterials through molecular self-assembly. *Nature Biotechnol.*, 21(10):1171–1178, October 2003.

[30] B. C. Haynie, A. V. Walker, T. B. Tighe, D. L. Allara, and N. Winograd. Adventures in molecular electronics: how to attach wires to molecules. *Appl. Surf. Sci.*, 203-204:433–436, January 2003.

[31] B. de Boer, M. M Frank, Y. J. Chabal, W. Jiang, E. Garfunkel, and Z. Bao. Metallic Contact Formation for Molecular Electronics: Interactions between Vapor-Deposited Metals and Self-Assembled Monolayers of Conjugated Mono- and Dithiols. *Langmuir*, 20(5):1539–1542, March 2004.

[32] H. Haick, J. Ghabboun, and D. Cahen. Pd versus Au as evaporated metal contacts to molecules. *Appl. Phys. Lett.*, 86(4):042113–042113–3, 2005.

[33] P. E. Laibinis, G. M. Whitesides, D. L. Allara, Y. T. Tao, A. N. Parikh, and R. G. Nuzzo. Comparison of the structures and wetting properties of self-assembled monolayers of n-alkanethiols on the coinage metal surfaces, copper, silver, and gold. *J. Am. Chem. Soc.*, 113(19):7152–7167, September 1991.

[34] J. P. Bucher, L. Santesson, and K. Kern. Thermal Healing of Self-Assembled Organic Monolayers: Hexane- and Octadecanethiol on Au(111) and Ag(111). *Langmuir*, 10(4):979–983, April 1994.

[35] A. Dhirani, M. A. Hines, A. J. Fisher, O. Ismail, and P. Guyot-Sionnest. Structure of Self-Assembled Decanethiol on Ag(111): A Molecular Resolution Scanning Tunneling Microscopy Study. *Langmuir*, 11(7):2609–2614, July 1995.

[36] R. Yamada, H. Wano, and K. Uosaki. Effect of temperature on structure of the self-assembled monolayer of decanethiol on Au(111) surface. *Langmuir*, 16(13):5523–5525, 2000.

[37] G. Gannon, J. C. Greer, J. A. Larsson, and D. Thompson. Molecular Dynamics Study of Naturally Occurring Defects in Self-Assembled Monolayer Formation. *ACS Nano*, 4(2):921–932, February 2010.

[38] P. Wagner, M. Hegner, H. J. Guentherodt, and G. Semenza. Formation and in Situ Modification of Monolayers Chemisorbed on Ultraflat Template-Stripped Gold Surfaces. *Langmuir*, 11(10):3867–3875, October 1995.

[39] J. S. Hsiao, B. P. Krueger, R. W. Wagner, T. E. Johnson, J. K. Delaney, D. C. Mauzerall, G. R. Fleming, J. S. Lindsey, D. F. Bocian, and R. J. Donohoe. Soluble Synthetic Multiporphyrin Arrays. 2. Photodynamics of Energy-Transfer Processes. *J. Am. Chem. Soc.*, 118(45):11181–11193, January 1996.

[40] J. Diebel, H. Löwe, P. Samorì, and J. P. Rabe. Fabrication of large-scale ultra-smooth metal surfaces by a replica technique. *Appl. Phys. A*, 73(3):273–279, September 2001.

[41] K. Unal, B. r.-O. Aronsson, Ya. Mugnier, and P. Descouts. Nano-oxidation of titanium films with large atomically flat surfaces by means of voltage-modulated scanning probe microscopy. *Surf. Interface Anal.*, 34(1):490–493, 2002.

[42] R. Naumann, S. M. Schiller, F. Giess, B. Grohe, K. B. Hartman, I. Kärcher, I. Köper, J. Lübben, K. Vasilev, and W. Knoll. Tethered Lipid Bilayers on Ultraflat Gold Surfaces. *Langmuir*, 19(13):5435–5443, June 2003.

[43] R. Ragan, D. Ohlberg, J. J. Blackstock, S. Kim, and R. S. Williams. Atomic Surface Structure of UHV-Prepared Template-Stripped Platinum and Single-Crystal Platinum(111). *J. Phys. Chem. B*, 108(52):20187–20192, December 2004.

[44] D. Zhou, A. Bruckbauer, M. Batchelor, D. J. Kang, C. Abell, and D. Klenerman. Influence of the Foundation Layer on the Layer-by-Layer Assembly of Poly- l-lysine and Poly(styrenesulfonate) and Its Usage in the Fabrication of 3D Microscale Features. *Langmuir*, 20(21):9089–9094, October 2004.

[45] L. He, J. W. F. Robertson, J. Li, I. Kärcher, S. M. Schiller, W. Knoll, and R. Naumann. Tethered Bilayer Lipid Membranes Based on Monolayers of Thiolipids Mixed with a Complementary Dilution Molecule. 1. Incorporation of Channel Peptides. *Langmuir*, 21(25):11666–11672, December 2005.

[46] E. A. Weiss, G. K. Kaufman, J. K. Kriebel, L. Li, R. Schalek, and G. M. Whitesides. Si/SiO$_2$-Templated formation of ultraflat metal surfaces on glass, polymer, and solder supports: Their use as substrates for Self-Assembled monolayers. *Langmuir*, 23(19):9686–9694, 2007.

[47] S. Borukhin and B. Pokroy. Formation and Elimination of Surface Nanodefects on Ultraflat Metal Surfaces Produced by Template Stripping. *Langmuir*, 27(22):13415–13419, 2011.

[48] E. A. Weiss, Chiechi R. C., Kaufman G. K., Kriebel J. K., Li Z., Duati M., Rampi M. A., and Whitesides G. M. Influence of defects on the electrical characteristics of Mercury-Drop junctions: Self-Assembled monolayers of n-Alkanethiolates on rough and smooth silver. *J. Am. Chem. Soc.*, 129(14):4336–4349, April 2007.

[49] J. A. DeRose, T. Thundat, L. A. Nagahara, and S. M. Lindsay. Gold grown epitaxially on mica: conditions for large area flat faces. *Surf. Sci.*, 256(1-2):102–108, 1991.

[50] D. Fracasso, H. Valkenier, J. C. Hummelen, G. C. Solomon, and Ryan C. Chiechi. Evidence for Quantum Interference in SAMs of Arylethynylene Thiolates in Tunneling Junctions with Eutectic Ga-In (EGaIn) Top-Contacts. *J. Am. Chem. Soc.*, 133(24):9556–9563, May 2011.

[51] G. M. Whitesides and P. E. Laibinis. Wet chemical approaches to the characterization of organic surfaces: self-assembled monolayers, wetting, and the physical-organic chemistry of the solid-liquid interface. *Langmuir*, 6(1):87–96, January 1990.

[52] L. H. Dubois and R.G. Nuzzo. Synthesis, Structure, and Properties of Model Organic Surfaces. *Annu. Rev. Phys. Chem.*, 43(1):437–463, October 1992.

[53] A. Ulman. Formation and Structure of Self-Assembled Monolayers. *Chem. Rev.*, 96(4):1533–1554, January 1996.

[54] J. Kondo. Resistance Minimum in Dilute Magnetic Alloys. *Prog. Theor. Phys.*, 32(1):37–49, July 1964.

[55] P. Chinwangso, A. C. Jamison, and T. R. Lee. Multidentate Adsorbates for Self-Assembled Monolayer Films. *Accounts of Chemical Research*, 44(7):511–519, July 2011.

[56] T.-C. Lee, D. J. Hounihan, R. Colorado, J.-S. Park, and T. R. Lee. Stability of aliphatic dithio-carboxylic acid self-assembled monolayers on gold. *J. Phys. Chem. B*, 108(8):2648–2653, 2004.

[57] Y.-S. Shon, S. Lee, R. Colorado, S. S. Perry, and T. R. Lee. Spiroalkanedithiol-Based SAMs Reveal Unique Insight into the Wettabilities and Frictional Properties of Organic Thin Films. *Journal of the American Chemical Society*, 122(31):7556–7563, August 2000.

[58] R. Colorado, R. J. Villazana, and T. R. Lee. Self-Assembled Monolayers on Gold Generated from Aliphatic Dithiocarboxylic Acids. *Langmuir*, 14(22):6337–6340, October 1998.

[59] Y. Selzer, A. Salomon, and D. Cahen. The Importance of Chemical Bonding to the Contact for Tunneling through Alkyl Chains. *J. Phys. Chem. B*, 106(40):10432–10439, October 2002.

[60] B. Xu and Tao N. J. Measurement of Single-Molecule resistance by repeated formation of molecular junctions. *Science*, 301(5637):1221 –1223, 2003.

[61] H. J. Yoon, N. D. Shapiro, K. M. Park, M. M. Thuo, S. Soh, and G. M. Whitesides. The rate of charge tunneling through self-assembled monolayers is insensitive to many functional group substitutions. *Angew. Chem.*, 51(19):4658–4661, May 2012.

[62] J. Jortner. Temperature dependent activation energy for electron transfer between biological molecules. *J. Chem. Phys.*, 64(12):4860–4867, 1976.

[63] R. A. Marcus and N. Sutin. Electron transfers in chemistry and biology. *Biochim. Biophys. Acta*, 811(3):265–322, August 1985.

[64] S. Datta. *Electronic transport in mesoscopic systems.* Cambrige University Press, 1995.

[65] S. Datta. *Electronic transport in mesoscopic systems.* Cambrige University Press, 2001.

[66] S. Datta. *Quantum transport: atom to transistor.* Cambrige University Press, 2005.

[67] E. Emberly and G. Kirczenow. Landauer theory, inelastic scattering, and electron transport in molecular wires. *Phys. Rev. B*, 61(8):5740–5750, February 2000.

[68] T. Seideman and H. Guo. Quantum transport and current-triggered dynamics in molecular tunnel junctions. *J. Theor. Comput. Chem.*, 02(03):439–458, September 2003.

[69] A. Troisi and M. A. Ratner. *Molecular nanoelectronics*, volume 1. American Scientific Publishers, Stevenson Ranch, CA, 2003.

[70] R. Liu, S.-H. Ke, H. U. Baranger, and W. Yang. Intermolecular effect in molecular electronics. *J. Chem. Phys.*, 122(4):044703–044703–4, 2005.

[71] H. A. Kramers. L'interaction Entre les Atomes Magnétogènes dans un Cristal Paramagnétique. *Physica*, 1(1-6):182–192, January 1934.

[72] P. Anderson. Antiferromagnetism. Theory of Superexchange Interaction. *Phys. Rev.*, 79(2):350–356, July 1950.

[73] R. A. Marcus. On the Theory of Electron-Transfer Reactions. VI. Unified Treatment for Homogeneous and Electrode Reactions. *J. Chem. Phys.*, 43(2):679–701, 1965.

[74] J. G. Simmons. Generalized formula for the electric tunnel effect between similar electrodes separated by a thin insulating film. *J. Appl. Phys.*, 1963.

[75] V. B. Engelkes, J. M. Beebe, and C. D. Frisbie. Length-Dependent Transport in Molecular Junctions Based on SAMs of Alkanethiols and Alkanedithiols: Effect of Metal Work Function and Applied Bias on Tunneling Efficiency and Contact Resistance. *J. Am. Chem. Soc.*, 126(43):14287–14296, November 2004.

[76] H. B. Akkerman and B. de Boer. Electrical conduction through single molecules and self-assembled monolayers. *J. Phys.: Condens. Physics*, 20:013001–013021, December 2007.

[77] X. D. Cui, A. Primak, X. Zarate, J. Tomfohr, O. F. Sankey, A. L. Moore, T. A. Moore, D. Gust, L. A. Nagahara, and S. M. Lindsay. Changes in the Electronic Properties of a Molecule When It Is Wired into a Circuit. *J. Phys. Chem. B*, 106(34):8609–8614, August 2002.

[78] R. L. York and K. Slowinski. Tunneling conductivity of one- and two-component alkanethiol bilayers in Hg-Hg junctions. *J. Electroanal. Chem.*, 550-551:327–336, July 2003.

[79] T. Lee, W. Wang, J. F. Klemic, J. J. Zhang, J. Su, and M. A. Reed. Comparison of Electronic Transport Characterization Methods for Alkanethiol Self-Assembled Monolayers . *J. Phys. Chem. B*, 108(25):8742–8750, June 2004.

[80] M. M. Thuo, W. F. Reus, C. A. Nijhuis, J. R. Barber, C. Kim, M. D. Schulz, and G. M. Whitesides. Odd-even effects in charge transport across self-assembled monolayers. *J. Am. Chem. Soc.*, 133(9):2962–2975, 2011.

[81] A. Nitzan. Electron transmission through molecules and molecular interfaces. *Audio, Transactions of the IRE Professional Group on*, 52(1):681–750, 2001.

[82] E. B. Troughton, C. D. Bain, G. M. Whitesides, R. G. Nuzzo, D. L. Allara, and M. D. Porter. Monolayer films prepared by the spontaneous self-assembly of symmetrical and unsymmetrical dialkyl sulfides from solution onto gold substrates: structure, properties, and reactivity of constituent functional groups. *Langmuir*, 4(2):365–385, March 1988.

[83] C. D. Bain, E. B. Troughton, Y. T. Tao, J. Evall, G. M. Whitesides, and R. G. Nuzzo. Formation of monolayer films by the spontaneous assembly of organic thiols from solution onto gold. *J. Am. Chem. Soc.*, 111(1):321–335, January 1989.

[84] C. D Bain and G. M. Whitesides. Formation of monolayers by the coadsorption of thiols on gold: variation in the length of the alkyl chain. *J. Am. Chem. Soc.*, 111(18):7164–7175, August 1989.

[85] M. A. Reed, C. Zhou, C. J. Muller, T. P. Burgin, and J. M. Tour. Conductance of a molecular junction. *Science*, 278(5336):252–254, 1997.

[86] D. J. Wold and C. D. Frisbie. Fabrication and characterization of metal-molecule-metal junctions by conducting probe atomic force microscopy. *J. Am. Chem. Soc.*, 123(23):5549–5556, January 2001.

[87] L. A. Bumm, J. J. Arnold, T. D. Dunbar, D. L. Allara, and P. S. Weiss. Electron Transfer through Organic Molecules. *J. Phys. Chem. B*, 103(38):8122–8127, September 1999.

[88] R. E. Holmlin, R. F. Ismagilov, R. Haag, V. Mujica, M. A. Ratner, M. A. Rampi, and G. M. Whitesides. Correlating electron transport and molecular structure in organic thin films. *Angew. Chem.*, 40(12):2316, 2001.

[89] R. E. Holmlin, R. Haag, M. L. Chabinyc, R. F. Ismagilov, A. E. Cohen, A. Terfort, M. A. Rampi, and Whitesides G. M. Electron transport through thin organic films in Metal-Insulator-Metal junctions based on Self-Assembled monolayers. *J. Am. Chem. Soc.*, 123(21):5075–5085, 2001.

[90] J. M. Beebe, V. B. Engelkes, L. L. Miller, and C. D. Frisbie. Contact Resistance in Metal–Molecule–Metal Junctions Based on Aliphatic SAMs: Effects of Surface Linker and Metal Work Function. *J. Am. Chem. Soc.*, 124(38):11268–11269, September 2002.

[91] M. A. Rampi and G. M. Whitesides. A versatile experimental approach for understanding electron transport through organic materials. *Chem. Phys.*, 281(2-3):373–391, August 2002.

[92] D. J. Wold, R. Haag, M. A. Rampi, and C. D. Frisbie. Distance dependence of electron tunneling through self-assembled monolayers measured by conducting probe atomic force microscopy: Unsaturated versus saturated molecular junctions. *J. Phys. Chem. B*, 106(11):2813 – 2816, 2002.

[93] J. C. Love, D. B Wolfe, R. Haasch, M. L. Chabinyc, K. E. Paul, G. M. Whitesides, and R. G. Nuzzo. Formation and Structure of Self-Assembled Monolayers of Alkanethiolates on Palladium. *J. Am. Chem. Soc.*, 125(9):2597–2609, 2003.

[94] E. Tran, M. A. Rampi, and G. M. Whitesides. Electron Transfer in a Hg-SAM//SAM-Hg Junction Mediated by Redox Centers. *Angew. Chem.*, 43(29):3835–3839, July 2004.

[95] E. Tran, C. Grave, G. M. Whitesides, and M. A. Rampi. Controlling the electron transfer mechanism in metal–molecules–metal junctions. *Electrochim. Acta*, 50(25-26):4850–4856, September 2005.

[96] M. Duati, C. Grave, N. Tcbeborateva, J. Wu, K. Müllen, A. Shaporenko, M. Zharnikov, J. K. Kriebel, G. M. Whitesides, and M. A. Rampi. Electron transport across hexa-peri-hexabenzocoronene units in a Metal–Self-Assembled Monolayer–Metal junction. *Adv. Mater.*, 18(3):329–333, 2006.

[97] S. Liao, Y. Shnidman, and A. Ulman. Adsorption Kinetics of Rigid 4-Mercaptobiphenyls on Gold. *J. Am. Chem. Soc.*, 122(15):3688–3694, April 2000.

[98] K. Heister, H. T. Rong, M. Buck, M. Zharnikov, M. Grunze, and L. S. O. Johansson. OddEven Effects at the S-Metal Interface and in the Aromatic Matrix of Biphenyl-Substituted Alkanethiol Self-Assembled Monolayers. *J. Phys. Chem. B*, 105(29):6888–6894, July 2001.

[99] T. Ishida, W. Mizutani, Y. Aya, H. Ogiso, S. Sasaki, and H. Tokumoto. Electrical Conduction of Conjugated Molecular SAMs Studied by Conductive Atomic Force Microscopy. *J. Phys. Chem. B*, 106(23):5886–5892, June 2002.

[100] F. Anariba and R. L. McCreery. Electronic Conductance Behavior of Carbon-Based Molecular Junctions with Conjugated Structures. *J. Phys. Chem. B*, 106(40):10355–10362, October 2002.

[101] J.-O. Lee, G. Lientschnig, F. G. H. Wiertz, M Struuijk, R. A. J. Janssen, R. Egberink, D. N. Reinhoudt, A. C. Grimsdale, K. Müllen, P. Hadley, and C. Dekkera. Electrical Transport Study of Phenylene-Based -Conjugated Molecules in a Three-Terminal Geometry. *Ann. N.Y. Acad. Sci.*, 1006(1):122–132, December 2003.

[102] R. L. McCreery. Molecular Electronic Junctions. *Chem. Mater.*, 16(23):4477–4496, November 2004.

[103] A. Shaporenko, K. Heister, A. Ulman, M. Grunze, and M. Zharnikov. The Effect of Halogen Substitution in Self-Assembled Monolayers of 4-Mercaptobiphenyls on Noble Metal Substrates. *J. Phys. Chem. B*, 109(9):4096–4103, March 2005.

[104] C. Kergueris, J. P. Bourgoin, S. Palacin, D. Esteve, C. Urbina, M. Magoga, and C. Joachim. Electron transport through a metal-molecule-metal junction. *Phys. Rev. B*, 59(19):12505–12513, May 1999.

[105] S. P. Dudek, H. D. Sikes, and C. E. D. Chidsey. Synthesis of Ferrocenethiols Containing Oligo(phenylenevinylene) Bridges and Their Characterization on Gold Electrodes. *J. Am. Chem. Soc.*, 123(33):8033–8038, August 2001.

[106] H. D. Sikes, J. F. Smalley, S. P. Dudek, A. R. Cook, M. D. Newton, C. E. D. Chidsey, and S. W. Feldberg. Rapid electron tunneling through oligophenylenevinylene bridges. *Science*, 291(5508):1519–1523, 2001.

[107] J. Reichert, R. Ochs, D. Beckmann, H. Weber, M. Mayor, and H. Löhneysen. Driving Current through Single Organic Molecules. *Phys. Rev. Lett.*, 88(17):176804, April 2002.

[108] G. Leatherman, E. N. Durantini, D. Gust, T. A. Moore, A. L. Moore, S. Stone, Z. Zhou, P. Rez, Y. Z. Liu, and S. M. Lindsay. Carotene as a Molecular Wire: Conducting Atomic Force Microscopy. *J. Phys. Chem. B*, 103(20):4006–4010, May 1999.

[109] G. K. Ramachandran, J. K. Tomfohr, J. Li, O. F. Sankey, X. Zarate, A. Primak, Y. Terazono, T. A. Moore, A. L. Moore, D. Gust, L. A. Nagahara, and S. M. Lindsay. Electron Transport Properties of a Carotene Molecule in a Metal(Single Molecule)Metal Junction. *J. Phys. Chem. B*, 107(25):6162–6169, June 2003.

[110] K. Slowinski, R. V. Chamberlain, R. Bilewicz, and M. Majda. Evidence for Inefficient Chain-to-Chain Coupling in Electron Tunneling through Liquid Alkanethiol Monolayer Films on Mercury. *J. Am. Chem. Soc.*, 118(19):4709–4710, January 1996.

[111] K. Slowinski, R. V. Chamberlain, C. J. Miller, and M. Majda. Through-Bond and Chain-to-Chain coupling. two pathways in electron tunneling through liquid alkanethiol monolayers on mercury electrodes. *J. Am. Chem. Soc.*, 119(49):11910–11919, December 1997.

[112] M. A. Rampi, O. J. A. Schueller, and G. M. Whitesides. Alkanethiol self-assembled monolayers as the dielectric of capacitors with nanoscale thickness. *Appl. Phys. Lett.*, 72(14):1781–1783, 1998.

[113] K. Slowinski, K. U. Slowinska, and M. Majda. Electron tunneling across hexadecanethiolate monolayers on mercury electrodes: reorganization energy, structure, and permeability of the alkane/water interface. *J. Phys. Chem. B*, 103(40):8544–8551, 1999.

[114] R. L. York, P. T. Nguyen, and K. Slowinski. Long-Range Electron Transfer through Monolayers and Bilayers of Alkanethiols in Electrochemically Controlled Hg-Hg Tunneling Junctions. *J. Am. Chem. Soc.*, 125(19):5948–5953, May 2003.

[115] E. Tran, A. E. Cohen, R. W. Murray, M. A. Rampi, and G. M. Whitesides. Redox Site-Mediated Charge Transport in a Hg–SAM//Ru(NH$_3$)$_6$$^{3+/2+}$//SAM–Hg Junction with a Dynamic Interelectrode Separation: Compatibility with Redox Cycling and Electron Hopping Mechanisms. *J. Am. Chem. Soc.*, 131(6):2141–2150, 2009.

[116] S. Frey, V. Stadler, K. Heister, W. Eck, M. Zharnikov, M. Grunze, B. Zeysing, and A. Terfort. Structure of Thioaromatic Self-Assembled Monolayers on Gold and Silver. *Langmuir*, 17(8):2408–2415, April 2001.

[117] S. J. French, D. J. Saunders, and G. W. Ingle. The system gallium-indium. *J. Phys. Chem.*, 42(2):265–274, 1938.

[118] D. Zrnic and D. S. Swatik. On the resistivity and surface tension of the eutectic alloy of gallium and indium. *J. Less Common Met.*, 18(1):67–68, May 1969.

[119] E. J. Lous, P. W. M. Blom, L. W. Molenkamp, and D. M. de Leeuw. Formation of a Schottky barrier between eutectic Ga,In and thiophene oligomers. *J. Appl. Phys.*, 81(8):3537–3542, 1997.

[120] A. D. Pasquier, S. Miller, and M. Chhowalla. On the use of Ga–In eutectic and halogen light source for testing P3HT–PCBM organic solar cells. *Sol. Energy Mater. Sol. Cells*, 90(12):1828–1839, July 2006.

[121] C. P. Rhodes, J. W. Long, M. S. Doescher, J. J. Fontanella, and D. R. Rolison. Nanoscale Polymer Electrolytes: Ultrathin Electrodeposited Poly(Phenylene Oxide) with Solid-State Ionic Conductivity. *J. Phys. Chem. B*, 108(35):13079–13087, September 2004.

[122] J. Wang, S. Liu, Z. V. Vardeny, and A. Nahata. Liquid metal-based plasmonics. *Opt. Express*, 20(3):2346–2353, 2012.

[123] E. A Weiss, J. K. Kriebel, M. A. Rampi, and G. M. Whitesides. The study of charge transport through organic thin films: mechanism, tools and applications. *Phil. Trans. R. Soc. A*, 365(1855):1509–1537, 2007.

[124] C. A. Nijhuis, W. F. Reus, and G. M. Whitesides. Mechanism of rectification in tunneling junctions based on molecules with asymmetric potential drops. *J. Am. Chem. Soc.*, 132(51):18386–18401, 2010.

[125] C. A. Nijhuis, W. F. Reus, and G. M. Whitesides. Molecular rectification in Metal-SAM-Metal Oxide-Metal junctions. *J. Am. Chem. Soc.*, 131(49):17814–17827, December 2009.

[126] A. C. Siegel, S. K. Y. Tang, C. A. Nijhuis, M. Hashimoto, S. T. Phillips, M. D. Dickey, and Whitesides G. M. Cofabrication: A strategy for building multicomponent microsystems. *Acc. Chem. Res.*, 43(4):518–528, April 2010.

[127] D. J. Lipomi and Z. Bao. Stretchable, elastic materials and devices for solar energy conversion. *Energy Enviro. Sci.*, 4(9):3314–3328, 2011.

[128] G. D. Lilly, A. C. Whalley, S. Grunder, C. Valente, M. T. Frederick, J. F. Stoddart, and E. A. Weiss. Switchable photoconductivity of quantum dot films using cross-linking ligands with light-sensitive structures. *J. Mater. Chem.*, 21(31):11492–11497, 2011.

[129] D. J. Lipomi, B. C. K. Tee, M. Vosgueritchian, and Z. Bao. Stretchable Organic Solar Cells. *Adv. Mater.*, 23(15):1771–1775, February 2011.

[130] M. M. Thuo, W. F. Reus, C. A. Nijhuis, J. R. Barber, C. Kim, M. D. Schulz, and G. M. Whitesides. Odd–even effects in charge transport across self-assembled monolayers. *J. Am. Chem. Soc.*, 133(9):2962–2975, March 2011.

[131] C. A. Nijhuis, W. F. Reus, A. C. Siegel, and G. M. Whitesides. A molecular half–wave rectifier. *J. Am. Chem. Soc.*, 133(39):15397–15411, August 2011.

[132] C. A. Nijhuis, W. F. Reus, and G. M. Whitesides. Mechanism of Rectification in Tunneling Junctions Based on Molecules with Asymmetric Potential Drops. *J. Am. Chem. Soc.*, 132(51):18386–18401, December 2010.

[133] K. S. Wimbush, W. F. Reus, W. G. van der Wiel, D. N. Reinhoudt, G. M. Whitesides, C. A. Nijhuis, and A. H. Velders. Control over Rectification in Supramolecular Tunneling Junctions. *Angew. Chem.*, 49(52):10176–10180, November 2010.

[134] C. A. Nijhuis, W. F. Reus, J. R. Barber, and G. M. Whitesides. Comparison of SAM-based junctions with Ga_2O_3/EGaIn top electrodes to other large-area tunneling junctions. *J. Phys. Chem. C*, 116(26):14139–14150, 2012.

[135] J. N. Hohman, M. Kim, G. A. Wadsworth, H. R. Bednar, J. Jiang, M. A. LeThai, and P. S. Weiss. Directing Substrate Morphology via Self-Assembly: Ligand-Mediated Scission of Gallium–Indium Microspheres to the Nanoscale. *Nano Letters*, 11(12):5104–5110, 2011.

[136] J.-H. So, H.-J. Koo, M. D. Dickey, and O. D. Velev. Ionic Current Rectification in Soft-Matter Diodes with Liquid-Metal Electrodes. *Adv. Funct. Mater.*, 22(3):625–631, 2011.

[137] G. J. Hayes, J. H. So, and A. Qusba. Flexible Liquid Metal Alloy (EGaIn) Microstrip Patch Antenna. *IEEE Antennas and Propagation Society*, 2012.

[138] M. M. Thuo, W. F. Reus, F. C. Simeone, C. Kim, M. D. Schulz, H. J. Yoon, and G. M. Whitesides. Replacing -CH_2CH_2- with -CONH- Does Not Significantly Change Rates of Charge Transport through Ag TS-SAM//Ga_2O_3/EGaIn Junctions. *J. Am. Chem. Soc.*, 134(26):10876–10884, July 2012.

[139] W. F. Reus, C. A. Nijhuis, J. R. Barber, M. M. Thuo, S. Tricard, and G. M. Whitesides. Statistical Tools for Analyzing Measurements of Charge Transport. *J. Phys. Chem. C*, 116(11):6714–6733, 2012.

[140] H. L. Filiatrault, G. C. Porteous, R. S. Carmichael, G. J. E. Davidson, and T. Breen. Carmichael. Stretchable Light-Emitting Electrochemical Cells Using an Elastomeric Emissive Material. *Adv. Mater.*, 24(20):2673–2678, March 2012.

[141] L. Cademartiri, M. M. Thuo, C. A. Nijhuis, W. F. Reus, S. Tricard, J. R. Barber, R. N. S. Sodhi, P. Brodersen, C. Kim, R. C. Chiechi, and G. M. Whitesides. Electrical Resistance of Ag TS–S$(CH_2)_{n-1}CH_3$//Ga_2O_3/EGaIn Tunneling Junctions. *J. Phys. Chem. C*, 116(20):10848–10860, May 2012.

[142] G. M. Lazzerini, S. Mian, F. Di Stasio, A. Merari Masillamani, N. Crivillers, F. Reinders, M. Mayor, P Samorì, and F. Cacialli. Increased efficiency of light-emitting diodes incorporating anodes functionalized with fluorinated azobenzene monolayers and a green-emitting polyfluorene derivative. *Appl. Phys. Lett.*, 101(15):153306, 2012.

[143] A. M. Masillamani, N. Crivillers, E. Orgiu, J. Rotzler, D. Bossert, R. Thippeswamy, M. Zharnikov, M. Mayor, and P. Samorì. Multiscale Charge Injection and Transport Properties in Self-Assembled Monolayers of Biphenyl Thiols with Varying Torsion Angles. *Chem. Eur. J.*, 18(33):10335–10347, July 2012.

[144] J. Park, S. Wang, M. Li, C. Ahn, J. K. Hyun, D. S. Kim, J. A. Rogers, Y. Huang, and S. Jeon. Three-dimensional nanonetworks for giant stretchability in dielectrics and conductors. *Nat. Comms*, 3:916, 2012.

[145] M. G. Mohammed and M. D. Dickey. Strain-controlled diffraction of light from stretchable liquid metal micro-components. *Sensors and Actuators A: Physical*, 2013.

[146] N. Nerngchamnong, L. Yuan, D.-C. Qi, J. Li, D. Thompson, and C. A. Nijhuis. The role of van der Waals forces in the performance of molecular diodes. *Nat. Nanotechnol.*, pages –, January 2013.

[147] D. Fracasso, M. I. Muglali, M. Rohwerder, A. Terfort, and R. C. Chiechi. Influence of an Atom in EGaIn/Ga$_2$O$_3$Tunneling Junctions Comprising Self-Assembled Monolayers. *The Journal of Physical Chemistry C*, 117(21):11367–11376, May 2013.

[148] C. A. Nijhuis, W. F. Reus, J. R. Barber, M. D. Dickey, and G. M. Whitesides. Charge transport and rectification in arrays of SAM-Based tunneling junctions. *Nano Lett.*, 10(9):3611–3619, 2010.

[149] M. F. Dumke, T. A. Tombrello, R. A. Weller, R. M. Housley, and E. H. Cirlin. Sputtering of the gallium–indium eutectic alloy in the liquid phase. *Surf. Sci.*, 124(2-3):407–422, January 1983.

[150] A. C Siegel, S. S. Shevkoplyas, D. B. Weibel, D. A. Bruzewicz, A. W. Martinez, and G. M. Whitesides. Cofabrication of Electromagnets and Microfluidic Systems in Poly(dimethylsiloxane). *Angew. Chem.*, 45(41):6877–6882, October 2006.

[151] A. C. Siegel, D. A. Bruzewicz, D. B. Weibel, and G. M. Whitesides. Microsolidics: Fabrication of Three-Dimensional Metallic Microstructures in Poly(dimethylsiloxane). *Adv. Mater.*, 19(5):727–733, March 2007.

[152] R M Metzger. Electrical rectification by a molecule: The advent of unimolecular electronic devices. *Acc. Chem. Res.*, 32:950–957, 1999.

[153] G. J. Ashwell, J. Ewington, and B. J. Robinson. Organic rectifying junctions fabricated by ionic coupling. *Chem. Commun.*, (6):618–620, 2006.

[154] W. J. Shumate, D. L. Mattern, A. Jaiswal, D. A. Dixon, T. R. White, J. Burgess, A. Honciuc, and R. M. Metzger. Spectroscopy and Rectification of Three DonorSigmaAcceptor Compounds, Consisting of a One-Electron Donor (Pyrene or Ferrocene), a One-Electron Acceptor (Perylenebisimide), and a C$_{19}$Swallowtail. *J. Phys. Chem. B*, 110(23):11146–11159, June 2006.

[155] M.-K. Ng, D.-C. Lee, and L. Yu. Molecular Diodes Based on Conjugated Diblock Co-oligomers. *J. Am. Chem. Soc.*, 124(40):11862–11863, October 2002.

[156] I. R. Peterson, D. Vuillaume, and R. M. Metzger. Analytical Model for Molecular-Scale Charge Transport. *J. Phys. Chem. A*, 105(19):4702–4707, May 2001.

[157] S. Lenfant, C. Krzeminski, C. Delerue, G. Allan, and D. Vuillaume. Molecular Rectifying Diodes from Self-Assembly on Silicon. *Nano Lett.*, 3(6):741–746, June 2003.

[158] N. Nishi, D. Hobara, M. Yamamoto, and T. Kakiuchi. Chain-length-dependent change in the structure of self-assembled monolayers of n-alkanethiols on Au(111) probed by broad-bandwidth sum frequency generation spectroscopy. *J. Chem. Phys.*, 118(4):1904–1911, 2003.

[159] F. Tao and S. L. Bernasek. Understanding OddEven Effects in Organic Self-Assembled Monolayers. *Chem. Rev.*, 107(5):1408–1453, May 2007.

[160] H. J. Yoon, N. D. Shapiro, K. M. Park, M. M. Thuo, S. Soh, and G. M. Whitesides. The rate of charge tunneling through self-assembled monolayers is insensitive to many functional group substitutions. *Angew. Chem. Int. Ed.*, 51(19):4658–4661, May 2012.

[161] E. A. Weiss, R. C. Chiechi, S. M. Geyer, V. J. Porter, D. C. Bell, M. G. Bawendi, and G. M. Whitesides. Size-Dependent Charge Collection in Junctions Containing Single-Size and Multi-Size Arrays of Colloidal CdSe Quantum Dots. *J. Am. Chem. Soc.*, 130(1):74–82, January 2008.

[162] E. A. Weiss, V. J. Porter, R. C. Chiechi, S. M. Geyer, D. C. Bell, M. G. Bawendi, and G. M. Whitesides. The Use of Size-Selective Excitation To Study Photocurrent through Junctions Containing Single-Size and Multi-Size Arrays of Colloidal CdSe Quantum Dots. *J. Am. Chem. Soc.*, 130(1):83–92, January 2008.

[163] C. Ladd, J.-H. So, J. Muth, and M. D. Dickey. 3D Printing of Free Standing Liquid Metal Microstructures. *Adv. Mater.*, 25(36):5081–5085, August 2013.

[164] M. R. Khan, G. J. Hayes, S. Zhang, M. D. Dickey, and G. Lazzi. A Pressure Responsive Fluidic Microstrip Open Stub Resonator Using a Liquid Metal Alloy. *Microwave and Wireless Components Letters, IEEE*, 22(11):577–579, 2012.

[165] B. L. Cumby, G. J. Hayes, M. D. Dickey, R. S. Justice, C. E. Tabor, and J. C. Heikenfeld. Reconfigurable liquid metal circuits by Laplace pressure shaping. *Appl. Phys. Lett.*, 101(17):174102, 2012.

2

Evidence of quantum interference in SAMs in tunneling junctions with Eutectic Gallium Indium

2.1 Introduction

Herein I report measurement of current-densities (J) through junctions comprising self-assembled monolayers (SAMs) of three arylethynylene thiolates (that differ only in their conjugation patterns) on Au substrates using eutectic Ga-In (EGaIn; 75 % Ga, 25 % In by weight, m.p. = 15.5 °C)[1] as a conformal top-contact. I compared the values of J at applied biases (V) between -0.4 and $+0.4$ V for three different ethynylthiophenol-functionalized anthracene derivatives, see Figure 2.1, with the predicted single molecule transport calculations (using gDFTB) for the molecules chemisorbed between two ideal gold electrodes. I observed a dramatic reduction in J where destructive quantum interference effects dominate the transport properties. I also found good qualitative agreement between experiment and theory; the linear-conjugation of the anthracene core is at least ten times more conductive than the broken-conjugation and cross-conjugation of the 9,10-dihydroanthracene and 9,10-anthraquionone cores. This is the first report of measurement of unsaturated molecules using EGaIn and the first experimental study showing the influence of cross-conjugation on J in molecular junctions containing a SAM.
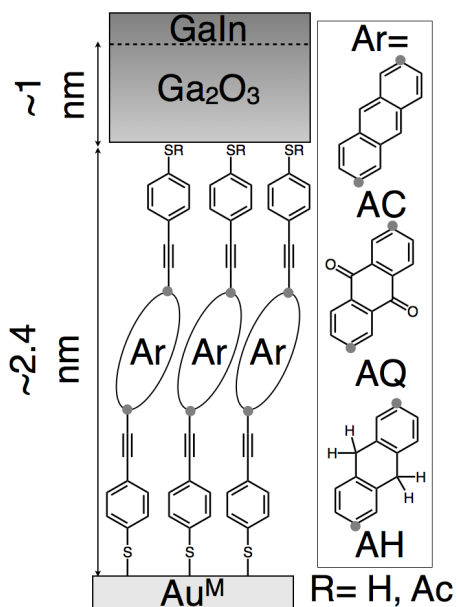
Figure 2.1: Not to scale schematic of the molecular junctions explore in this chapter. SAMs of thiolated arylethynylenes with cores of anthracene (AC; linear-conjugation), 9,10-anthraquinone (AQ; cross-conjugation), or 9,10-dihydroanthracene (AH; broken-conjugation) connected at the 2,6 positions (indicated with grey circles). The thiolate groups at the GaIn—Ga_2O_3 interface comprise a random mixture of free thiols and thioacetates.

2.1.1 Quantum Interference Effects

Minor manipulation in the chemical structure of a molecule often results in significant changes in a physical property of the system. In the case of conjugated molecules, there are particular relationships between parts of the molecule that govern a whole range of physical and chemical properties. For example, the substitution patterns of benzene derivatives are well established; electrophiles prefer to add *ortho* or *para* to electron-rich substituents. This effect is enhanced in the case of substituents with a lone pair due to the contribution of the resonance structures which place negative charges *ortho* and *para* to the substituent. The reason why there are no resonance contributors with negative charges on the meta positions is that the *ortho* and *para* positions are linearly-conjugated, while the *meta* position is cross-conjugated (with respect to the substituent). Thus, while the *meta* position is in the same π circuit—and one carbon atom away from either the *ortho* or *para* positions—there is no resonance structure that places the lone pair of a substituent on the *meta* position of the benzene ring. The conductivity of molecules is related to the same underlying physical processes that determine the types of resonance structures that are permitted for the molecule; however, electrical current due to a tunneling process need not be described by single charges hopping through a molecule. Cross-conjugation, whether it be through *meta* substitution on a benzene ring, [2–15] or other cyclic [16,17] or acyclic [18,19] structures, results in significantly reduced electron transport, as destructive interference effects can dominate the low-bias current. Theoretical models predict that this effect extends to anthracene systems. [20] For these molecules, instead of having to alter the connectivity to the aromatic system, conjugation can be controlled by chemically modifying the anthracene moieties; for example, via redox switching between anthraquinone and anthrahydroquinone [17,21]. More recently, quantum interference effects were observed for photoinduced electron transfer across linearly- and cross-conjugated acyclic bridges, [22] but to the best of our knowledge, before our contribution, there were only two observations of the influence of cross-conjugation in tunneling junctions, both of which concluding only that *meta* contacts lead to less current passing through a single-molecule junction than *para* contacts. [14,15] Another study observed a decrease in the conductance of single-molecule junctions that are photochemically switched between linear and cross-conjugated states, however the authors did not ascribe this effect to cross-conjugation or quantum interference. [23]

2.1.2 EGaIn Top Electrode for Tunneling Junctions

A central challenge for Molecular Electronics (ME) still remains the formation of reproducible electrical contacts to molecules that allow the measurement of current through individual molecules, *i.e.*, molecular junctions.[24,25] Two common strategies for forming these junctions are: let the molecules define the smallest dimensions in the junction (*i.e.*, bottom-up) or pre-forming a molecule-sized gap and subsequently populating it with the molecules (*i.e.*, top-down). The former strategy utilizes a top-contact that is placed directly on top of pre-formed SAM, while the latter is almost exclusively used for single-molecule measurements, which are not easily comparable to SAM-based measurements comprising micron-sized areas of molecules. To perform the measurement, a small drop of EGaIn ($< 2\ \mu\text{L}$) is extruded such that it remains adhered to the end of the syringe needle subsequently the drop is brought into contact with a sacrificial metal substrate (which can consist of a corner of the substrate used for the measurement) and the syringe raised using the piezo (this step can also be done by hand), forming and hourglass shape that cleaves in the center, leaving a tip attached to the syringe needle and a drop of EGaIn attached to the sacrificial substrate, see Figure 2.2.
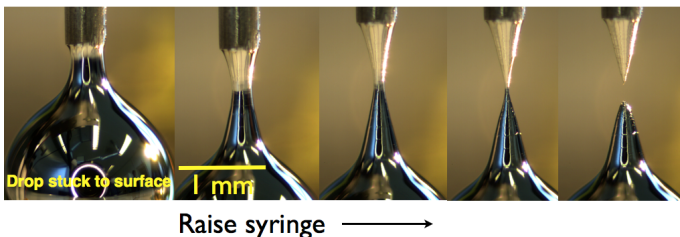
Figure 2.2: Left to right the sequence of the formation of an EGaIn tip. First, a drop is stuck to a sacrificial substrate, then the syringe is raised slowly, forming an hourglass shape. At a certain point the hourglass shape snap at the thinnest point, leaving behind an EGaIn tip and a drop that is discarded. The difference in color between the top and bottom of the hourglass shapes comes from the reflection of the gold surface.

The speed and the step-size affect the size and shape of the EGaIn tip, but the diameter of the tip is always $\sim 25\ \mu\text{m}$. In our hands, sharper tips not only allow the formation of smaller junctions, but enable the use of the same tip for multiple junctions, which speeds the acquisition of data, which is particularly important for fragile SAMs. The more slowly the syringe is withdrawn, the sharper the EGaIn tips, thus the

piezo affords control and reproducibility that cannot be achieved by hand. It is also important that there is a visible amount of EGaIn in the barrel of the syringe; as the syringe runs out, it becomes more difficult to produce long, sharp tips because the angle of the hourglass shape becomes more obtuse. By doing so I reproducibly form probes of EGaIn that are $\sim$ 25 μm in diameter, position them laterally with an adjustable stage, and bring them into contact with a SAM using a piezo stepper (open-loop, $\sim$ 5 nm resolution). We chose phenylethynylene-substituted anthracene moieties because the electronic structure can be synthetically manipulated with relatively minor perturbations to the molecules and the subsequent SAMs. The synthetic manipulation of the central aromatic ring (by substitutions at the 9 and 10 positions of the anthracene) allows the direct comparison of different conjugated pathways through the same molecular framework. I measured three different anthracene derivatives, see Figure 2.1, (the syntheses of which are described elsewhere [21,26]) functionalized at the 2,6 positions with para-ethynylthiophenols: i) anthracene (AC), which is linearly-conjugated, ii) anthraquinone (AQ), which is cross-conjugated, and iii) dihydroanthracene (AH), in which the conjugation is broken.

2.2 Results and Discussion

I formed SAMs on freshly prepared, thermally evaporated gold on mica (Au^M). [27,28] Au^M consists of large islands of atomically flat Au(111) and these islands are separated by large step-edges and crevices that function as defects that are absent in Au^{TS}surfaces. I measured fewer scans per junction and encountered a higher percentage of junctions that immediately short ($20-30\%$, compared to classical measurements of alkanethiolates) because of the relative fragility of the SAMs of AC, AQ, and AH (compared to alkanethiolates) and the possibility that numerous J/V cycles can induce chemical reactions (*e.g.*, dimerization of AC, redox of AQ, or elimination of H$_2$ from AH). Of the junctions that did not immediately short, I also observed lower yields of junctions that did not short during scanning ($\sim$80%) and broader distributions of $log|J|$ than for junctions of alkanethiols on template stripped metals. Using a piezo stepper to lower the EGaIn tip to the surface (instead of doing it by hand with a micromanipulator) enables us to measure these more fragile SAMs, but also introduces lower J, hysteretic "no-contact" traces. I therefore used an algorithm to filter these traces by defining shorts

as I/V curves where $I > 10$ mA ($J \approx 10^3$ A/cm^2) at 0.2 V and no-contact traces where $J \neq 0$ at 0 V, or in which dI/dV changes sign five or more times during a forward or reverse trace (*i.e.*, the trace is noisy). An example of collective J/V curves showing before (global) and after pruning (global_pruned) is shown in Figure 2.3.
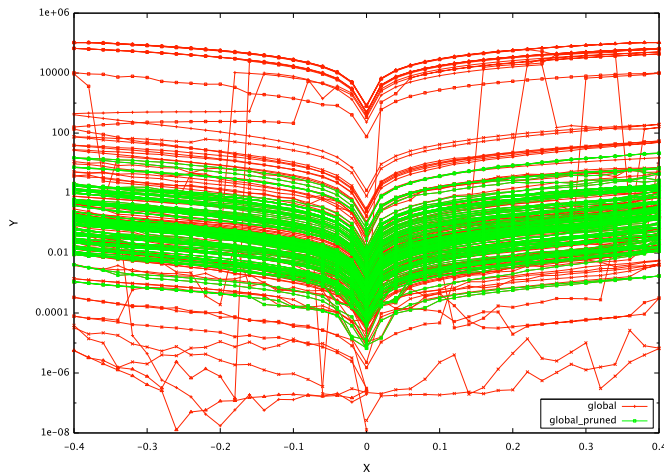
Figure 2.3: A plot of the raw data from one AC substrate showing the raw data (global, red) and the data after pruning the data using a custom algorithm (global_pruned, green). The X and Y axes are Potential (V) and Current-Density (A/cm^2) respectively.

A junction that shorts either immediately or after several scans will often result in a filament of EGaIn between the SAM and the tip as it is moved away from the SAM; that is, shorts are most likely caused by the EGaIn penetrating the SAM and contacting the Au^M substrate. The net effect of all of these factors is that it is much more difficult to collect large datasets for AC, AQ, and AH than it is for alkanethiolates. The variance (σ_{log}^2) of the histograms of $log|J|$ is also roughly doubled; $\sim 0.25 - 0.5$ $log|$ A/cm$^2|$ for alkanethiolates compared with $\sim 0.5 - 1.0$ $log|$ A/cm$^2|$ for AC, AQ, and AH. I initially prepared two substrates each for AC, AQ, and AH using Et$_3$N to de-protect the thioacetates *in situ* to form SAMs. Using a combination of ellipsometry and XPS we measured the thicknesses of the SAMs and found: 25.1 Å for AC, 24.3 Å for AQ, and 19.0 Å for AH. The predicted (B3LYP/6-311g**) S–S distances are; 24.5, 24.5, and 24.6 Å for AC, AQ, and AH respectively. (The bent form of AH differs in energy by only 2.04 kcal/mol is 23.8 Å; see below). These measured values predict, based on thickness, the order of

conductivities to be AH > AQ > AC, while the minimized values predict no observable difference.

Our chosen method of preparing SAMs of conjugated molecules produces dense monolayers, but leaves a mixture of free thiols and thioacetates at the SAM//Ga_2O_3—EGaIn interface. (The procedure for forming and measuring the thicknesses of SAMs of conjugated thiolates is presented in detail elsewhere).[29] I measured each substrate by recording five complete traces on each of 20-40 junctions on each substrate, for a total of ~ 200 traces each for AC, AQ, and AH after discarding the shorts and no-contact traces. I then computed the geometric average, $\bar{J}$, for each value of V and the standard error, SE.[30] These data are summarized in Figure 2.4. I initially chose to use the geometric average because the relatively low number (typical numbers for alkanethiolates are > 1000) of traces makes it difficult to fit Gaussians using least squares fitting algorithms, resulting in distorted line-shapes of the resulting traces. (And while more complex statistical analyses are available,[31] their use is not necessary to understand our data and undermines the simple and straightforward nature of EGaIn measurements). Typically $log|\bar{J}|$ and SE are good approximations of μ_{log} and σ_{log}, particularly with smaller datasets. I also computed the rectification ratio, R, for each value of $|V|$ from each trace and then computed the arithmetic mean (R is not a normal or log-normal distributed), $\bar{R}$. Junctions of EGaIn—Ga_2O_3//$CH_3(CH_2)_nS$/Ag^{TS} give $1.0 < \bar{R} < 1.5$ and I expect the same for AC, AQ, and AH because the molecules are symmetrical, but the interfaces with the electrodes are not. (Thus the voltage drop across the EGaIn—Ga_2O_3//SAM interface is presumably greater than the S/Au^M interface). The work function of EGaIn is about -4.3 eV which is in between Au (-5.1 eV) and Ag (-4.7 eV), thus I do not expect a large change in $\bar{R}$ moving from Ag^{TS} to Au^M substrates. I found $1.3 < \bar{R} < 1.5$ for AC, AQ, and AH, supporting the hypothesis that the current is the result of tunneling through the SAMs and not an artifact of the EGaIn—Ga_2O_3//SAM interface. The geometric-averaged J/V data for AC, AH, and AQ, Figure 2.4, show two trends: i) J for AC is at least ten times higher than AQ and AH, plus ii) the error increases with decreasing J. The latter trend is most likely because the instrument is less accurate at low currents (10^{-2} A/$cm^2 \approx 100$ nA) and thus the instrument error is superimposed on the distribution of J that is intrinsic to the SAM. The former trend suggests that the linear-conjugation of AC makes it more conductive than the broken-conjugation of AH and the cross-conjugation of AQ. I ascribe this result to the fact that, although both AC
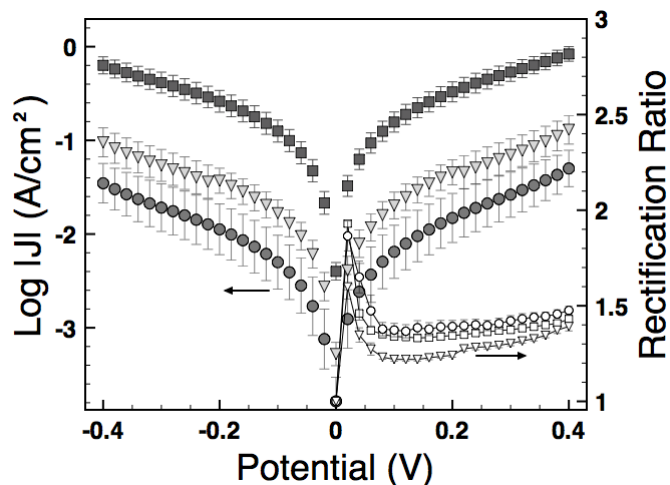
Figure 2.4: *Left axis*: plots of the geometric mean of $log|J|$ versus V for AC (dark squares), AQ (dark circles), AH (dark triangles). Error bars represent the standard error. *Right axis*: plots of the rectification ratios for AC (open squares), AQ (open circles), and AH (open triangles) versus $|V|$ computed from the arithmetic mean of $J(+V)/J(-V)$ for each trace. Error bars are computed from the standard error, SE_m. These data show that AC (linear-conjugation) is at least one order of magnitude more conductive than AH (broken-conjugation) and AQ (cross-conjugation) while AH is slightly more conductive than AQ, though in some places the error bars overlap, thus I cannot conclude that they differ significantly from each other.

(a) $V = 0.0$

(b) $V = 0.1$

(c) $V = 0.2$

(d) $V = 0.3$
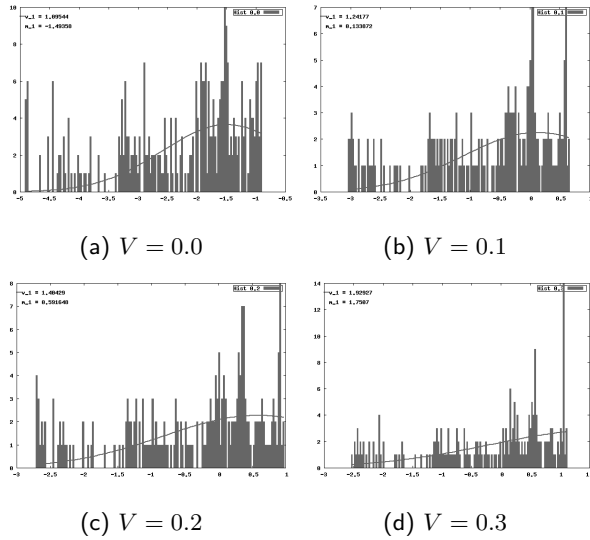
Figure 2.5: Histograms of AC for $V = 0.0, 0.1, 0.2,$ and 0.3 V.

and AQ provide a continuous pathway of p orbitals (*i.e.*, sp^2 and sp carbons between the S anchors) from EGaIn—Ga$_2$O$_3$ to Au^M, because the p orbitals of the carbonyl oxygens are exocyclic, their π bonds are perpendicular to the ring system, creating a cross-conjugated pathway between the electrodes. In order to gain more insight into this finding I fit the histograms of $log|J|$ for AC, AQ, and AH for each value of V to a Gaussian function and plotted μ_{log} versus V. Examples of the histograms for AC, AQ, and AH comprising 218, 268, and 232 traces respectively are pictured in Figure 2.5, 2.6, 2.7. In some cases the histogram looks incomplete and for clarity I decided to acquire more scans for AC (782 traces total), the resulting histograms are pictured in Figure 2.8.

These data are plotted together with $log|\bar{J}|$ in Figure 2.9 (the error bars representing the variance are omitted for clarity, $\sigma_{log}^2 \approx 1 \ log|\,\mathrm{A/cm^2}|$ for AC, AQ, and AH). The histograms of $log|J|$ at $V = 0.4$ V are shown to the right of the J/V traces. These fits show the expected agreement between $log|\bar{J}|$ and μ_{log} for AH and AQ, as well as the distorted line-shapes induced by the low number of traces. The J/V traces derived from the values of μ_{log} clearly show that the experiment cannot discern a statistically significant difference between AH and AQ. The data for AC differ greatly between the

(a) $V = 0.0$

(b) $V = 0.1$

(c) $V = 0.2$

(d) $V = 0.3$
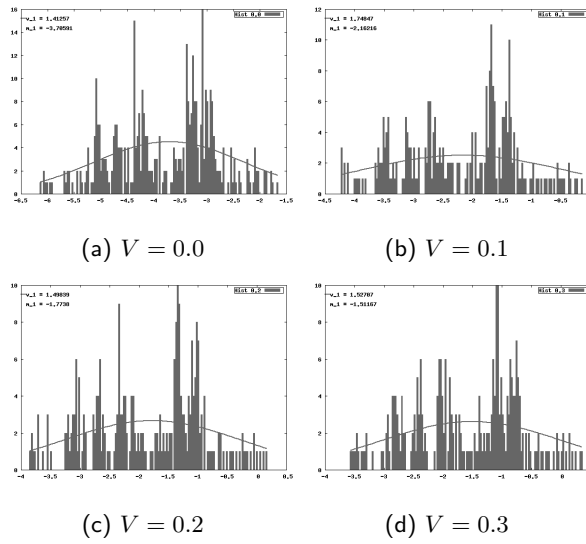
Figure 2.6: Histograms of AQ for $V = 0.0, 0.1, 0.2,$ and 0.3 V.

(a) $V = 0.0$

(b) $V = 0.1$

(c) $V = 0.2$

(d) $V = 0.3$
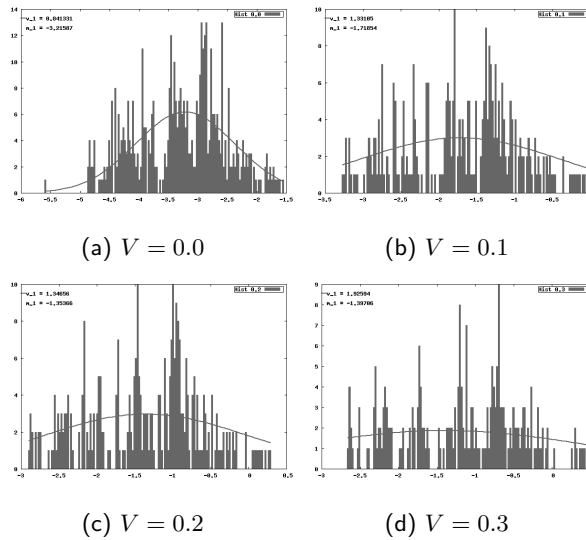
Figure 2.7: Histograms of AH for $V = 0.0, 0.1, 0.2,$ and 0.3 V.

(a) $V = 0.0$

(b) $V = 0.1$

(c) $V = 0.2$

(d) $V = 0.3$
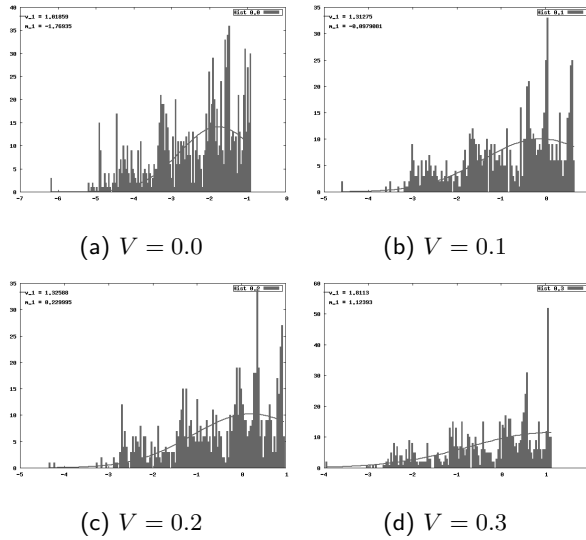
Figure 2.8: Histograms of AC for $V = 0.0, 0.1, 0.2,$ and 0.3 V including the additional two substrates.

geometric average and Gaussian fits, with the latter giving values of J that about one order of magnitude higher. The reason for this discrepancy can be seen in the histogram for AC at $V = 0.4$ V (see Figure 2.9). The data form a truncated Gaussian, the fit for which predicts values of μ_{log} that are about one order of magnitude higher than $log|\bar{J}|$ (and are higher even than the maximum measured value of J). To address this discrepancy, I measured AC twice more (*i.e.*, two substrates each, on two separate days, several weeks later, from freshly-prepared Au^M and solutions of AC) and the resulting histogram (Figure 2.8) did not change apart from the total number of counts; $log|\bar{J}|$ did not change, nor did μ_{log}. These results suggest that this histogram reflects the tunneling properties of AC, which are converging on μ_{log}. I hypothesize that the data are being truncated by J_0 for this system which means that, although the peak conductance of AC is very close to that of the EGaIn—Ga_2O_3//AC interface, I am still able to observe it by virtue of the fact that the data are distributed log-normal. This cropping is evident through the entire range of V but is more obvious at higher voltages. The values of $log|\bar{J}|$, which agree very well with those of μ_{log} for AQ and AH, diverge for AC because they are weighted by the lack of high values of J. Nevertheless, both the geometric
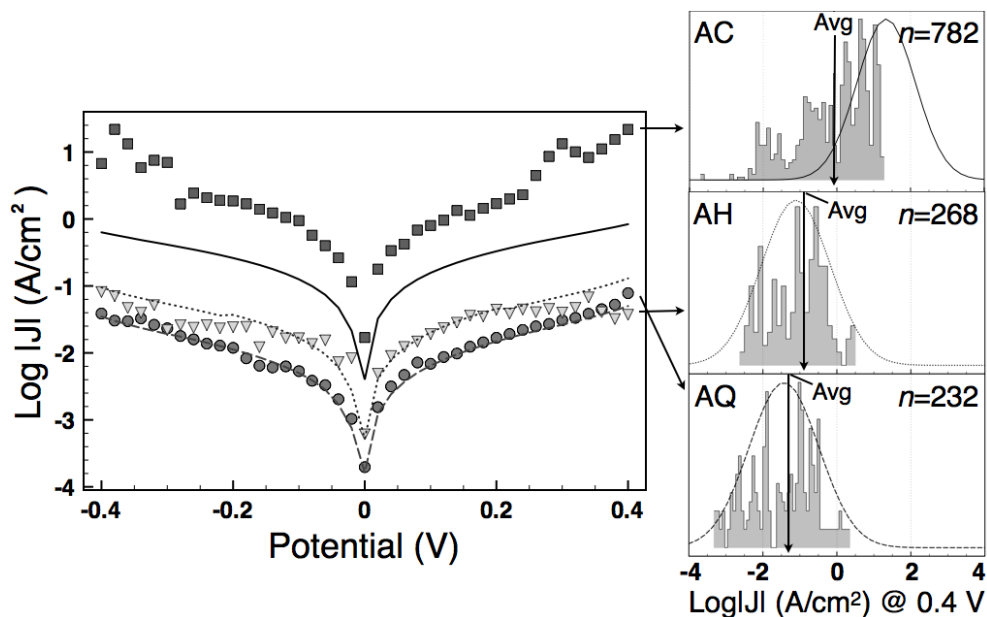
Figure 2.9: Left: plots of the geometric mean (lines) and Gaussian (μ_{log}) mean (symbols) of $log|J|$ versus V for AC (solid line; squares), AH (dotted line; triangles), and AQ (dashed line; circles). Right: plots of the normalized histograms of $log|J|$ at 0.4 V and the Gaussian fits for AC (top; solid line), AH (center; dotted line), and AQ (bottom; dashed line). The value of the geometric mean of $log|J|$ is indicated with a solid arrow and n is the total number of traces. These data reveal no appreciable difference between the geometric and Gaussian means for AH and AQ and clearly show that I cannot make a meaningful distinction between AH and AQ. The data for AC, however, form a truncated Gaussian distribution such that the Gaussian mean is more than an order or magnitude higher than the geometric mean. In either case, AC is clearly more conductive than either AH or AQ.

average and Gaussian data clearly show that AC is more conductive than either AH or AQ. The only ambiguity is the magnitude of this difference: geometric-averaged values of J for AC are $\sim 10^1\,\text{A/cm}^2$ larger than AH and AQ, while Gaussian-derived values of J are $\sim 10^2\,\text{A/cm}^2$ larger.

2.2.1 Transport Calculations

The work described in this section was performed by prof. dr. Gemma Solomon in collaboration with us. Assumptions need to be made when comparing single molecule transport calculations with experimental large-area charge-transport studies. The atomic structure of the SAM//Ga_2O_3—EGaIn interface is unknown, so the problem is further simplified by considering the individual molecules chemisorbed between two Au electrodes. The structures of the isolated AC, AQ and AH molecules were optimized (with terminal thiol groups) using Qchem [32] (DFT, B3LYP/6-311g**) and then chemisorbed them on the FCC hollow sites of two Au electrodes with a binding distance taken from the literature. [33] The minimized structure for AH is a bent conformation 2.04 kcal/mol lower in energy than the planar conformation. Both conformations were included in the transport calculations as this energy difference indicates that both conformations would be present at room temperature and we cannot predict which is dominant in the SAM. The transport were calculated using gDFTB [34–38] with no gold atoms included in the extended molecule. We integrated the bias-dependent transmission through the system over an energy window, the size of which is controlled by the magnitude of the applied bias, in order to obtain the current through the system. As the molecules are symmetrically bound to the two electrodes in the transport calculations, we assume that the applied bias drops symmetrically across the junction—a further difference with EGaIn. From transmission probability I/V curves can be extracted. These results are shown in Figure 2.10, clearly reproducing the experimental finding that AC is significantly more conductive than AQ or either conformation of AH. It is interesting to note that the transport through the bent conformation of AH is actually higher than that through the planar conformation. The opposite trend would generally be expected for a predominantly conjugated molecule because deviations from planarity decrease electronic coupling. For AH, however, modulating the σ/hyperconjugative coupling with bending has a different effect and evidently the same "rules of thumb" do not apply. In any case, the difference between the two conformations is minimal. The transport calculations

appear to suggest that the magnitude of the current through AQ and AH should be clearly distinguishable, with AQ exhibiting higher levels of transport and thus higher measured values of J. In this sense, the calculations and experiment are in agreement: AC is more conductive than AH and AQ, but the differences between AQ and AH cannot necessarily be resolved. The predicted difference between AC and AQ (*i.e.*, between the most and least conductive molecules) is 10^2, which agrees perfectly with the values of J derived from the Gaussian fits (Figure 2.9), but is one order of magnitude larger than the geometric-average values of J. While care must be exercised when comparing these theoretical predictions to experimental data, this result strengthens the hypothesis that the Gaussian fits for the truncated histograms of $log|J|$ are indeed correct in that they reflect the physical and electronic properties of AC.

The qualitative agreement between theory and experiment also suggests that interactions within the monolayer may not significantly influence the observed transport properties. In the transport measurements of densely packed monolayers, it is always possible that favorable transport pathways exist where current flows through multiple molecules connected by "through-space" [39] interactions in the monolayer. Recently, it was suggested that intermolecular interactions influenced the transport properties of alkanethiol monolayers on the basis of simulated inelastic electron tunneling spectra. [40] In molecules such as AQ and AH, where the coupling between large conjugated units is disrupted by small elements in the central part of the anthracene, it is plausible that current could flow through the monolayer by tunneling from one side of one molecule to the other side of a neighbor, possibly with similar ease to passing through a single molecule if π-stacking interactions were significant. While this scenario cannot be ruled out on the basis of these experiments, the qualitative agreement with single molecule transport calculations would tend to suggest that "through-bond" transport dominates.
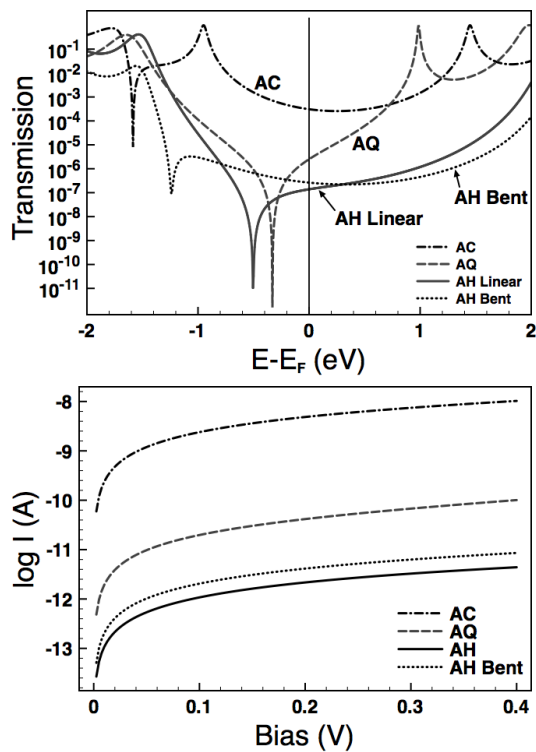
Figure 2.10: Top: The transmission curves as a function of energy. Bottom: current as a function of voltage. The three systems, AC, AQ, AH in the linear conformation, and AH in the bent conformation, shown as dot-dash, dashed, solid, and dotted lines respectively. The currents were calculated by integrating the transmission over increasing windows of bias.

2.3 Conclusions

I have successfully demonstrated that EGaIn can be used as a top-contact for tunneling junctions comprising SAMs of highly conjugated molecules and differentiate molecules with broken-conjugation, cross-conjugation, and linear-conjugation even though they are of approximately the same length. The calculated transport properties agree qualitatively, in fact AC (linear-conjugation) is significantly more conductive than AQ (cross-conjugated) and AH (broken-conjugation). While I was able to easily and rapidly collect statistically-significant amounts of data on (chemically) fragile SAMs under ambient conditions, the data appear to be limited by the conductivity of the EGaIn—Ga_2O_3//SAM interface. This limit is evident in the histograms of $log|J|$, which are truncated at $\sim 10^1$ A/cm^2 at 0.4 V, a value for J_0 that has been estimated by two other studies of EGaIn tunneling junctions. [41,42] However gaussian fits of these histograms predict mean values of J that are higher than the maximum measured (and average) values of J, but agree perfectly with the values predicted by our transport calculations. These results highlight the importance of the Ga_2O_3 layer in EGaIn measurements; it simultaneously enables the simple, rapid measurement of myriad different types of SAMs on different substrates, but limits the conductivity of the molecules that can currently be measured.

2.3.1 Recent Contribution of QI after our publication

In the last two years several experimental works regarding quantum interference and anthraquinone molecular junctions appear in literature. Quantum interference is of particular relevance to molecular electronics because it could be used to control the operation of molecular devices at the wave function level. Guedon et al., almost simultaneously with us, measured the same three molecules with a conductive probe finding similar results. Between the three molecule studied in this chapter, the anthraquinone have garnered much attention. Darwish et al. reported electrochemical studies on single-molecule switch anthraquinone molecular bridge with a conductance on/off ratio of an order of magnitude. This magnitude, which is attributed to destructive QI effects operating in the AQ form. The AQ moiety can be electrochemically switched in situ between the high-conducting H_2AQ system and the low-conducting AQ system. [43] Darwish et al. also used the bridge molecule into an STM break-junction with similar finding. Different approach was used by Vazquez et al. who investigate the conduc-

tance superposition law for parallel components in single-molecule circuits, particularly the role of interference.[44] Kaliginedi et al. measured a series of molecules by STM-BJ and MCBJ (mechanically controlled break junction) among which anthraquinone and dihydroanthracene were present.[45] Similarly to the others the authors found that the introduction of a cross-conjugated anthraquinone or a dihydroanthracene central unit results in lower conductance values, which are attributed to a destructive quantum interference phenomenon for the former and a broken π-conjugation for the latter. Arroyo et al. using MCBJ studied the effect of quantum interference through a single benzene ring by having *para* and *meta* substituents finding that *meta*-coupled benzene is more then one order of magnitude less conductive then the *para*-coupled.[46] By considering the conductive probe AFM technique a few-to-single molecule technique then EGaIn is the real only large-area techniques so far which demonstrate quantum interference effect in SAMs. Furthermore MCBJ and STM-BJ have the molecules in solution, thus there are great uncertainties in the binding mode. The good agreement between single molecule calculations and experimental work done by different laboratories using different techniques is a strong proof that this effect is real and by no chance an artifacts of the experiments.

Bibliography

[1] S. J. French, D. J. Saunders, and G. W. Ingle. The system gallium-indium. *J. Phys. Chem.*, 42(2):265–274, 1938.

[2] P. Sautet and C. Joachim. Electronic interference produced by a benzene embedded in a polyacetylene chain. *Chem. Phys. Lett.*, 153(6):511–516, 1988.

[3] C. Patoux, C. Coudret, J.-P. Launay, C. Joachim, and A. Gourdon. Topological Effects on Intramolecular Electron Transfer via Quantum Interference. *Inorg. Chem.*, 36(22):5037–5049, 1997.

[4] S. N. Yaliraki and Mark A. Ratner. Interplay of topology and chemical stability on the electronic transport of molecular junctions. *Ann. N.Y. Acad. Sci.*, 960(MOLECULAR ELECTRONICS II):153–162, 2002.

[5] M. H. Hettler, W. Wenzel, M. R. Wegewijs, and H. Schoeller. Current collapse in tunneling transport through benzene. *Phys. Rev. Lett.*, 90(7):076805, 2003.

[6] R. Stadler, S. Ami, C. Joachim, and M. Forshaw. Integrating logic functions inside a single molecule. *Nanotech.*, 15(4):S115–S121, 2004.

[7] D. Walter, D. Neuhauser, and R. Baer. Quantum interference in polycyclic hydrocarbon molecular wires. *Chem. Phys.*, 299(1):139–145, 2004.

[8] D. M. Cardamone, C. A. Stafford, and S. Mazumdar. Controlling quantum transport through a single molecule. *Nano Lett.*, 6(11):2422–2426, 2006.

[9] C. A. Stafford, D. M. Cardamone, and S. Mazumdar. The quantum interference effect transistor. *Nanotech.*, 18(42):424014, 2007.

[10] S.-H. Ke, W. Yang, and H. U. Baranger. Quantum-Interference-Controlled Molecular Electronics. *Nano Lett.*, 8(10):3257–3261, 2008.

[11] G. C. Solomon, D. Q. Andrews, R. P. Van Duyne, and M. A. Ratner. Electron transport through conjugated molecules: When the π system only tells part of the story. *Chem. Phys. Chem.*, 10(1):257–264, 2009.

[12] H. Thorsten, G. C. Solomon, D. Q. Andrews, and M. A. Ratner. Interfering pathways in benzene: An analytical treatment. *J. Chem. Phys.*, 131(19):194704, 2009.

[13] A. A. Kocherzhenko, F. C. Grozema, and L. D. A. Siebbeles. Charge Transfer Through Molecules with Multiple Pathways: Quantum Interference and Dephasing. *J. Phys. Chem. C*, 114(17):7973–7979, May 2010.

[14] M. Mayor, H. B Weber, J. Reichert, M. Elbing, C. von Hänisch, D. Beckmann, and M. Fischer. Electric current through a molecular Rod—Relevance of the position of the anchor groups. *Angew. Chem.*, 42(47):5834–5838, 2003.

[15] M. Kiguchi, H. Nakamura, Y. Takahashi, T. Takahashi, and T. Ohto. Effect of anchoring group position on formation and conductance of a single disubstituted benzene molecule bridging au electrodes: Change of conductive molecular orbital and electron pathway. *J. Phys. Chem. C*, 114(50):22254–22261, December 2010.

[16] N. S. Hush, J. R. Reimers, L. E. Hall, L. A. Johnston, and M. J. Crossley. Optimization and Chemical Control of Porphyrin-Based Molecular Wires and Switches. *Ann. N.Y. Acad. Sci.*, 852(1):1–21, 1998.

[17] T. Markussen, J. Schiötz, and K. S. Thygesen. Electrochemical control of quantum interference in anthraquinone-based molecular switches. *J. Chem. Phys.*, 132(22):224104, 2010.

[18] G. C. Solomon, D. Q. Andrews, R. P. Van Duyne, and M. A. Ratner. When things are not as they seem: Quantum interference turns molecular electron transfer "rules" upside down. *J. Am. Chem. Soc.*, 130(25):7788–7789, 2008.

[19] G. C. Solomon, D. Q. Andrews, T. Hansen, R. H. Goldsmith, M. R. Wasielewski, R. P. Van Duyne, and M. A. Ratner. Understanding quantum interference in coherent molecular conduction. *J. Chem. Phys.*, 129(5):054701–8, 2008.

[20] T. Markussen, R. Stadler, and K. S. Thygesen. The relation between structure and quantum interference in single molecule junctions. *Nano Lett.*, 10(10):4260–4265, October 2010.

[21] E. H. van Dijk, D. J. T. Myles, M. H. van der Veen, and J. C. Hummelen. Synthesis and properties of an Anthraquinone-Based redox switch for molecular electronics. *Org. Lett.*, 8(11):2333–2336, May 2006.

[22] A. B. Ricks, G. C. Solomon, M. T. Colvin, A. M. Scott, K. Chen, M. A. Ratner, and M. R. Wasielewski. Controlling electron transfer in Donor-Bridge-Acceptor molecules using Cross-Conjugated bridges. *J. Am. Chem. Soc.*, 132(43):15427–15434, November 2010.

[23] D. Dulić, S. J. van der Molen, T. Kudernac, H. T. Jonkman, J. J. D. de Jong, T. N. Bowden, J. van Esch, B. L. Feringa, and B. J. van Wees. One-way optoelectronic switching of photochromic molecules on gold. *Phys. Rev. Lett.*, 91(20):207402, Nov 2003.

[24] H. B. Akkerman and B. de Boer. Electrical conduction through single molecules and self-assembled monolayers. *J. Phys.: Condens. Physics*, 20:013001–013021, December 2007.

[25] L. A. Bumm. Measuring molecular junctions: What is the standard? *ACS Nano*, 2(3):403–407, January 2008.

[26] C. M. Guedon, H. Valkenier, T. Markussen, K. S. Thygesen, J. C. Hummelen, and S. J. van der Molen. Observation of quantum interference in molecular charge transport. *Nat. Nanotechnol.*, 7(5):305–309, 2012.

[27] J. A. DeRose, T. Thundat, L. A. Nagahara, and S. M. Lindsay. Gold grown epitaxially on mica: conditions for large area flat faces. *Surf. Sci.*, 256(1-2):102–108, 1991.

[28] D. Porath, Y. Goldstein, A. Grayevsky, and O. Millo. Scanning tunneling microscopy studies of annealing of gold films. *Surf. Sci.*, 321(1-2):81 – 88, 1994.

[29] H. Valkenier, E. H. Huisman, P. A. van Hal, D. M. de Leeuw, R. C. Chiechi, and J. C. Hummelen. Formation of high-quality self-assembled monolayers of conjugated dithiols on gold: Base matters. *J. Am. Chem. Soc.*, 133(13):4930–4939, 2011.

[30] E. A. Weiss, Chiechi R. C., Kaufman G. K., Kriebel J. K., Li Z., Duati M., Rampi M. A., and Whitesides G. M. Influence of defects on the electrical characteristics of Mercury-Drop junctions: Self-Assembled monolayers of n-Alkanethiolates on rough and smooth silver. *J. Am. Chem. Soc.*, 129(14):4336–4349, April 2007.

[31] V. B. Engelkes, J. M. Beebe, and C. D. Frisbie. Analysis of the causes of variance in resistance measurements on metal–molecule–metal junctions formed by conducting-probe atomic force microscopy. *J. Phys. Chem. B*, 109(35):16801–16810, 2005.

[32] Shao et al. Advances in methods and algorithms in a modern quantum chemistry program package. *Phys. Chem. Chem. Phys.*, 8(27):3172–3191, 2006.

[33] A. Bilic, J. R. Reimers, and N. S. Hush. The structure, energetics, and nature of the chemical bonding of phenylthiol adsorbed on the au(111) surface: Implications for density-functional calculations of molecular-electronic conduction. *J. Chem. Phys.*, 122(9):094708–15, 2005.

[34] M. Elstner, D. Porezag, G. Jugnickel, J. Elsner, M. Haugk, T. Frauenheim, S. Suhai, and G. Seifert. Self-consistent-charge density-functional tight-binding method for simulations of complex materials properties. *Phys. Rev. B*, 58:7260–7268, 1998.

[35] T. Frauenheim, G. Seifert, M. Elstner, Z. Hagnal, G. Jungnickel, D. Porezag, S. Suhai, and R. Scholz. A self-consistent charge density-functional based tight-binding method for predictive materials simulations in physics, chemistry and biology. *Phys. Stat. Sol. (b)*, 217(1):41–62, 2000.

[36] T. Frauenheim, G. Seifert, M. Elstner, T. Niehaus, C. Koehler, M. Amkreutz, M. Sternberg, Zoltan Hajnal, Aldo Di Carlo, and S. Suhai. Atomistic simulations of complex materials: ground-state and excited-state properties. *J. Phys.: Condens. Matter*, 14:3015–3047, 2002.

[37] D. Porezag, T. Frauenheim, T. Kohler, G. Seifert, and R. Kaschner. Construction of tight-binding-like potentials on the basis of density-functional theory: Application to carbon. *Phys. Rev. B*, 51:12947–12957, 1995.

[38] A. Pecchia and A. Di Carlo. Atomistic theory of transport in organic and inorganic nanostructures. *Rep. Prog. Phys.*, 67(8):1497–1561, 2004.

[39] R. Hoffmann. Interaction of orbitals through space and through bonds. *Acc. Chem. Res.*, 4(1):1–9, 1971.

[40] N. Okabayashi, M. Paulsson, H. Ueba, Y. Konda, and T. Komeda. Inelastic tunneling spectroscopy of alkanethiol molecules: High-resolution spectroscopy and theoretical simulations. *Phys. Rev. Lett.*, 104(7):077801, 2010.

[41] C. A. Nijhuis, W. F. Reus, and G. M. Whitesides. Molecular rectification in Metal-SAM-Metal Oxide-Metal junctions. *J. Am. Chem. Soc.*, 131(49):17814–17827, December 2009.

[42] M. M. Thuo, W. F. Reus, C. A. Nijhuis, J. R. Barber, C. Kim, M. D. Schulz, and G. M. White-sides. Odd-even effects in charge transport across self-assembled monolayers. *J. Am. Chem. Soc.*, 133(9):2962–2975, 2011.

[43] N. Darwish, I. Díez-Pérez, P. Da Silva, N. Tao, J. J. Gooding, and M. N. Paddon-Row. Observation of Electrochemically Controlled Quantum Interference in a Single Anthraquinone-Based Norbornylogous Bridge Molecule. *Angew. Chem.*, 124(13):3257–3260, February 2012.

[44] H. Vazquez, R. Skouta, S. Schneebeli, M. Kamenetska, R. Breslow, L. Venkataraman, and M. S. Hybertsen. Probing the conductance superposition law in single-molecule circuits with parallel paths. *Nature Nanotech.*, 7(10):663–667, September 2012.

[45] V. Kaliginedi, P. Moreno-García, H. Valkenier, W. Hong, V. M. García-Suárez, P. Buiter, J. L. H. Otten, J. C. Hummelen, C. J. Lambert, and T. Wandlowski. Correlations between molecular structure and single-junction conductance: A case study with oligo(phenylene-ethynylene)-type wires. *J. Am. Chem. Soc.*, 134(11):5262–5275, 2012.

[46] C. R. Arroyo, S. Tarkuc, R. Frisenda, J. S. Seldenthuis, C. H. M. Woerde, R. Eelkema, F. C. Grozema, and H. S. J. van der Zant. Signatures of Quantum Interference Effects on Charge Transport Through a Single Benzene Ring. *Angew. Chem. Int. Ed.*, 52(11):3152–3155, February 2013.

3

The Influence of an Atom in EGaIn/Ga$_2$O$_3$ Tunneling Junctions Comprising Self-Assembled Monolayers

3.1 Introduction

In this chapter I describe the measurement of current-densities, J, arising from the tunneling of charges through junctions comprising self-assembled monolayers (SAMs) on template-stripped[1] gold substrates Au^{TS} using EGa-In, as previously described, as conformal top contact. In Chapter 2 we changed the conjugation pattern of fully conjugated molecules. In this chapter I will instead describe two homologous series of oligo(phenylene)s, Scheme 3.1, bearing alkylthiol tails. One series is terminated with phenyl groups (Ph-SAMs) whereas the others terminated with 4-pyridyl groups (Py-SAMs). Thus, these two series of SAMs vary only by the substitution of C-H for N. I know from previous work that changing the head-group in the case of alkanethiols SAMs does not result in a substantial difference in J.[2] Research in Molecular Electronics (ME) often seeks both to elucidate the mechanisms by which charges flow across electrical junctions bridged by individual molecules and to construct electronic devices where molecules act as the active component.[3] The latter goal also represents a challenge of nanotechnology, making SAMs particularly useful because they are capable of defining the smallest dimension of a device by self-assembling onto the "bottom" electrode.[4]

The minutia of their structure also become important handles for manipulating tunneling currents, if they can be successfully incorporated into devices. An open question in ME is how—or if—the molecules in a tunneling junction modulate the transport properties of the junction.[5] The ease of the formation of tunneling junctions using EGaIn has led to the rapid buildup of large sets of data from SAMs of disparate molecules from which a seeming contradiction has arisen; it has been unambiguously established that the SAM dominates charge transport in EGaIn/Ga_2O_3//SAM/metal junctions,[6] while at the same time these junctions are completely insensitive to the inclusion of amides[7] and to a wide variety of head-groups at the SAM//Ga_2O_3 interface.[8] It has even been suggested that the transport properties of EGaIn/Ga_2O_3//SAM/metal junctions are dominated by the offset between the Fermi energy of the metal and the valence/conduction bands of Ga_2O_3, reducing the role of the SAM to a dielectric spacer layer.[9] It would seem, therefore, that the role of the SAM in charge transport has not yet been unambiguously determined; however, despite the layer of Ga_2O_3, EGaIn is sensitive enough to resolve the odd-even effect in SAMs of alkanethiolates,[10] rectification in SAMs incorporating ferrocene,[11–13] different torsional angles in biphenyl moieties,[14] and quantum interference (*i.e.*, the influence of conjugation patterns) in SAMs incorporating anthracene moieties.[15] Closer inspection of the SAMs in these studies reveals that, in the cases in which the conductance properties—or phenomenon such as rectification—are clearly modulated by the SAM, the molecules are (at least partially) conjugated, which places the HOMO of the molecule relatively close to the Fermi energy of the bottom electrode. In cases in which the conductance properties are independent of the structure of the SAM, the molecules are (mostly) aliphatic, placing the HOMO much further from the Fermi energy and possibly promoting transport through the LUMO. In these cases, it is reasonable to assume that either the valence or conduction band of the Ga_2O_3 is the state closest in energy to the Fermi energy of the electrode, thus it is this coupling, modulated by the tunneling distance (*i.e.*, the thickness of the SAM), that dominates the conductance properties. In the current chapter I investigate the conductance properties of two nearly identical series of SAMs, Scheme 3.1, that differ by only a single atom (N to C-H).
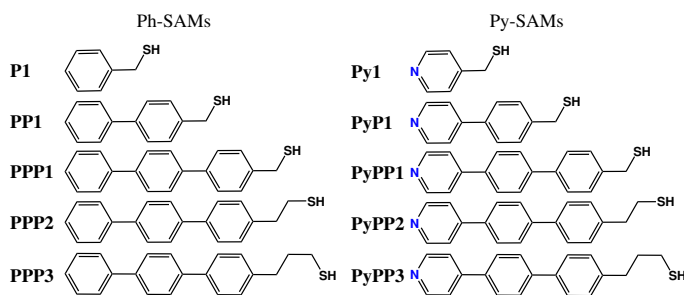
Figure 3.1: Left: Ph-SAM, Right: Py-SAM; **P** stand for phenylene and the number **(1-3)** indicate the number of methylene(s) spacer between the sulphur and the first phenylene. In the case of the Py-SAMs Py indicate the pyridine unit.

3.1.1 SAMs of Oligoarylene-alkanethiolates

The Ph-SAM series belongs to the particularly well-characterized series of oligo(phenylene)-alkanethiols known to form high-quality SAMs, the compactness of which rival that of alkanethiols. [16] Similar to SAMs of alkanethiolates, SAMs of oligo(phenylene)-alkanethiols show a pronounced odd-even effect (with respect to the alkane portion), which has a strong impact on the tilt angle and the structure of the SAM. [17–20] The torsional angle of oligo(phenylene)s is much smaller in the solid phase than in solution, and can vary widely with packing in the solid state due to intermolecular interaction. [21] In SAMs of oligo(phenylene)s this angle is not expected to vary significantly with the number of phenyl rings, however, in oligo(phenylene)-alkanethiols, the odd-even effect can manifest as a significant (six-fold) change in torsional angle. [22] This property makes the Ph-SAM series particularly interesting to study using EGaIn, as the changing torsional angle is known to affect the HOMO level of the molecules in the SAM, which is electronically decoupled from the Au^{TS} by the alkane spacer (*i.e.*, it should not be broadened significantly by the gold electrode). An open question in EGaIn-based junctions is how the EGaIn couples via the Ga$_2$O$_3$ layer to the SAM; evidence suggests weak coupling. [8,23] Strong coupling would theoretically broaden the levels in the SAM, reducing the effects on conductance simply to length dependance, while weak coupling—the expected outcome—would likely be more sensitive to small changes in the relative positions of the HOMOs. The Py-SAM series is well-characterized and shares many of the same structural features as the Ph-SAM series. [24–26] Pyridines terminated SAMs have been used

in several applications for their ligand properties. The odd-even effect in the Py-SAM series, however, differs from that of the Ph-SAMs in two important ways; i) the effect on the tilt angle is more pronounced and ii) the effect on the torsional angle is apparently subdued. [25] The first point is important because the lone pair of the nitrogens points towards the EGaIn electrode in SAMs of PyP1, PyPP1, and PyPP3, but not PyPP2. Here, strong electronic coupling between the SAMs and EGaIn would be expected to lead to a deviation from simple length dependence, while weak coupling would remove any significant influence from the orientation of the lone pairs. The second point is of interest because of dependence of the HOMO levels of oligo(arylene)s on torsion angle. The conjugated portions of the Ph-SAM and Py-SAM series are isolated from the Au$^{\text{TS}}$ by alkane chains, but if the Ga_2O_3 layer also isolates them from the bulk Ga-In, then one would expect a deviation from length dependence for the Ph-SAM series, but not for the Py-SAM series; i.e., the effect of the torsional angle on the relative HOMO levels should only be apparent when they are sufficiently decoupled from EGaIn. Grave et al. observed a ten-fold difference in conductivity for SAMs in Hg bilayer junctions comprising oligo(arylenes) with different torsional angles, however their effect on conductance could not be fully disentangled from the 0.5 eV difference in HOMO levels induced by the inclusion of several nitrogen atoms. [27] The Ph-SAM and Py-SAM series, by contrast, separate the influence of the heteroatom from the torsional angle by offering two series (as opposed to molecules) of molecules against which to compare.

3.2 Conductance Length Dependence

Similar to what I described in chapter 2, I measured the conductances of the Ph-SAM and Py-SAM series by stretching small drops of EGaIn into sharp tips, applying them to the surface of each SAM and sweeping them through a range of voltages (± 0.4 V for the Py-SAMs and ± 0.7 V for the Ph-SAMs). I used Au$^{\text{TS}}$ for the Ph-SAMs and Py-SAMs instead of gold-on-mica. In addition, these SAMs were robust enough that I did not have to exclude any aberrant J/V traces arising from defects, only a few shorts (i.e., the Ohmic traces resulting from a junction failing after several scans). In that respect, these SAMs behave much more like SAMs of alkanethiolates, i.e., the yield of working junction is $> 90\%$, and I was therefore able to treat the data similarly. [10] I chose to analyze the data sets using geometric averages rather than Gaussian fits because

the raw conductance data for Py1, PP1, and PyP1 were for some biases bi-modal. Figure 3.2 shows a comparison of the values of J derived from geometric averages and Gaussian fits, only Py1, PP1, and PyP1 differ substantially. I could have chosen to fit the tallest Gaussians from these SAMs, but without a detailed understanding of the physical meaning of the bi-modality it is more reasonable to use geometric averages, which include the entire distribution of J values, weighted according to frequency. Thus the geometric average values of J are slightly higher for Py1 and PyP1 and slightly lower for PP1 than the Gaussian values.
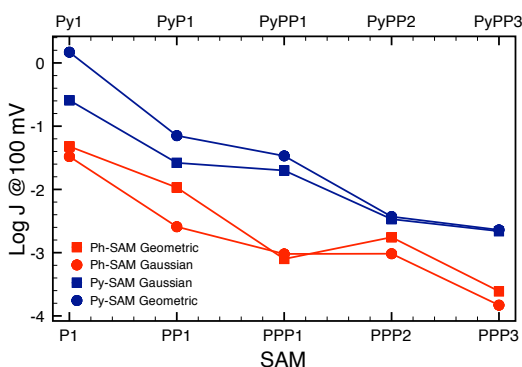
Figure 3.2: Plots of the values of J at 100 mV for the Ph-SAM (red, bottom axis) and Py-SAM (blue, top axis) series from Gaussian fits (squares) and geometric means (circles). This color scheme is used throughout this chapter.

I formed SAMs from each of the molecules in Scheme 3.1 by immersing $\mathrm{Au^{TS}}$ substrates in 20 μM solutions in ethanol at room temperature for 24 hours. The resulting J/V traces are shown in Figure 3.3. Table 3.1 is a summary of the number of traces and the percentage of junctions that shorted for each SAM. I calculated this percentage from the number of junctions that shorted during a measurement, however, since I collected an average of five scans per junction, these yields can be described as the percentage of junctions that shorted within approximately five scans. That is why two SAMs, PyPP1 and PyPP2, exhibit 0% shorts. Statistics in ME is very often underestimated if not omitted completely from scientific reports, which unfortunately does not give a clear picture of the system under investigation and reduces its impact for applications.

SAMs	number of traces	% of junctions that shorted
P1	420	7%
PP1	1460	4%
PPP1	1200	16%
PPP2	1402	5%
PPP3	870	6%
Py1	1040	3%
PyP1	1010	3%
PyPP1	760	0%
PyPP2	750	0%
PyPP3	1340	4%

Table 3.1: Number of traces acquired and the % of shorted junctions for the Ph-SAM and Py-SAM series

In Figure 3.3 the Ph-SAM series is represented by red traces and the Py-SAM by blue traces (this color scheme is used throughout this chapter). The symbols correspond to the equivalent SAM in each series (*e.g.*, PPP1 and PyPP1). The conductances of the two series of SAMs significantly overlap and without prior knowledge of which trace belonged to which SAM, they could not be unambiguously distinguished without either further experiments or a deeper analysis of the data. This is an important point, as it demonstrates that the shift in the relative HOMO levels induced by the inclusion of a nitrogen atom is not sufficient to separate the Py-SAMs from the Ph-SAMs simply by inspecting the J/V data. The trends within each series also differ; Py1 > PyP1 > PyPP1 > PyPP2 > PyPP3, but P1 > PP1 > PPP2 > PPP1 > PPP3. I expected the conductance to depend both on the length of the molecules and on their respective HOMO levels (because they are closer to the Fermi levels of Au and EGaIn than the LUMO levels), but I found that the calculated energies of the minimized structures follow the lengths (see Figure 3.4).

Therefore, the overall trend should be decreasing conductance with length, but that decrease should not be as uniform as it is with SAMs of alkanethiolates if the HOMOs of the SAMs affect the transport properties. The Py-SAMs behaves in this manner; by looking closer at Figure 3.4 I notice that the conductance drops in two large steps, one between Py1 and PyP1 and one between PyPP1 and PyPP2. There are also two significantly smaller steps between PyPP1 and PyPP2 and between PyPP2 and PyPP3.
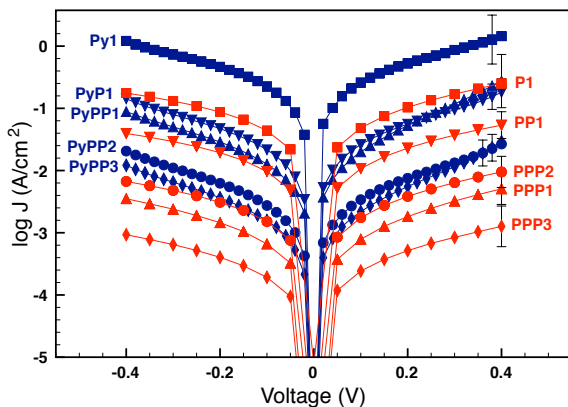
Figure 3.3: Plots of $\log$ current-density versus voltage for the two series Ph-SAMs (red) and Py-SAMs (blue); P1/Py1 (squares), PP1/PyP1 (triangle down), PPP1/PyPP1 (triangle up), PPP2/PyPP2 (circle), and PPP3/PyPP3 (diamond). Values of $\log J$ at $V = 0$ are omitted for clarity. The error bars are variances. The two different series of SAMS are almost indistinguishable except that Py1 is the most conductive and PPP3 is the least conductive. The trends within each series also differ; *e.g.*, PPP2 is more conductive than PPP1, while PyPP2 is less conductive than PyPP1.
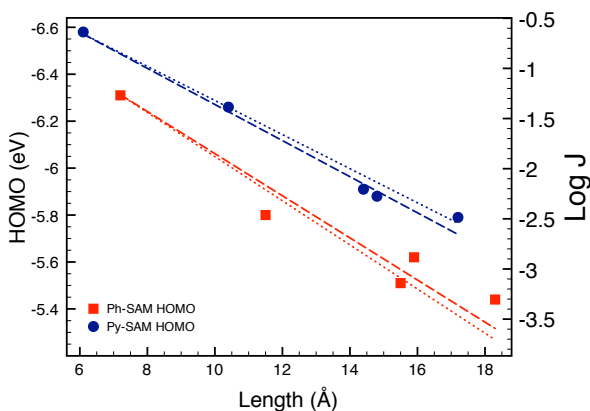
Figure 3.4: Plots of the calculated energies of the HOMOs (left axis) of the Ph-SAM (red squares) and Py-SAM (blue circles) versus XPS-derived molecular lengths. The dotted and dashed lines (right axis) are the fits to $J = J_0 e^{-\beta d}$ from Figure 3.6.

The change in conductivity in the Ph-SAM series, however, is almost uniform except that PPP1 and PPP2 are reversed with respect to PyPP1 and PyPP2 (*i.e.*, PPP2 > PPP1, but PyPP1 > PyPP2) and with respect to length dependence. Taken together, the conductance data for the Py-SAM and Ph-SAM series do not follow an obvious trend. The conductance result could be describe as a sort of superposition of length and molecular levels.

3.2.1 Beta Value Calculations

According to Simmons' approximation, when the effects of image charges are excluded, J as a function of the width of the junction, d, follows Equation 3.1, where β is the characteristic tunneling decay and J_0 is the theoretical value of J when $d = 0$.[28]

$$J = J_0 e^{-d\beta} \tag{3.1}$$

The parameter β is often used to "validate" a particular method for constructing tunneling junctions (while J_0 varies widely and is not reported as often as β). Detailed statistical analyses of EGaIn/Ga_2O_3 junctions show that $\beta \approx 1\ n_C^{-1}$ (*i.e.*, per methylene unit; 0.8 Å^{-1}) at 200-500 mV for SAMs of alkanethiolates,[29] which is in good agreement with literature values from other experimental techniques.[10,30–32] Conjugated molecules, owing to their increased polarizability (*i.e.*, delocalized electrons) and HOMO/LUMO levels that are closer to the Fermi level of the metal electrodes, yield lower values of β; values as low as 0.2 Å^{-1} have been reported for SAMs of oligo(phenylene)s using PEDOT:PSS as a top contact[33] and high as 0.61 Å^{-1} in a bilayer with hexadecanethiol using Hg.[34] Ishida et al. measured the Ph-SAM series using conducting probe AFM (CP-AFM), but they did not report a value for β for the entire series.[35] Instead, they calculated β for the phenylene units (P1, PP1, and PPP1) and methylene units (PPP1, PPP2, and PPP3) separately, giving values of ~ 0.5 and ~ 1.2 Å^{-1} respectively. The reason for separating the values was an unexpectedly sharp increase in resistance at PPP2. They ascribe this increase to the localization of the HOMO density at the center phenyl ring (using MOPAC/AM1 calculations), however, they reached this conclusion using the minimized structures, not the more planar conformations that are adopted in SAMs (conformation which is determined by surface characterization, *i.e.*, they ignored the effects of solid-state packing on torsional angles). The B3LYP/DFT calculations show

that the HOMO density is spread evenly over the phenylene rings, see Figure 3.5. To the best of my knowledge, no tunneling junctions comprising any of the Py-SAMs have been reported, thus some assumption must be made.
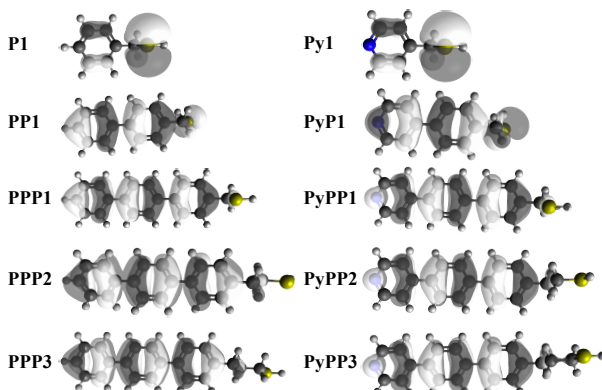
Figure 3.5: DFT calculations of the Ph-SAM series (left) and Py-SAM series (right) showing the even distribution of the density of the HOMO orbitals.

Figure 3.6 is a β plot representing values of J at 100 mV (taken from Figure 3.3) versus length for the Py-SAM and Ph-SAM series. I used values for the layer thickness derived from XPS data for molecular lengths because, with the exception of PPP2 and PyPP2, the molecules pack with the oligoarylene portions perpendicular to the substrate.[24,25] The XPS-derived values are also $\sim 3\%$ larger than the end-to-end distances predicted by AM1 minimization for every SAM except PPP2 and PyPP2. Thus, assuming that the tunneling pathway follows the backbones of the molecules in the SAMs, these values are more reasonable than using estimated lengths. Due to the increased tilt angle, the theoretical lengths are longer than the XPS-derived values for PPP2 and PyPP2; those values are plotted as an open square and open circle respectively. Fits to Equation 3.1 yielded $J_0 = 1.18 \pm 1.44$ A/cm^2 and $\beta = 0.44 \pm 0.04$ Å^{-1} for the Ph-SAM series and $J_0 = 2.46 \pm 3.00$ A/cm^2 and $\beta = 0.42 \pm 0.08$ Å^{-1} for the Py-SAM series. β values are significantly higher than the lowest values reported for oligo(phenylene)s and significantly lower than the values for alkanethiolates using EGaIn/Ga$_2$O$_3$. The fact that they are within 10% of each other is a reflection of the structural and electronic similarity and is evidence that one is not electronically coupled to EGaIn/Ga$_2$O$_3$ differently than the other. These two β values are, however, not statistically different from each other,

in fact the two linear fit fall between the 95% confidence bands, see Figure 3.7, and therefore β cannot be used to distinguish the two series of SAMs.
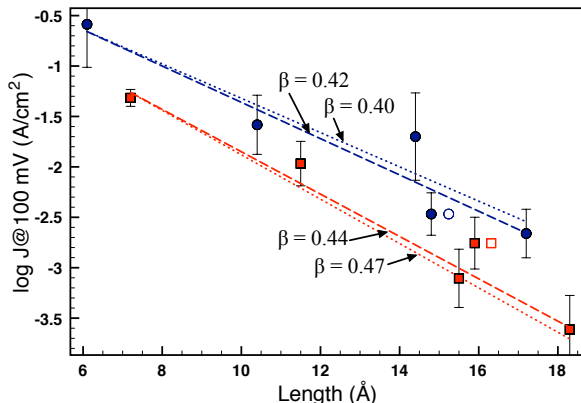
Figure 3.6: Plots of $\log J$ at 100 mV versus molecular length (derived from XPS data) for the Ph-SAM series (red squares) and the Py-SAM series (blue circles). The offset in the X-axis between the two series reflects the 1.1 Å added by the C-H bond in the Ph-SAM series. The fits shown with dashed lines correspond to $J_0 = 1.18$ A/cm^2 and $\beta = 0.44$ Å^{-1} ($R^2 = 0.97$) for the Ph-SAM series and $J_0 = 2.46$ A/cm^2 and $\beta = 0.42$ Å^{-1} ($R^2 = 0.87$) for the Py-SAM series. When PPP2 is omitted (*i.e.*, only the SAMs with odd-numbered carbons are plotted; dotted line) $J_0 = 1.45$ A/cm^2 and $\beta = 0.47$ Å^{-1} ($R^2 = 0.98$). For comparison, the same fit for the Py-SAM series (*i.e.*, omitting PyPP2; dotted line) yields $J_0 = 2.35$ A/cm^2 and $\beta = 0.40$ Å^{-1} ($R^2 = 0.90$). The open circle and open square are the theoretical lengths for PyPP2 and PPP2, respectively, which are larger than the XPS-derived values due to the increased tilt angle as compared to the SAMs with odd-numbered alkane spacers.

Values of J_0 are more difficult to compare, as they are not frequently reported. Reus et al. derived values of J_0 of $\sim 10^2$ A/cm^2 from plots of $\log J$ versus n_C^{-1} for SAMs of alkanethiolates using EGaIn/Ga$_2$O$_3$.[29] Kim et al. determined R_0 (the theoretical resistance at $d = 0$) from the Y-intercept of plots of length (in Å) versus resistance for series of mono- and di-thiol acenes using CP-AFM.[36] While not directly comparable to our results, they found that R_0 was ~ 10x larger for monothiols than for dithiols, and that R_0 decreased as a function of increasing work function of the electrode. They concluded that R_0 (or, analogously, J_0) is sensitive to the degree of electronic coupling of the SAM to the electrodes; physisorbed contacts gave higher values of R_0 (lower values of J_0) than chemisorbed contacts. From these results, I conclude that the values
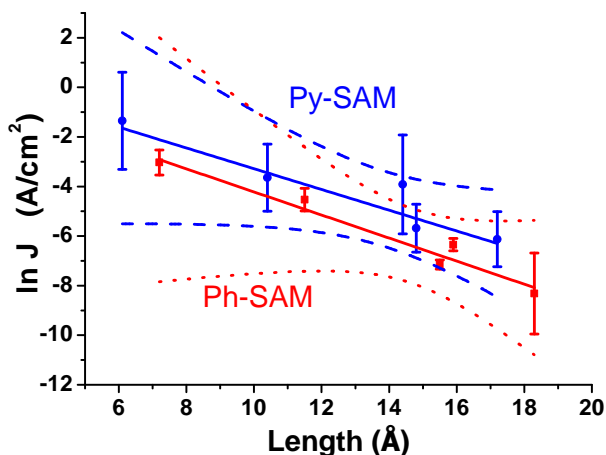
Figure 3.7: The same data as in Figure 2 from the main text, plotted with 99% confidence bands, showing that the two vales of β are within the confidence limit and are therefore statistically indistinguishable.

of J_0 for the Ph-SAM and Py-SAM series are reasonable (*i.e.*, compared to SAMs of alkanethiolates using $EGaIn/Ga_2O_3$) and more importantly that the nitrogen lone pairs of the Py-SAM series do not significantly affect the electronic coupling of the SAM to $EGaIn/Ga_2O_3$ as compared to the Ph-SAM series. It could have been possible that the nitrogen coupling was better, resulting in a overall better interface, however, our results as well as the report from Yoon et al. found no difference in conductance between many head groups (including between phenyl and pyridyl).[8]

In order to compare our results to those of Ishida et al.,[35] I fit the aryl and alkyl portions to Equation 3.1 separately (using theoretical molecular lengths)[35]. The results are listed in the aryl and alkyl entries of Table 3.2 and show that, for both SAMs, β was higher for the alkyl portion than the aryl portion. The value of β for the aryl portion of the Ph-SAMs series is in good agreement with Ishida et al., but the Py-SAM series yielded a significantly smaller value of β. For both series of SAMs, I observed a larger value of β for the alkyl portion. Unfortunately the error associated with J_0 was too high to produce a reasonable value for the alkyl fits. The value of β for the alkane portion of the Ph-SAM series is roughly half of the value measured by Ishidia et al., but their value was also higher than expected. In fact, they made two interesting observations that may be explained by our data and in light of the more complete structural picture

of oligo(phenylene)-alkane SAMs that has emerged in the past decade; i) in contrast to the other SAMs in the Ph-SAM series, the resistance of the SAMs of PPP2 increased as a function of load applied by the AFM tip and ii) the resistance increased dramatically and unexpectedly between PPP1 and PPP2. The first observation makes sense if the odd-even effect is taken into account; applying pressure to the SAMs with odd numbers of methylenes compresses the alkyl portion and presses the aryl groups closer to the gold substrate, reducing the tunneling distance. Due to the increased tilt angle, pressing on PPP2 distorts the sigma framework of the molecules in the SAMs by bending (rather than compressing) the alkane spacers, which hinders tunneling down the backbone.[18] Though I cannot explain the magnitude of the change, the second observation fits with our observation that the decreased torsional angles of the Ph-SAMs with odd numbers of methylenes leads to lower values of J (*i.e.*, higher resistance). While the values of β for the aryl portions of the Ph-SAM and Py-SAM series are within the ranges of literature values ($0.20 - 0.61$ Å^{-1}), the values for the alkyl portions are lower than what has been reported for EGaIn/Ga$_2$O$_3$ on Ag$^{\text{TS}}$ substrates (0.8 Å^{-1}); however, there are too many variables between SAMs of alkanethiolates and the alkyl portion of the Ph-SAM and Py-SAM series to expect perfect agreement (*e.g.*, they pack completely differently).

Table 3.2: Values of β and J_0 for Subsets and Combinations of the Ph-SAM and Py-SAM Series

Trend	Molecules	β (Å^{-1})	J_0 (A/cm^2)
Full series	Ph-SAM	0.44 ± 0.04	1.18 ± 1.44
	Py-SAM	0.42 ± 0.08	2.46 ± 3.00
Odd only	P1, PP1, PPP1, PPP3	0.47 ± 0.04	1.45 ± 1.43
	Py1, PyP1, PyPP1, PyPP3	0.40 ± 0.07	2.35 ± 2.77
Aryl	P1, PP1, PPP1	0.46 ± 0.07	1.32 ± 1.85
	Py1, PyP1, PyPP1	0.32 ± 0.17	1.11 ± 6.00
Alkyl	PPP1, PPP2, PPP3	0.56 ± 0.41	n.d.
	PyPP1, PyPP2, PyPPP3	0.36 ± 0.41	n.d.

To examine the influence of the odd-even effect, I fit the Ph-SAM and Py-SAM series to Equation 3.1 omitting PPP2 and PyPP2 (the fits are shown as dotted lines in Figure 3.6 and summarized in Table 3.2). From these fits I obtained, $J_0 = 1.43 \pm 1.43$ A/cm^2 and $\beta = 0.47 \pm 0.04$ Å^{-1} for the Ph-SAM series and $J_0 = 2.35 \pm 2.77$ A/cm^2 and $\beta = 0.40 \pm 0.07$ Å^{-1} for the Py-SAM series, meaning that β and J_0 increased for the Ph-SAM series and

decreased for the Py-SAM series. Numerically, the reason for these opposing trends is clear; the data for the Py-SAM series in Figure 3.6 are distributed around the linear fit and have larger variances than the data for the Ph-SAMs, which lie almost directly on the fit, except PPP2. I interpret these differences as further evidence that the odd-even effect influences the two series differently. Namely, that the increased tilt-angles for PPP2 and PyPP2 change the orientation of the head groups at the EGaIn/Ga$_2$O$_3$ interface, but that the change in torsional angle—which is more pronounced in the Ph-SAM series—adds the additional influence of the commensurate change to the energy of the HOMO. The differences in the length dependent measurements between the Ph-SAM series and the Py-SAM series are small, but detectible with EGaIn. They arise from the amplification of the influence of the change from C to N induced by packing into a SAM; namely, the odd-even effect influences the torsional angles differently. From these data alone, however, the two series could not be distinguished without prior knowledge of what was being measured. I demonstrated that EGaIn is sensitive enough to detect minor differences in parameters such as β and J_0, but not that it is sensitive enough to actually differentiate the two series. This type of sensitivity requires that EGaIn be able to differentiate subtle differences in the positions of the HOMO (or LUMO) energies with respect to the Fermi level(s) of the electrode(s). Conductance data alone suffer from the same problem encountered by Grave et al.—that these differences are intertwined with other structural parameters (i.e., length dependence and torsional angles.) However, it is clear from these results that even subtle differences in the structure of the SAM affect the transport properties of the junctions. Our studies further emphasize the importance of well characterized SAMs, since deep information about packing, torsional angle, tilt angles and so on are essential to make strong conclusions.

3.2.2 Transition Voltages

The J/V traces, *i.e.*, conductance is not the only information that can be achieved. In addition to the magnitude of J and the values of β, and J_0, J/V curves can provide indirect information about the relative positions of the accessible electronic states of the Ph- and Py-SAMs via the transition voltage, V_{trans}, which is derived either from inflection points in $\log-\log I/V$ plots or the minima of plots of $ln(I/V^2)$ versus $1/V$ (*i.e.*, Fowler-Nordheim plots) of each SAM. Also called transition voltage spectroscopy (TVS), values of V_{trans} were first compared in SAMs by Beebe et al. [37,38] as a method for measuring

ϕ (the barrier height) in metal-molecule-metal (MMM) junctions. Though the initial interpretation of V_{trans} as a transition to Fowler-Nordheim tunneling was challenged by Huisman et al. [39], the simplicity of TVS has piqued the interest of both theorists and experimentalists working with MMM junctions. [36,40–47] Experimental data for aliphatic and conjugated SAMs from crossed-wire and CP-AFM measurements have shown that (above a certain length) V_{trans} is independent of length for alkanethiols, but not for oligo(phenyleneethynylene) (OPE) thiols and that V_{trans} is sensitive to the work function of the substrate/CP-AFM tip for OPE thiols. [38] These data imply that V_{trans} is sensitive to the difference between the work function of the metal, Φ, and the energy of the frontier orbital closest in energy to Φ (E_{HOMO} for OPEs). A followup study found a linear dependence of V_{trans} on the difference between the Fermi energy of the substrate/CP-AFM tip, E_f, and the onset of E_{HOMO} for oligo(acenes) as determined by the divergence between the UPS spectra of the bare metal and the metal supporting a SAM of the oligo(acene). [36] Combined with theoretical studies, there is growing evidence that V_{trans} is directly related to $E_f - E_{orbital}$ (where orbital is either HOMO or LUMO). A recent study by Ricœur et al. measured V_{trans} in a variety of alkane-based monolayers with CP-AFM, Hg drops, EGaIn, and vacuum-deposited Al. [9] They found that, within (in some cases a rather substantial) error, EGaIn, Hg, and Al always produced values of $-0.3 < V_{trans} < 0.3$ whereas CP-AFM produced values of $-1.3 < V_{trans} < 1.3$. The authors describe this discrepancy to the presence of an oxide in EGaIn, Hg, and Al, suggesting that V_{trans} was related to the difference between E_{LUMO} and the conduction bands of the oxides present on these electrodes. This interpretation assumes a lot of similarities between native Ga_2O_3, HgO, and Al_2O_3, despite the unique nature of EGaIn/Ga_2O_3; [23,48] however, their data do clearly show consistently lower values of V_{trans} for EGaIn than CP-AFM measurements. Thus, the Ph-SAM and Py-SAM series provide a perfect opportunity to probe how sensitive V_{trans} is to electronic structure. Based on the assumption by Ricœur et al. if V_{trans} is only a measure of the offset between Φ_{Au} and Ga_2O_3, in our case both the Ph-SAM and Py-SAM series should yield values of $V_{trans} \sim 0.3$ V and TVS should be even less effective at differentiating the two series than the conductance/length dependence data.

I calculated $V_{trans}(+)$ by re-plotting the raw I/V data as $ln(I/V^2)$ versus $1/V$ and determining the minimum for positive biases and made histograms of these values for each SAM, histograms fitted to Gaussian distribution. Two examples of distribution of

$V_{trans}(+)$ are represented in Figure 3.8. As above mentioned the V_{trans} is determine from the minimum, as is shown in Figure 3.9.
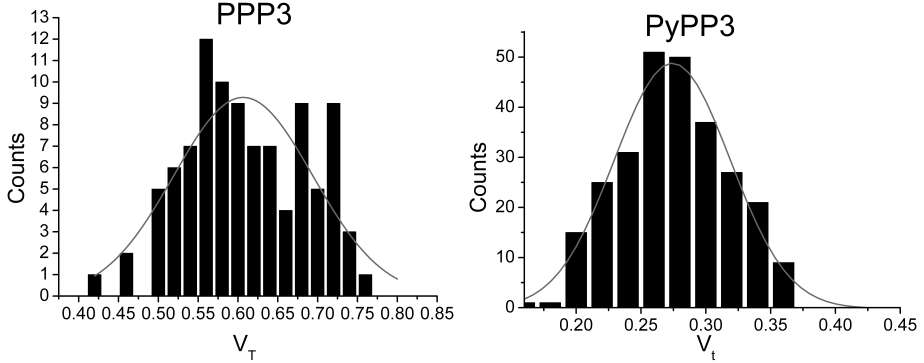
Figure 3.8: Representative histograms of $V_{trans}(+)$, for SAMs of PPP3 and PyPP3. The log-normal distribution of V_{trans} allows fitting with a Gaussian function. I found this method to be superior to deriving $V_{trans}(+)$ plots of mean values of J vs V, which obfuscates the true distribution of V_{trans}.
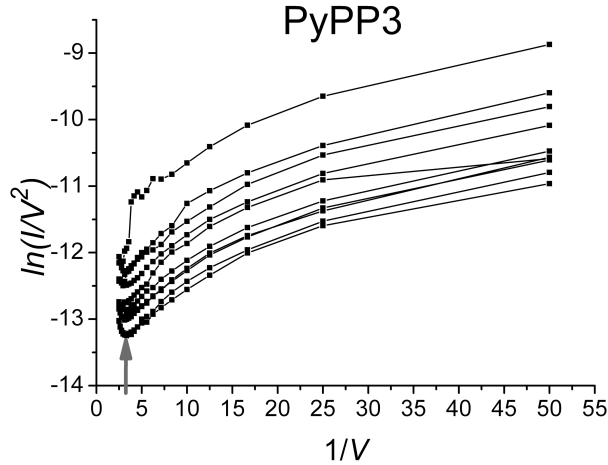
Figure 3.9: Representative Fowler-Nordheim plots of 10 traces for SAMs of PyPP3. The arrow shows the minima in these plots ($V_{trans}(+)$) which I used to construct the histograms in Figure 3.8.

I found $V_{trans}(+) \sim 0.6$ V for the Py-SAM series and $V_{trans}(+) \sim 0.3$ V for the

Ph-SAM series which suggests that V_{trans} for these SAMs does in fact depend on the properties of the molecules and not only on Φ_{Au} and Ga_2O_3 and therefore is capable of differentiating the Ph-SAM series from the Py-SAM series without any prior knowledge of what was being measured. One possible explanation for this difference is partial charge-transfer between the lone pairs of the nitrogens in the Py-SAM series and Ga_2O_3, but such an interaction should affect J and β. Other studies have also found that the electronic properties of the SAM and not the Ga_2O_3 layer dominate the transport properties in EGaIn junctions.[6] Thus, the ~ 0.3 V difference in V_{trans} between the Ph-SAM and Py-SAM series most likely does not originate from the Ga_2O_3//SAM interface. To determine whether the effect on V_{trans} is related to the energies of the frontier orbitals, we determined E_{HOMO} using DFT/B3LYP calculations with Gaussian 03 on a 12-CPU GNU/Linux cluster. Molecular structures were first minimized by AM1. The torsional angles, θ, were then fixed to known values in SAMs and then the point-energies calculated DFT using the B3LYP/6-311+g(2d,2p) basis set. In accordance to literature procedures, the hydrogen atoms were removed from the thiol groups before calculating the dipole moments, μ.[49] The net perpendicular dipole moment, $\mu_\perp$, was calculated by summing the contributions along the X and Z axes (Y lies completely parallel to the substrate) using the formula $\mu_\perp = \mu_{x,z} \cos \alpha$ where α is the tilt angle along the respective axis.[50] Figure 3.5 shows the densities of the HOMO orbitals for the Ph-SAM and Py-SAM series and Table 3.3 is a summary of the parameters for and results of the DFT calculations. Figure 3.4 is a plot of the calculated energies of the HOMO levels as a function of XPS-derived SAM thickness along with the linear fits of $J = J_0 e^{-\beta d}$ from Figure 3.6 showing that the HOMO energies track very closely with the length of the molecules and that the presence of the nitrogen atom in the Py-SAM series shifts the values more negative, but does not substantially affect the overall trend.

DFT calculations done on molecules in the gas phase do not perfectly capture their properties in SAMs, but by calculating the Ph-SAM and Py-SAM series in the geometries that they adopt in SAMs, I compensate for many of the discrepancies. I assumed that E_{LUMO} is too far in energy from Φ_{Au} to participate significantly in charge transport. To account for the decreased torsional angles induced by packing in a SAM, I used values from detailed studies of alkyl-substituted oligo(phenylene)s[22] and the Py-SAM series.[25] The results of these calculations are plotted along with values of $\log J$ at 100 mV in Figure 3.10 and show that the Py-SAM series is slightly more conductive and

Molecule	E_{HOMO} (eV)[a]	μ_X (D)[b]	μ_Z (D)[b]	$\mu_\perp$ (D)[b]	α_x (°)[c]	α_z (°)[c]	θ (°)[d]	$N \times 10^{18}$ (m^{-2})[c]
P1	−6.43	0.97	−1.16	1.46	0.26	1.31	5	4.30
PP1	−6.14	1.08	−1.29	1.63	0.26	1.31	5	4.20
PPP1	−5.75	1.11	−1.35	1.68	0.26	1.31	5	4.20
PPP2	−5.94	1.65	−0.06	1.28	0.68	1.31	18	3.10
PPP3	−5.74	0.53	−1.28	1.50	0.26	0.89	5	4.20
Py1	−6.87	−1.49	−1.77	−2.24	0.26	1.31	5	4.30
PyP1	−6.60	−2.01	−1.58	−2.47	0.26	1.31	5	4.20
PyPP1	−6.31	−2.07	−1.45	−2.46	0.26	1.31	5	4.20
PyPP2	−6.19	−1.68	−0.15	−1.316	0.68	0.89	27	3.10
PyPP3	−6.08	−2.77	−1.71	−3.23	0.26	1.31	5	4.20

[a] Calculated with the thiol hydrogen intact
[b] Calculated with the thiol hydrogen removed [49]
[c] Experimental values from the literature [18,25,51]
[d] Combined theoretical and experimental values from the literature [18,19,22,25,26,51,52]

Table 3.3: Parameters for and results of B3LYP/6-311+g(2d,2p) DFT calculations of the Ph-SAM and Py-SAM series.

has slightly deeper HOMO levels than the Ph-SAM series, though the majority of the molecules overlap in both values of $\log J$ and E_{HOMO}; only Py1, PPP1, and PPP3 lie outside the range of overlapping values of both E_{HOMO} and $\log J$. The close correlation between $\log J$ and E_{HOMO} I believe is just coincidence, since there is no reason why that should be the case; the magnitude of J is dominated by the length of the molecules (*i.e.*, tunneling currents flow along the backbones of the molecules) at 100 mV and the values of E_{HOMO} follow the length of the molecules, see Figure 3.4. Though the inflection points at PPP2, which has a much higher torsional angle due to an odd-even effect in the alkyl tails, are probably related—*i.e.*, the deviation from length dependence in the Ph-SAM series at PPP2 could arise from the influence of E_{HOMO}. In any case, the presence of a nitrogen atom in the Py-SAM series shifts V_{trans} by 0.3 V compared to the Ph-SAM series, which is not reflected in any systematic differences between J or E_{HOMO} for the two series. Therefore I deduce that the nitrogen atom is affecting some other property of the SAMs in the junctions which had not been considered previously.

3.2.3 The Influence of Dipole Moments

The last remaining molecular property that is likely to vary significantly between the Py-SAM and Ph-SAM series is dipole moment. Metal-thiol bonds produce a dipole moment that is dependent only on the metal and thus is invariant across both series.
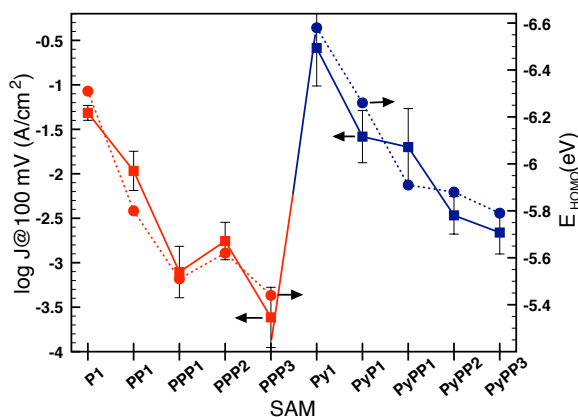
Figure 3.10: Plots of $\log J$ at 100 mV taken from Figure 3.3 (squares, solid line; left axis) and DFT-calculated E_{HOMO} (circles, dashed line; right axis) of the molecule from Scheme 3.1 that forms each SAM listed on the X-axis. The values of E_{HOMO} were calculated using torsional angles derived from experiment and calculation. This plot does not imply that the trends in J are the direct result of the trends in E_{HOMO}, but shows that neither E_{HOMO} nor J follow the same trend as V_{trans} (i.e., because J and E_{HOMO} are nearly equal for several SAMs from different series).

The inclusion of a nitrogen atom at the head of the molecules in the Py-SAM series is, however, expected to create a dipole moment that is inverse to and larger in magnitude than the dipole moment in the Ph-SAM series. These molecular dipole moments likely have little influence on the transport properties of single-molecule MMM junctions, but their collective action in a SAM can have a strong influence on the vacuum level at the surface of the metal, shifting Φ significantly.[49,50,53,54] In the case of alkanethiols the metal-thiol dipole dominates and since it is constant across alkanes of any length, it is typically ignored in charge transport studies. In their discussion of the influence of Φ on V_{trans}, Kim et al. ascribe the shifts in Φ upon adsorption of the SAMs of oligo(acene)s to the bond dipole arising from the metal-thiol bond, which dominate the net dipole moment of the SAM because, much like the Ph-SAM series, oligo(acene)s do not possess a strong inherent dipole moment.[36] Thus, as is typically the case, the influence of these dipoles is considered a constant and is not discussed further in the context of tunneling transport or V_{trans}. In our case, I am varying the dipole moments of the series of SAMs, while keeping the metals in the MMM junction constant. I measured the shift in

work function, $\Delta\Phi$, using a Kelvin probe referenced to highly ordered pyrolytic graphite (HOPG) by comparing the value obtained by measuring bare Au^{TS} to Au^{TS} bearing the Ph-SAM and Py-SAM series. These measurements determine the surface potential of the Au^{TS}/SAM surfaces, from which $\Delta\Phi$ is calculated. To gain insight into the vacuum level shift inside an Au^{TS}/SAM//Ga_2O_3/EGaIn junction, I calculated the Fermi energy, E_f, according to de Boer et al. [50] using Equation 3.2 where N is the density of molecules in the SAM, $\mu_{\perp,SAM}$ and μ_{M-S} are the net dipole moment perpendicular to the substrate from the SAM and the metal-thiolate bond respectively, $\mu_{\perp,SAM} = \mu_{molecule}\cos\alpha$, where α is the tilt angle, and κ_{SAM} and κ_{M-S} are the dielectric constants of the SAM and metal-thiolate layer.

$$E_f = \Phi_{Au} + N\left(\frac{\mu_{\perp,SAM}}{\epsilon_0\kappa_{SAM}} + \frac{\mu_{M-S}}{\epsilon_0\kappa_{M-S}}\right) \tag{3.2}$$

This calculation assumes that the shift in Φ occurs primarily at the SAM/Au^{TS} interface because the (free carriers in the) band structure of the Ga_2O_3 layer screens the influence of the SAM from the bulk Ga-In. I used experimental values for N and α [18,25] and used experimentally-derived values of $\frac{\mu_{M-S}}{\epsilon_0\kappa_{M-S}} = -0.5$ eV. [49] I estimated $\kappa_{SAM} = 2$ for the Ph-SAM series ($\kappa_{benzene} \sim 2$) and $\kappa_{SAM} = 5$ for the Py-SAM series ($\kappa_{pyridine} \sim 10$). (In reality, κ varies from SAM to SAM, but in the absence of a reliable way to measure κ, I used estimations, which is common practice.) The experimental and calculated values are shown in Table 3.4 along with the measured values of $V_{trans}(+)$ determined from Gaussian fits as described above. I decided to use 2σ as error, instead of the more often used σ, to cover a probability interval equal to 95.4% instead of only 68%. This analysis means that the next value of $V_{trans}(+)$ measured would have a 95.4% probability of lying within the interval $\mu \pm 2\sigma$. There are no obvious trends in the calculated or measured data except that the Ph-SAM series produces values of V_{trans} that are ~ 0.3 V larger than those of the Py-SAM series and that the two series give values of $\Delta\Phi$ of opposite signs. In all cases E_f over-estimates the influence of the dipoles as compared to Φ, which is normal for this calculation. [50]

Figure 3.11 is a plot of V_{trans} versus $\Delta\Phi$ (from Table 3.4). The plot is roughly linear, fitting to $y = 0.51x + 0.44$ with $R^2 = 0.81$, demonstrating that V_{trans} is influenced by the shift in vacuum level induced by the dipoles of the SAM—i.e., V_{trans} varies with Φ. Beebe et al. observed a similar trend with SAMs of OPE thiols by varying

SAM on Au$^{\mathrm{TS}}$	$\lvert E_f \rvert$ (eV)	$\lvert \Phi \rvert$ (eV)	$\Delta\Phi$ (eV)	$V_{trans} \pm 2\sigma$ (+V)
Blank	-	4.77	0	-
P1	4.12	4.45	+0.32	0.64 ± 0.10
PP1	4.01	4.58	+0.19	0.60 ± 0.12
PPP1	3.97	4.47	+0.30	0.55 ± 0.10
PPP2	4.55	4.43	+0.34	0.57 ± 0.14
PPP3	4.12	4.73	+0.05	0.61 ± 0.18
Py1	6.02	5.00	−0.23	0.36 ± 0.06
PyP1	6.08	4.88	−0.11	0.34 ± 0.06
PyPP1	6.08	4.99	−0.22	0.25 ± 0.08
PyPP2	5.67	5.01	−0.24	0.33 ± 0.06
PyPP3	6.32	5.16	−0.39	0.27 ± 0.08

Table 3.4: Calculated Fermi energies (E_f), measured work functions (Φ), work functions shift upon surface modification ($\Delta\Phi$), and measured V_{trans} (+) of the Ph-SAM and Py-SAM series on Au$^{\mathrm{TS}}$.

the work function of the metal in CP-AFM measurements.[38] If the interpretation of TVS in EGaIn/Ga$_2$O$_3$ junctions by Ricœur et al. is correct, then the linearity of this plot is a result of the shift in Φ_{Au} with respect to the conduction band of Ga$_2$O$_3$. They observed that $V_{trans} \sim 0.3$ V for alkanethiols (except C18) on Au[9] for which $\Delta\Phi = +0.8$ (the value reported is -0.8 eV, however, I used the opposite sign convention for Φ), measured by Kelvin probe, identically to our data[50]. The largest value of $\Delta\Phi$ for our series is $+0.34$ eV (PPP2), for which I measured $V_{trans} = 0.57 \pm 0.14$. Furthermore, the trend in our data predicts $V_{trans} = 0.85$ at $\Delta\Phi = +0.8$, which is lower than, but in good agreement with values reported for hydrocarbons on gold using both CP-AFM and PEDOT:PSS top contacts.[38,45] I also measured $V_{trans} \sim 0.5$ V for SAMs of hexadecanethiolate using EGaIn, which is well within the range of 0.37 ± 0.33 reported by Ricœur et al. From these data it is apparent that V_{trans} may be dominated by the energy difference between Φ_{Au} and the bands of Ga$_2$O$_3$ for SAMs of alkanethiolates, but clearly not for the Ph-SAM or Py-SAM series. I hypothesize that, when E_{HOMO} is sufficiently far (*i.e.*, decoupled) from the Fermi level of the gold electrode, V_{trans} is dominated by the offset between Φ_{Au} and Ga$_2$O$_3$; this is the situation with all alkanethiolates. With the Ph-SAM and Py-SAM series, however, E_{HOMO} is close enough to the Fermi level of the gold electrode that it influences V_{trans}.
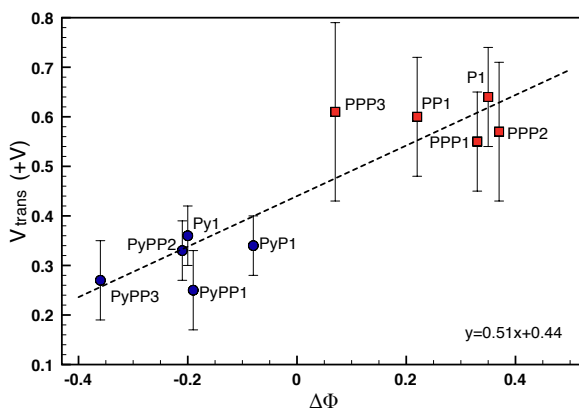
Figure 3.11: Plots of V_{trans} versus the measured shift in work function, $\Delta\Phi$ (from Table 3.4), for the Ph-SAM (red squares) and Py-SAM (blue circles) series. The parameters of the linear fit (dashed line) are shown in the lower right ($R^2 = 0.81$). The error bars are $\pm 2\sigma$. These data show that V_{trans} varies approximately linearly with $\Delta\Phi$, which directly influences $E_f - E_{\text{HOMO}}$.

For symmetrical Metal/SAM/Metal junctions (*i.e.*, lacking an oxide layer), V_{trans} is most likely related to the difference in energy between the tail of the distribution of E_{orbital} (E_{HOMO} for the Ph-SAM and Py-SAM series) and the Fermi energy of the electrodes.[40,41,47] To gain insight into the influence of E_{HOMO} on V_{trans} for the Ph-SAM and Py-SAM series, I plotted V_{trans} versus $E_f - E_{\text{HOMO}}$ (from Table 3.4 and Figure 3.10), which I referenced to UPS data from a previous study of PPP3.[55] Figure 3.12 is a plot of these data, showing a similar trend to Figure 3.11 except that the fit is, $y = 0.17x + 0.19$, $R^2 = 0.92$, and the order of the SAMs is different. If we assume that V_{trans} is correlated to $E_{\text{HOMO,onset}}$ (*i.e.*, the tail of E_{HOMO}, which is $\sim 30\%$ of the peak value) and multiply the X-axis by 0.3, the fit changes to $y = 0.58x + 0.19$ which is remarkably close to the fit to values of $E_{\text{HOMO,onset}}$ measured by UPS, $y = 0.55x + 0.26$, $R^2 = 0.92$, reported by Kim et al.[36] Many assumptions were used calculating both E_f and E_{HOMO}, not the least of which is κ_{SAM}, however, DFT/B3LYP calculations of $\mu_{\perp,SAM}$ for alkanethiolates[49] and of E_{HOMO} for oligo(phenylene)-alkanethiols[55] have been shown to agree closely with UPS data. I am confident that this simple method of calculating $E_f - E_{\text{HOMO}}$ (provided accurate conformational data are available for the SAM) is a valid estimation of the combined influences of dipole moments and

orbital energies on V_{trans}. Furthermore, in combination with the Kelvin probe data, I demonstrate that V_{trans} for the Ph-SAM and Py-SAM series is dominated by the intrinsic properties of the molecules in the SAM and not simply the Fermi energy of the substrate and the valence/conduction bands of Ga_2O_3, adding V_{trans} to the growing body of evidence that "the SAM, not the electrodes, dominates charge transport in metal-monolayer//Ga_2O_3/gallium–indium eutectic junctions." [6]
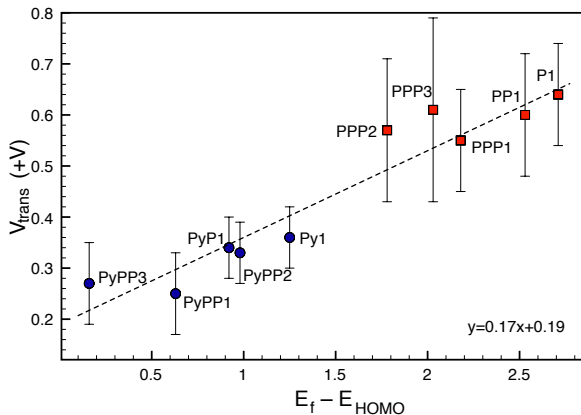
Figure 3.12: Plots of V_{trans} versus the calculated values of $E_f - E_{\mathrm{HOMO}}$, which are referenced to UPS data for PPP3. The parameters of the linear fit (dashed line) are shown in the lower right ($R^2 = 0.92$). The error bars are $\pm 2\sigma$. If $E_f - E_{\mathrm{HOMO}}$ is adjusted to simulate values of $E_{\mathrm{HOMO,onset}}$ from UPS data, the fit becomes $y = 0.58x + 0.19$.

3.3 Conclusions

In this chapter I have demonstrated unambiguously that tunneling junctions based on $EGaIn/Ga_2O_3$ are sensitive enough to discriminate between two series of SAMs that differ by the substitution of C-H to N. Conductance data (J/V curves) and length dependence (β and J_0) are barely sufficient to differentiate the two series, Ph-SAM and Py-SAM, but the differences are subtle and require prior knowledge of the two series being measured; by removing the colors from Figure 3.3, the J/V data are overlapping and therefore could not be distinguished. Re-plotting the J/V data to derive V_{trans}, however, provides a clear distinction between the two series—V_{trans} differs by ~ 0.3

V—without any prior knowledge. Thus, $EGaIn/Ga_2O_3$ has enough sensitivity that can be used to distinguish between and differentiate two series of SAMs that differ by the substitution of a carbon atom for a nitrogen atom. I have shown that $EGaIn/Ga_2O_3$ is sensitive not only to subtle variations in tilt and torsional angle, but more important to the substitution of single atoms. Furthermore, these subtle changes are brought about by the inclusion of the molecules in a SAM. A single-molecule study of the Ph-SAM and Py-SAM series would likely yield entirely different results as the torsional angles would not be reduced by packing in a SAM and the influence of dipoles on vacuum level is a collective property of SAMs. This observation highlights the importance of considering the differences between SAMs, which are far more practical for potential applications, from single-molecule studies, which are more relevant to spectroscopy and theory. The observation that V_{trans} varies with the surface potentials (*i.e.*, $\Delta\Phi$) measured by Kelvin probe highlights the importance of considering the influence of dipole moments on the vacuum level as ME studies move towards complex molecules. I observed a linear relationship ($R^2 = 0.92$) between V_{trans} and the offset of the Fermi energy of Au and the HOMOs of the Ph-SAM and Py-SAM series using straightforward DFT calculations to estimate the HOMO levels and the shift in vacuum level induced by the dipole moments of the SAMs. Our calculations rely heavily on experimentally-derived parameters, of which there is an abundance for SAMs of oligo(phenylene)-alkanethiols, but they are dramatically simpler than pure theoretical methods for calculating V_{trans} and are therefore accessible to physical-organic chemists working in ME.

Bibliography

[1] E. A. Weiss, G. K. Kaufman, J. K. Kriebel, L. Li, R. Schalek, and G. M. Whitesides. Si/SiO_2-Templated formation of ultraflat metal surfaces on glass, polymer, and solder supports: Their use as substrates for Self-Assembled monolayers. *Langmuir*, 23(19):9686–9694, 2007.

[2] H. J. Yoon, N. D. Shapiro, K. M. Park, M. M. Thuo, S. Soh, and G. M. Whitesides. The rate of charge tunneling through self-assembled monolayers is insensitive to many functional group substitutions. *Angew. Chem.*, 51(19):4658–4661, May 2012.

[3] R. L. Carroll and C. B. Gorman. The genesis of molecular electronics. *Angew. Chem. Int. Ed.*, 41(23):4378–4400, 2002.

[4] J. C. Love, L. A. Estroff, J. K. Kriebel, R. G. Nuzzo, and G. M. Whitesides. Self-assembled monolayers of thiolates on metals as a form of nanotechnology. *Chem. Rev.*, 105(4):1103–1170, 2005.

[5] S. L. Bernasek. Can We Understand the Molecule in Molecular Electronics? *Angew. Chem. Int. Ed.*, 51(39):9737–9738, August 2012.

[6] W. F. Reus, M. M. Thuo, N. D. Shapiro, C. A. Nijhuis, and G. M. Whitesides. The sam, not the electrodes, dominates charge transport in metal-monolayer//ga_2o_3/gallium–indium eutectic junctions. *ACS Nano*, 6(6):4806–4822, 2012.

[7] M. M. Thuo, W. F. Reus, F. C. Simeone, C. Kim, M. D. Schulz, H. J. Yoon, and G. M. Whitesides. Replacing -CH_2CH_2- with -CONH- Does Not Significantly Change Rates of Charge Transport through Ag TS-SAM//Ga_2O_3/EGaIn Junctions. *J. Am. Chem. Soc.*, 134(26):10876–10884, 2012.

[8] H. J. Yoon, N. D. Shapiro, K. M. Park, M. M. Thuo, S. Soh, and G. M. Whitesides. The rate of charge tunneling through self-assembled monolayers is insensitive to many functional group substitutions. *Angew. Chem. Int. Ed.*, 51(19):4658–4661, May 2012.

[9] G. Ricœur, S. Lenfant, D. Guérin, and D. Vuillaume. Molecule/electrode interface energetics in molecular junction: A "transition voltage spectroscopy" study. *J. Phys. Chem. C*, 116(39):20722–20730, 2012.

[10] M. M. Thuo, W. F. Reus, C. A. Nijhuis, J. R. Barber, C. Kim, M. D. Schulz, and G. M. Whitesides. Odd-even effects in charge transport across self-assembled monolayers. *J. Am. Chem. Soc.*, 133(9):2962–2975, 2011.

[11] C. A. Nijhuis, W. F. Reus, A. C. Siegel, and G. M. Whitesides. A molecular half–wave rectifier. *J. Am. Chem. Soc.*, 133(39):15397–15411, 2011.

[12] C. A. Nijhuis, W. F. Reus, and G. M. Whitesides. Molecular rectification in Metal-SAM-Metal Oxide-Metal junctions. *J. Am. Chem. Soc.*, 131(49):17814–17827, December 2009.

[13] C. A. Nijhuis, W. F. Reus, and G. M. Whitesides. Mechanism of rectification in tunneling junctions based on molecules with asymmetric potential drops. *J. Am. Chem. Soc.*, 132(51):18386–18401, 2010.

[14] A. M. Masillamani, N. Crivillers, E. Orgiu, J. Rotzler, D. Bossert, R. Thippeswamy, M. Zharnikov, M. Mayor, and P. Samorì. Multiscale Charge Injection and Transport Properties in Self-Assembled Monolayers of Biphenyl Thiols with Varying Torsion Angles. *Chem. Eur. J.*, 18(33):10335–10347, July 2012.

[15] D. Fracasso, H. Valkenier, J. C. Hummelen, G. C. Solomon, and Ryan C. Chiechi. Evidence for Quantum Interference in SAMs of Arylethynylene Thiolates in Tunneling Junctions with Eutectic Ga-In (EGaIn) Top-Contacts. *J. Am. Chem. Soc.*, 133(24):9556–9563, May 2011.

[16] T. Leung, P. Schwartz, G. Scoles, F. Schreiber, and A. Ulman. Structure and growth of 4-methyl-4-mercaptobiphenyl monolayers on Au (111): a surface diffraction study. *Surf. Sci.*, 458(1):34–52, 2000.

[17] W. Azzam, P. Cyganik, G. Witte, M. Buck, and Ch. Wöll. Pronounced odd–even changes in the molecular arrangement and packing density of biphenyl–based thiol sams: A combined stm and leed study. *Langmuir*, 19(20):8262–8270, 2003.

[18] W. Azzam, A. Bashir, A. Terfort, T. Strunskus, and C. Wöll. Combined stm and ftir characterization of terphenylalkanethiol monolayers on au(111): Effect of alkyl chain length and deposition temperature. *Langmuir*, 22(8):3647–3655, 2006.

[19] Y. Long, H. Rong, M. Buck, and M. Grunze. Odd-even effects in the cyclic voltammetry of self-assembled monolayers of biphenyl based thiols. *J. Electroanal. Chem.*, 524–525:62–67, 2002.

[20] P. Cyganik, G. Witte, M. Buck, and C. Wöll. Pronounced odd-even changes in the molecular arrangement and packing density of biphenyl-based thiol SAMs: A combined STM and LEED study. *Langmuir*, 2003.

[21] P. Bordat and R. Brown. A molecular model of p-terphenyl and its disorder-order transition. *Chem. Phys.*, 246:323–334, 1999.

[22] G. Heimel, L. Romaner, J.-L. Bredas, and E. Zojer. Odd-Even Effects in Self-Assembled Monolayers of ω–(Biphenyl–4–yl)alkanethiols: A First-Principles Study. *Langmuir*, 24(2):474–482, January 2008.

[23] L. Cademartiri, M. M. Thuo, C. A. Nijhuis, W. F. Reus, S. Tricard, J. R. Barber, R. N. S. Sodhi, P. Brodersen, C. Kim, R. C. Chiechi, and G. M. Whitesides. Electrical Resistance of Ag TS–S(CH$_2$)$_{n-1}$CH$_3$//Ga$_2$O$_3$/EGaIn Tunneling Junctions. *J. Phys. Chem. C*, 116(20):10848–10860, May 2012.

[24] M. I. Muglali, A. Bashir, A. Terfort, and M. Rohwerder. Electrochemical investigations on stability and protonation behavior of pyridine-terminated aromatic self-assembled monolayers. *Phys. Chem. Chem. Phys.*, 13:15530–15538, 2011.

[25] J. Liu, B. Schuepbach, A. Bashir, O. Shekhah, A. Nefedov, M. Kind, A. Terfort, and C. Wöll. Structural characterization of self-assembled monolayers of pyridine-terminated thiolates on gold. *Phys. Chem. Chem. Phys.*, 12(17):4459–4472, 2010.

[26] J. Liu, L. Stratmann, S. Krakert, M. Kind, F. Olbrich, A. Terfort, and C. Wöll. A study on oxygen reduction inhibition at pyridine-terminated self assembled monolayer modified Au (111) electrodes. *J. Electron Spec. Rel. Phen.*, 172(1-3):793–800, April 2009.

[27] C. Grave, C. Risko, A. Shaporenko, Y. Wang, C. Nuckolls, M. A. Ratner, M. A. Rampi, and M. Zharnikov. Charge Transport through Oligoarylene Self-assembled Monolayers: Interplay of Molecular Organization, Metal–Molecule Interactions, and Electronic Structure. *Adv. Funct. Mater.*, 17(18):3816–3828, December 2007.

[28] J. G. Simmons. Generalized formula for the electric tunnel effect between similar electrodes separated by a thin insulating film. *Appl. Phys. Lett.*, 34(6):1793–1803, 1963.

[29] W. F. Reus, C. A. Nijhuis, J. R. Barber, M. M. Thuo, S. Tricard, and G. M. Whitesides. Statistical tools for analyzing measurements of charge transport. *J. Phys. Chem. C*, 116(11):6714–6733, 2012.

[30] H. Song, Y. Kim, H. Jeong, M. A. Reed, and T. Lee. Coherent Tunneling Transport in Molecular Junctions. *J. Phys. Chem. C*, 114(48):20431–20435, December 2010.

[31] W. Y. Wang, T. Lee, and M. A. Reed. Mechanism of Electron Conduction in Self-Assembled Alkanethiol Monolayer Devices. *Phys. Rev. B*, 68(3):035416–1–035416–7, 2003.

[32] E. A. Weiss, Chiechi R. C., Kaufman G. K., Kriebel J. K., Li Z., Duati M., Rampi M. A., and Whitesides G. M. Influence of defects on the electrical characteristics of Mercury-Drop junctions: Self-Assembled monolayers of n-Alkanethiolates on rough and smooth silver. *J. Am. Chem. Soc.*, 129(14):4336–4349, April 2007.

[33] A. J. Kronemeijer, E. H. Huisman, H. B. Akkerman, A. M. Goossens, I. Katsouras, P. A. van Hal, T. C. T. Geuns, S. J. van der Molen, P. W. M. Blom, and D. M. de Leeuw. Electrical characteristics of conjugated self-assembled monolayers in large-area molecular junctions. *Appl. Phys. Lett.*, 97(17):173302–173302–3, 2010.

[34] R. E. Holmlin, R. Haag, M. L. Chabinyc, R. F. Ismagilov, A. E. Cohen, A. Terfort, M. A. Rampi, and Whitesides G. M. Electron transport through thin organic films in Metal-Insulator-Metal junctions based on Self-Assembled monolayers. *J. Am. Chem. Soc.*, 123(21):5075–5085, 2001.

[35] T. Ishida, W. Mizutani, Y. Aya, H. Ogiso, S. Sasaki, and H. Tokumoto. Electrical Conduction of Conjugated Molecular SAMs Studied by Conductive Atomic Force Microscopy. *J. Phys. Chem. B*, 106(23):5886–5892, June 2002.

[36] B. Kim, S. H. Choi, X. Y. Zhu, and C. D. Frisbie. Molecular Tunnel Junctions Based on π-Conjugated Oligoacene Thiols and Dithiols between Ag, Au, and Pt Contacts: Effect of Surface Linking Group and Metal Work Function. *J. Am. Chem. Soc.*, 133(49):19864–19877, December 2011.

[37] J. M. Beebe, B. Kim, J. Gadzuk, D. C. Frisbie, and J. G. Kushmerick. Transition from Direct Tunneling to Field Emission in Metal-Molecule-Metal Junctions. *Phys. Rev. Lett.*, 97(2):26801, July 2006.

[38] J. M. Beebe, B. Kim, C. D. Frisbie, and J. G. Kushmerick. Measuring relative barrier heights in molecular electronic junctions with transition voltage spectroscopy. *ACS Nano*, 2(5):827–832, 2008.

[39] E. H. Huisman, C. M. Guedon, B. J. van Wees, and S. J. van der Molen. Interpretation of Transition Voltage Spectroscopy. *Nano Lett.*, 9(11):3909–3913, 2009.

[40] M. Araidai and M. Tsukada. Theoretical calculations of electron transport in molecular junctions: Inflection behavior in Fowler-Nordheim plot and its origin. *Phys. Rev. B*, 81(23), June 2010.

[41] J. Chen, T. Markussen, and K. Thygesen. Quantifying transition voltage spectroscopy of molecular junctions: Ab initio calculations. *Phys. Rev. B*, 82(12):121412–1–121412–4, September 2010.

[42] F. Mirjani, J. Thijssen, and S. J. van der Molen. Advantages and limitations of transition voltage spectroscopy: A theoretical analysis. *Phys. Rev. B*, 84(11):115402–1–115402–8, September 2011.

[43] G. Wang, T.-W. Kim, G. Jo, and T. Lee. Enhancement of Field Emission Transport by Molecular Tilt Configuration in MetalMoleculeMetal Junctions. *J. Am. Chem. Soc.*, 131(16):5980–5985, April 2009.

[44] N. Bennett, G. Xu, L. J. Esdaile, H. L. Anderson, J. E. Macdonald, and M. Elliott. Transition Voltage Spectroscopy of Porphyrin Molecular Wires. *Small*, 6(22):2604–2611, October 2010.

[45] G. Wang, Y. Kim, S.-I. Na, Y. H. Kahng, J. Ku, S. Park, Y. H. Jang, D.-Y. Kim, and T. Lee. Investigation of the Transition Voltage Spectra of Molecular Junctions Considering Frontier Molecular Orbitals and the Asymmetric Coupling Effect. *J. Phys. Chem. C*, 115(36):17979–17985, September 2011.

[46] K. Smaali, N. Clément, G. Patriarche, and D. Vuillaume. Conductance Statistics from a Large Array of Sub-10 nm Molecular Junctions. *ACS Nano*, 6(6):4639–4647, June 2012.

[47] I. Bâldea. Ambipolar transition voltage spectroscopy: Analytical results and experimental agreement. *Phys. Rev. B*, 85(3):035442–1–035442–5, January 2012.

[48] M. D. Dickey, R. C. Chiechi, R. J. Larsen, E. A. Weiss, D. A. Weitz, and G. M. Whitesides. Eutectic Gallium-Indium (EGaIn): A Liquid Metal Alloy for the Formation of Stable Structures in Microchannels at Room Temperature. *Adv. Funct. Mater.*, 18(7):1097–1104, April 2008.

[49] D. M. Alloway, M. Hofmann, D. L. Smith, N. E. Gruhn, A. L. Graham, R. Colorado, V. H. Wysocki, T. R. Lee, P. A. Lee, and N. R. Armstrong. Interface Dipoles Arising from Self–Assembled Monolayers on Gold: UV–Photoemission Studies of Alkanethiols and Partially Fluorinated Alkanethiols. *J. Phys. Chem. B*, 107(42):11690–11699, October 2003.

[50] B. de Boer, A. Hadipour, M. M. Mandoc, T. van Woudenbergh, and P. W. M. Blom. Tuning of Metal Work Functions with Self-Assembled Monolayers. *Adv. Mater.*, 17(5):621–625, March 2005.

[51] P. Cyganik, M. Buck, W. Azzam, and C. Wöll. Self–assembled monolayers of ω–biphenylalkanethiols on au(111): influence of spacer chain on molecular packing. *J. Phys. Chem. B*, 108(16):4989–4996, 2004.

[52] A. Shaporenko, M. Elbing, A. Błaszczyk, C. von Hänisch, M. Mayor, and M. Zharnikov. Self–assembled monolayers from biphenyldithiol derivatives: optimization of the deprotection procedure and effect of the molecular conformation. *J. Phys. Chem. B*, 110(9):4307–4317, 2006. PMID: 16509728.

[53] D. A. Egger, F. Rissner, G. M. Rangger, O. T. Hofmann, L. Wittwer, G. Heimel, and E. Zojer. Self-assembled monolayers of polar molecules on Au(111) surfaces: distributing the dipoles. *Phys. Chem. Chem. Phys.*, 12(17):4291–4294, 2010.

[54] D. A. Egger, F. Rissner, E. Zojer, and G. Heimel. Polarity Switching of Charge Transport and Thermoelectricity in Self-Assembled Monolayer Devices. *Adv. Mater.*, Volume 24(32):4403—4407, August 2012.

[55] L. Kong, F. Chesneau, Z. Zhang, F. Staier, A. Terfort, P. A. Dowben, and M. Zharnikov. Electronic Structure of Aromatic Monomolecular Films: The Effect of Molecular Spacers and Interfacial Dipoles. *J. Phys. Chem. C*, 115(45):22422–22428, November 2011.

<div style="text-align: right; font-style: italic; font-size: 2em">4</div>

Self-Assembled Monolayers of Terminal Acetylenes as Replacements for Thiols in Tunneling Junctions

4.1 Introduction

The strong, selective binding of organothiols to gold and other noble metals is widely exploited in Molecular Electronics (ME) to bind molecules to one or both electrodes in a device. Bottom-up tunneling junctions rely almost exclusively on self-assembled monolayers (SAMs) of thiols to define the gap between the electrodes. So why do we use thiols in Molecular Electronics? Alkanethiols, in particular, are favored because they reproducibly form dense monolayers quickly and in a variety of conditions and tolerate a wide variety of head groups. Thus thiolates have been an ideal tool to functionalize metal surfaces. Nevertheless despite their popularity, there are significant disadvantages that are common to virtually all organothiols: They oxidize to disulfides under ambient conditions; their stench is detectible at concentrations of parts per billion and long term exposure can lead to permanent olfactory damage; and the reactivity of thiols and their tendency to poison catalysts can limit their synthetic accessibility and/or require the use of protecting groups that complicate or preclude synthetic efforts. Furthermore, in ME applications, the gold-thiolate interface introduces non-trivial complexities to modeling studies and acts as a barrier to change transport from the involvement of sulphur 3d orbitals in bonding metals.[1–3] Researchers in ME—particularly in top-down, single-

---

† Manuscript submitted.

<div style="text-align: right">105</div>

molecule experiments—have explored alternative anchoring groups, such as isonitriles, aryl diazoniums, aryl iodoniums, and thiocyanates, dithiocarbamate, and selenium, but none have matched the facile, selective self-assembly of thiols that is required to form stable tunneling junctions in high yields. [4]

4.2 SAMs of Alkynes

In this chapter I study SAMs of terminal alkynes, and I believe that the former could be a drop-in replacement for thiols in tunneling junctions comprising SAMs on gold and silver. Alkynes are known to have an affinity for and chelate with metals, [5–9] but their self-assembly on surfaces had been thought to require the formation of acetylides electrochemically [10] or by deprotonation. [11] Gorman and co-workers characterized SAMs formed by exposing solutions of n-alkyl terminal alkynes (acetylenes) in ethanol to gold, showing that alkynes spontaneously form densely packed monolayers analogously to thiols. [12] However, while acetylides have been used in single-molecule ME devices (break-junctions), [13] to the best of our knowledge, tunneling junctions based on the self-assembly of terminal alkynes—particularly into SAMs—have not been reported. I used eutectic Ga-In (EGaIn) as top electrode [14] to contact SAMs of n-alkyl terminal alkynes on template-stripped [15] gold (Au^{TS}) and silver (Ag^{TS}) and measure tunneling currents. I characterized the SAMs on Au^{TS} using surface enhanced Raman spectroscopy (SERS), polarization modulation infrared reflection adsorption spectroscopy (PMIRRAS), and contact angles to confirm the presence of the terminal alkynes on the surface (by comparison to Zhang et al. [12]) and the relative density of the monolayers.

4.3 Results and Discussion

I performed Raman and attenuated total reflectance (ATR) measurements on neat 1-hexyne, 1-octyne, 1-decyne, and 1-dodecyne, which I abbreviate AC6-12, respectively. All four alkynes clearly showed the expected $\nu(C\equiv C)$ mode at 2118 cm^{-1} (see Figure 4.1 and Figure 4.2), which corresponds to the alkyne stretching vibration. While surface-enhanced Raman spectroscopy (SERS) studies have established that terminal alkynes bind to Au and Ag, [16–18] the unambiguous characterization of SAMs of alkynes has only been performed on Au. [12] Thus I first analyzed AC6-12 by SERS on roughened

Au beads. Gold beads were used as working electrodes for SERS measurements. The gold beads were prepared from 0.5 mm 99.999% Au wire (SCHÖNE EDELMETAAL B.V), melted in a H_2 gas flame to form a bead with a diameter of 2-3 mm. The freshly prepared bead was cleaned chemically and electrochemically. Roughening of the gold bead electrode was performed according to the procedure described by Tian et al.[19] SERS active surfaces were obtained after 9 cycles and the measured electrochemically active surface area did not change significantly with further cycling. Immediately after cleaning, the substrates were immersed into a solution of the compound for subsequent monolayer formation. Excitation wavelength λ_{exc} at 785 nm was used for SER measurement. The resulting data, shown in Figure 4.3 (Top), confirm the binding of all four alkynes to Au via the ~ 100 cm^{-1} red-shift in the alkyne stretching vibrations in the SER spectra, which occurs upon the adsorption/complexation of alkyne species to Au and Ag.[6,7,9,16–18] These peaks (at ~ 2000 cm^{-1} in Figure 4.3) are red-shifted and broader than the Raman peaks due to the roughness of the polycrystalline surfaces of the gold beads and the presence of numerous defects induced by the Au surface reconstruction. Other peaks of interest are the CH_2 and CH_3 stretches at $\sim$2800-2900 cm^{-1} (which are also shown in Figure 4.1 and Figure 4.2). These stretching modes are often used to compare the density of molecules and their packing, *e.g.*, shifts to higher frequencies are an indication of a densely-packed SAM.[20] Furthermore, typical modes for alkanes are present at $\sim$1450 and $\sim$1300 cm^{-1}, which I assign to scissoring vibrations of CH_2.[12,18]

I formed SAMs of AC6-12, by simply exposing 1 mM ethanolic solutions of the appropriate *n*-alkyl terminal alkyne to Au^{TS} and Ag^{TS} substrates for $\sim$20 h. To prove that densely-packed SAMs form on these ultra-smooth substrates, I measured AC12, which is long enough to give reasonable intensities, by PMIRRA (unlike on roughened Au, the signal intensity is extremely low on Au^{TS}). A blow-up of this spectrum is shown in Figure 4.3 (Bottom), showing the characteristic CH_2 and CH_3 peaks associated with trans-extended SAMs. The values of the peaks are within 1% of values reported for densely-packed SAMs of dodecanethiolate on Au, which is a strong indication that the alkyl portion of the SAMs of AC12 pack identically to the thiol equivalent.[21] Taken together, the vibrational spectra unambiguously show the formation of ordered SAMs on Au, regardless of any uncertainties in the specific binding mode of the alkyne anchoring groups.

I compared the static sessile water contact angles (CA) of SAMs of AC6-12 on Au^{TS}
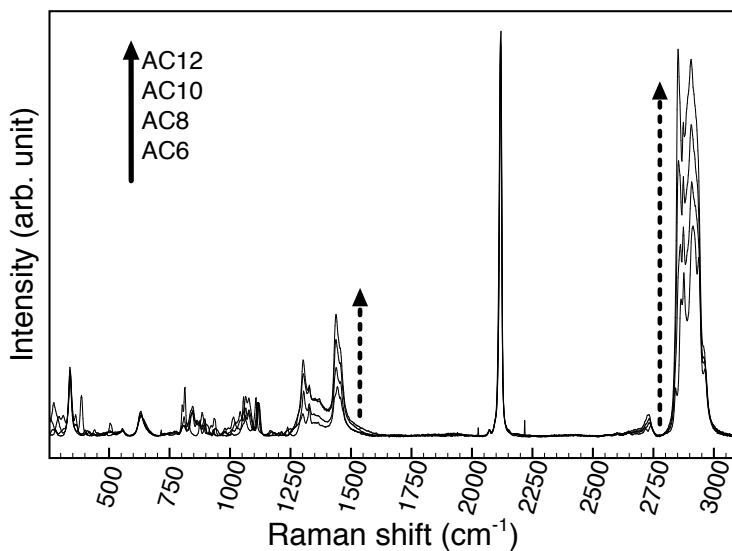
Figure 4.1: Ordinary Raman spectra of 1-Hexyne (AC6), 1-Octyne (AC8), 1-Decyne (AC10), 1-Dodecyne (AC12).
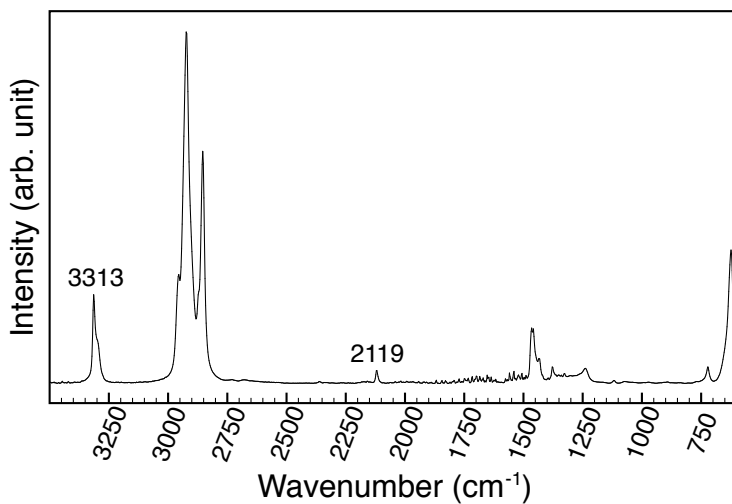
Figure 4.2: FTIR spectra of 1-Dodecyne with Attenuated total reflectance (ATR)
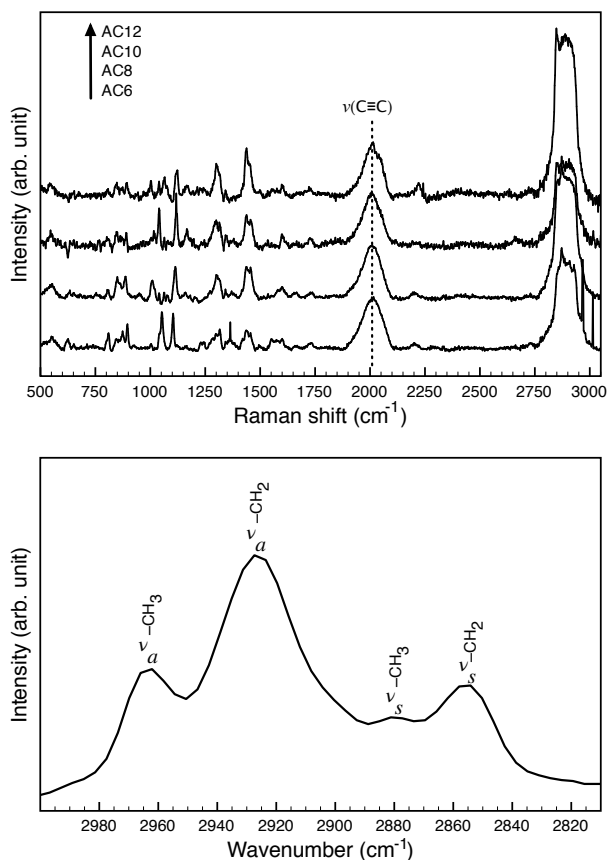
Figure 4.3: Top; SER spectra of AC6-12 SAMs on electrochemically roughened gold beads showing the characteristic peak for surface-bound alkynes. Bottom; PMIRRA spectra of AC12 on Au^{TS} showing the characteristics methyl and methylene modes for trans-extended alkanes in a densely-packed monolayer.
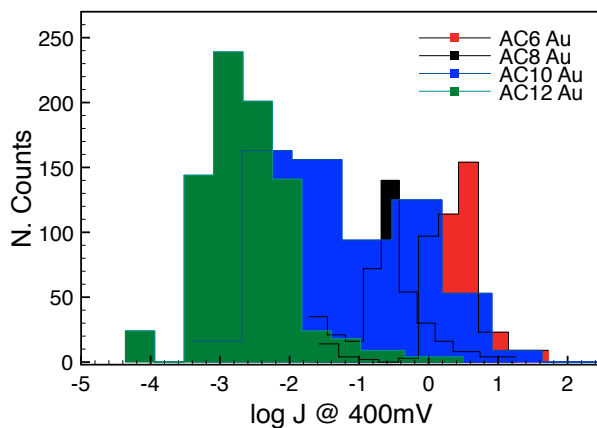
Figure 4.4: Histograms of log J at 400mV for SAMs on $\mathrm{Au}^{\mathrm{TS}}$
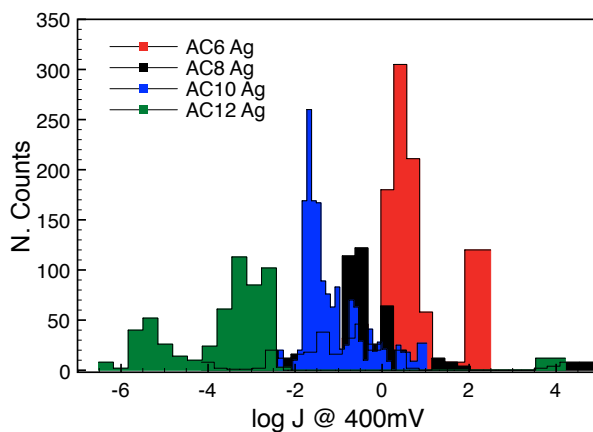
Figure 4.5: Histograms of log J at 400mV for SAMs on $\mathrm{Ag}^{\mathrm{TS}}$

and silver Ag$^{\text{TS}}$, shown in Table 4.1, showing a clear increase with the increasing molecular length (*i.e.*, number of methylene units), which is an indication of increasing order in SAMs of alkanethiolates.[22] The values for SAMs of AC6-12 have been reported on Au surfaces, and are in excellent agreement with our data,[12] but they have not been reported on Ag. The contact angles are higher for Au$^{\text{TS}}$ than Ag$^{\text{TS}}$, which suggests looser packing on Ag, however, in the absence of literature data against which to compare, I cannot draw any firm conclusions. Nevertheless taking together the CA and conductance measurements of AC6-12 SAMs on Ag$^{\text{TS}}$ suggest that there is little structural difference between SAMs of AC6-12 on Ag$^{\text{TS}}$ and Au$^{\text{TS}}$. Swanson et al. investigated the properties of diisocyanide SAMs; isocyanide is isoelectronic with acetylene. The authors found that isocyanides bind to gold with a terminal η^1 geometry in which only one atom (a carbon atom) is coordinate to the metal[23]. I therefore tentatively suggest that the binding mode on Au could be the same for terminal alkyne SAMs but potentially not the same for Ag.

SAMs	θ Au	θ Ag
AC6	80.1°	61.4°
AC8	89.7°	71.2°
AC10	91.2°	86.7°
AC12	98.7°	97.3°

Table 4.1: Static contact angles measured for Milli-Q water on SAMs of AC6-12 on Au$^{\text{TS}}$ and Ag$^{\text{TS}}$

I constructed tunneling junctions of the SAMs of AC6-12 on Ag$^{\text{TS}}$ and Au$^{\text{TS}}$ by contacting them with sharp tips of EGaIn, sweeping through a potential range of ± 0.6 V, and collecting current density versus voltage (J/V) plots at different positions on each of multiple substrates. As previously describe in Chapter 2 and 3, I analyzed the resulting data by fitting a histogram of $\log J$ for each value of V to a Gaussian distribution: see Figure 4.4 and 4.5. The symbols in Figure 4.6 represent the Gaussian mean for the corresponding SAMs on Au$^{\text{TS}}$ (yellow) and Ag$^{\text{TS}}$ (grey). The error bars are the standard deviation. The SAMs of AC6-12 behaved identically to alkanethiolates—forming robust junctions in high yields—thus I was able to treat the data identically. A further proof of the robustness of terminal alkyne SAMs can be found in the report of Tucker et al. where they study the rate and extent of chemical exchange of thiols and terminal alkynes.[24] It was observed from STM images that the replacement of terminal

alkyne SAMs into $C_{12}S^-$ occurred exclusively at defect sites and did not proceed into domains. Thus alkynes have a good affinity for gold, however they can not fully replace thiolated SAMs. The conductances for AC6-12 on Ag^{TS} and Au^{TS} are within error of each other and nearly indistinguishable. This remarkable similarity means that charge-transport most likely occurs through the backbones of the molecules and/or that the packing on Au^{TS} and Ag^{TS} is identical and that there is little, if any, difference in the binding modes on Ag and Au. The magnitude of J in Figure 4.6 is also remarkably similar to SAMs of alkanethiolates with the same number of carbons,[25] which suggests that the electronic coupling formed by the spontaneously assembly of alkynes on Au and Ag is similar to that of thiols. The yields of working junctions, determined by the percentage of junctions that failed during a series of potential sweeps, and the total number of traces acquired for each SAM are shown in Table 4.2. The yields are in all cases excellent. The lowest yield is for AC10 on Ag^{TS}, which I compensated for by acquiring more scans on more junctions.
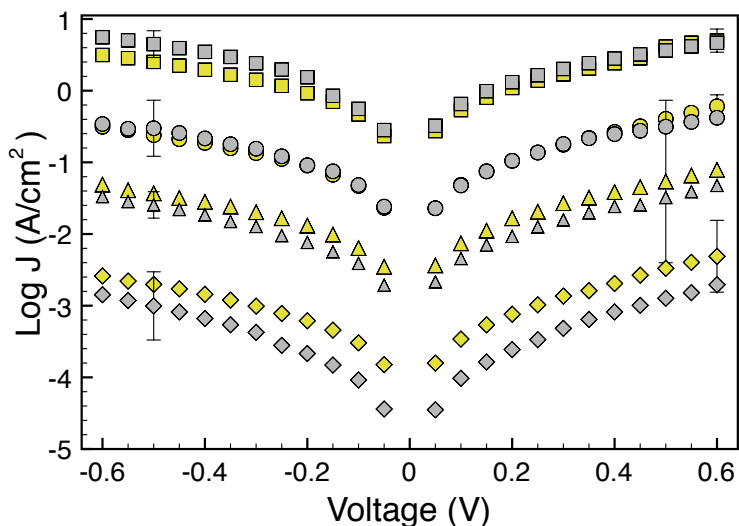
Figure 4.6: Plots of current density (J) versus voltage (V) for SAMs of AC6 (squares), AC8 (circles), AC10 (triangles), and AC12 (diamonds) on Au^{TS} (yellow) and Ag^{TS} (grey) determined by fitting log-normal plots of J at each value of V to a Gaussian. The error bars (shown on one point per trace for clarity) represent the variance.

The length-dependence of J for SAMs of n-alkanethiolates is well established as fol-

SAM	Traces		Yield	
	Au^{TS}	Ag^{TS}	Au^{TS}	Ag^{TS}
AC6	420	1140	100%	90%
AC8	800	528	92%	96%
AC10	660	3084	93%	80%
AC12	822	808	98%	98%

Table 4.2: Number of J/V traces acquired and the % of junctions that did not fail during measurement (yield).

lowing Simmons' approximation, $J = J_0 e^{-d\beta}$.[26] Values of β are often used to compare to or "validate" a method of measuring tunneling currents using values from the literature. There are no reported values of β (or tunneling junctions comprising SAMs) for alkynes against which to compare AC6-12, thus, to contextualize our data, I fit plots of $\ln J$ versus the total number of carbons in the alkynes (as opposed to guessing the molecular length). These data are shown in Figure 4.7. I found $\beta_{Au}=$ $1.16 \pm 0.04 \ n_C^{-1}$, $J_0 = (2.836 \pm 0.001) \times 10^3$ A/cm^2 for Au^{TS}, and $\beta_{Ag} = 1.23 \pm 0.09 \ n_C^{-1}$, $J_0 = (4.722 \pm 0.002) \times 10^3$ A/cm^2 for Ag^{TS}. These values of Beta are in excellent agreement with reported values for SAMs of alkanethiolates measured using a variety of experimental techniques, which is further evidence that charges tunnel through the backbones of the molecules of the SAM and that the packing of the molecules is similar to that of alkanethiolates, *i.e.*, that the alkyl portion is trans-extended. Furthermore, it implies that the alkyne anchoring groups are oriented approximately perpendicular to the metal surface on both Au^{TS} and Ag^{TS}, which is supported by ellipsometric thicknesses and electrochemical studies on Au.[12] Further evidence of this conformation, *i.e.*, η^1 geometry, is the low percentage of short, which implies high density.

Values of J_0 are more difficult to compare than β, as they are reported less frequently and are more sensitive to experimental variations. However, our values are in good agreement, if not a bit higher, than those reported for EGaIn junctions comprising SAMs of alkanethiolates on Ag^{TS}.[25] Since J_0 reflects the theoretical value of J at $d = 0$, it can be thought of as the total contact resistance of a junction. In this case, the values are relatively high, particularly in comparison to data we recently reported on partially conjugated SAMs on Au^{TS} in EGaIn junctions.[27] I therefore suggest that alkynes couple to Au and Ag as well or even slightly better than thiols. Better coupling
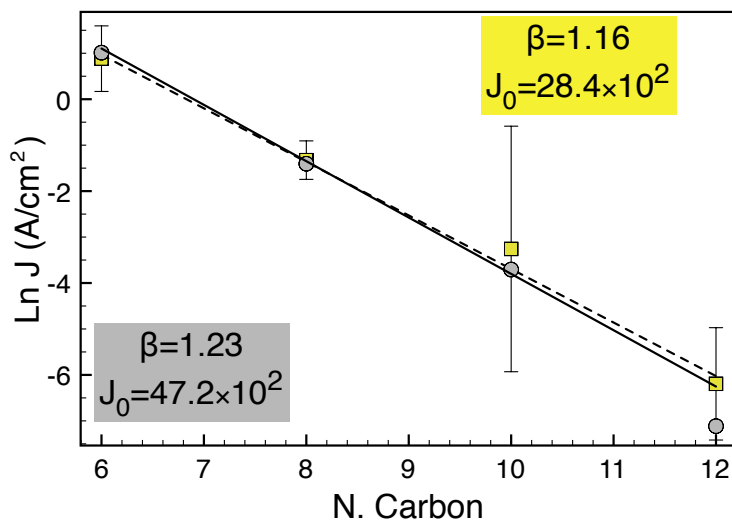
Figure 4.7: Plots of $\ln J$ at 400mV versus the number of carbons in the backbones of AC6-12 on $\mathrm{Au^{TS}}$ (yellow) and $\mathrm{Ag^{TS}}$ (grey). The insets show β (the negative slope) and J_0 ($e^{\mathrm{Y-intercept}}$).

to the electrodes is, in some cases, highly desirable.

4.4 Conclusions

Further studies are necessary to establish the behavior of conjugated and more exotic molecular motifs in SAMs of alkynes, especially fully conjugated molecules, and possibly to better understand the structure of AC6-12 on Ag^{TS}. The data presented in this chapter unambiguously show that SAMs of n-alkyl terminal alkynes can act as drop-in replacements for SAMs of alkanethiolates. In light of the ease of the myriad practical advantages of alkynes over thiols, we would like to move towards thiols and use terminal alkynes. I would like to end this chapter with an open question: Why not use alkynes instead of thiols in Molecular Electronics?

Bibliography

[1] Y. Xue, S. Datta, and M. A. Ratner. Charge transfer and "band lineup" in molecular electronic devices: A chemical and numerical interpretation. *J. Chem. Phys.*, 115:4292, 2001.

[2] T. Ishida, M. Hara, I. Kojima, S. Tsuneda, N. Nishida, H. Sasabe, and W. Knoll. High Resolution X-ray Photoelectron Spectroscopy Measurements of Octadecanethiol Self-Assembled Monolayers on Au(111). *Langmuir*, 14(8):2092–2096, April 1998.

[3] H. Sellers, A. Ulman, Y. Shnidman, and J. E. Eilers. Structure and binding of alkanethiolates on gold and silver surfaces: implications for self-assembled monolayers. *J. Am. Chem. Soc.*, 115(21):9389–9401, October 1993.

[4] E. Adaligil, Y.-S. Shon, and K. Slowinski. Effect of Headgroup on Electrical Conductivity of Self-Assembled Monolayers on Mercury: n-Alkanethiols versus n-Alkaneselenols. *Langmuir*, 26(3):1570–1573, 2010.

[5] N. J. Long and C. K. Williams. Metal Alkynyl σ Complexes: Synthesis and Materials. *Angew. Chem. Int. Ed.*, 42(23):2586–2617, June 2003.

[6] M. L. Patterson and M. J. Weaver. Surface-enhanced Raman spectroscopy as a probe of adsorbate-surface bonding: simple alkenes and alkynes adsorbed at gold electrodes. *J. Phys. Chem.*, 89(23):5046–5051, 1985.

[7] H. Feilchenfeld and M. J. Weaver. Binding of alkynes to silver, gold, and underpotential deposited silver electrodes as deduced by surface-enhanced Raman spectroscopy. *J. Phys. Chem.*, 93(10):4276–4282, May 1989.

[8] J. Howard and Z. A. Kadir. Infrared studies of the interaction of acetylene with silver A zeolite. *Zeolites*, 4(1):45–50, January 1984.

[9] D. C. Kennedy, C. S. McKay, L.-l. Tay, Y. Rouleau, and J. P. Pezacki. Carbon-bonded silver nanoparticles: alkyne-functionalized ligands for SERS imaging of mammalian cells. *Chem. Commun.*, 47(11):3156–3158, 2011.

[10] Q. Li, C. Han, M. Fuentes-Cabrera, H. Terrones, B. G. Sumpter, W. Lu, J. Bernholc, J. Yi, Z. Gai, A. P. Baddorf, P. Maksymovych, and M. Pan. Electronic Control over Attachment and Self-Assembly of Alkyne Groups on Gold. *ACS Nano*, 6(10):9267–9275, October 2012.

[11] A. M. McDonagh, H. M. Zareie, M. J. Ford, C. S. Barton, M. Ginic-Markovic, and J. G. Matisons. Ethynylbenzene Monolayers on Gold: A Metal-Molecule Binding Motif Derived from a Hydrocarbon. *J. Am. Chem. Soc.*, 129(12):3533–3538, March 2007.

[12] S. Zhang, K.L. Chandra, and C.B. Gorman. Self-assembled monolayers of terminal alkynes on gold. *J. Am. Chem. Soc.*, 129(16):4876–4877, 2007.

[13] W. Hong, H. Li, S.-X. Liu, Y. Fu, J. Li, V. Kaliginedi, S. Decurtins, and T. Wandlowski. Trimethylsilyl-Terminated Oligo(phenylene ethynylene)s: An Approach to Single-Molecule Junctions with Covalent Au-C sigma-Bonds. *J. Am. Chem. Soc.*, 134(47):19425–19431, November 2012.

[14] M. D. Dickey, R. C. Chiechi, R. J. Larsen, E. A. Weiss, D. A. Weitz, and G. M. Whitesides. Eutectic Gallium-Indium (EGaIn): A Liquid Metal Alloy for the Formation of Stable Structures in Microchannels at Room Temperature. *Adv. Funct. Mater.*, 18(7):1097–1104, April 2008.

[15] E. A. Weiss, G. K. Kaufman, J. K. Kriebel, L. Li, R. Schalek, and G. M. Whitesides. Si/SiO$_2$-Templated formation of ultraflat metal surfaces on glass, polymer, and solder supports: Their use as substrates for Self-Assembled monolayers. *Langmuir*, 23(19):9686–9694, 2007.

[16] J. K. Lim, S.-W. Joo, and K. S. Shin. Concentration dependent Raman study of 1,4-diethynylbenzene on gold nanoparticle surfaces. *Vib. Spectrosc.*, 43(2):330–334, March 2007.

[17] B. K. Yoo and S.-W. Joo. In situ Raman monitoring triazole formation from self-assembled monolayers of 1,4-diethynylbenzene on Ag and Au surfaces via "click" cyclization. *J. Colloid Interface Sci.*, 311(2):491–496, July 2007.

[18] Y. H. Jang, S. Hwang, J. J. Oh, and S.-W. Joo. Adsorption change of cyclohexyl acetylene on gold nanoparticle surfaces. *Vib. Spectrosc.*, 51(2):193–198, November 2009.

[19] Z.-Q. Tian, B. Ren, and D.-Y. Wu. Surface-Enhanced Raman Scattering: From Noble to Transition Metals and from Rough Surfaces to Ordered Nanostructures. *J. Phys. Chem. B*, 106(37):9463–9483, September 2002.

[20] V. S. Dilimon, J. Denayer, J. Delhalle, and Z. Mekhalif. Electrochemical and Spectroscopic Study of the Self-Assembling Mechanism of Normal and Chelating Alkanethiols on Copper. *Langmuir*, 28(17):6857–6865, May 2012.

[21] M. D. Porter, T. B. Bright, D. L. Allara, and C. E. D. Chidsey. Spontaneously organized molecular assemblies. 4. Structural characterization of n-alkyl thiol monolayers on gold by optical ellipsometry, infrared spectroscopy, and electrochemistry. *J. Am. Chem. Soc.*, 109(12):3559–3568, June 1987.

[22] C. D. Bain, E. B. Troughton, Y. T. Tao, J. Evall, G. M. Whitesides, and R. G. Nuzzo. Formation of monolayer films by the spontaneous assembly of organic thiols from solution onto gold. *J. Am. Chem. Soc.*, 111(1):321–335, 1989.

[23] S. A. Swanson, R. McClain, K. S. Lovejoy, N. B. Alamdari, J. S. Hamilton, and J. C. Scott. Self-Assembled Diisocyanide Monolayer Films on Gold and Palladium. *Langmuir*, 21(11):5034–5039, May 2005.

[24] E. Z. Tucker and C. B. Gorman. Terminal Alkynes as an Ink or Background SAM in Replacement Lithography: Adventitious versus Directed Replacement. *Langmuir*, 26(18):15027–15034, September 2010.

[25] M. M. Thuo, W. F. Reus, C. A. Nijhuis, J. R. Barber, C. Kim, M. D. Schulz, and G. M. White-sides. Odd-even effects in charge transport across self-assembled monolayers. *J. Am. Chem. Soc.*, 133(9):2962–2975, 2011.

[26] J. G. Simmons. Generalized formula for the electric tunnel effect between similar electrodes separated by a thin insulating film. *Appl. Phys. Lett.*, 34(6):1793–1803, 1963.

[27] D. Fracasso, M. I. Muglali, M. Rohwerder, A. Terfort, and R. C. Chiechi. Influence of an Atom in EGaIn/Ga_2O_3Tunneling Junctions Comprising Self-Assembled Monolayers. *The Journal of Physical Chemistry C*, 117(21):11367–11376, May 2013.

A Simple Method for Forming Dense Self-Assembled Monolayers of Thiolated Double-Stranded DNA on Gold for Solid-State Charge-Transport Junctions

5.1 Introduction

Great effort has been devoted to tuning the density of surface-attached polynucleotides on glass, silicon, indium tin oxide (ITO), highly ordered pyrolytic graphite (HOPG), and gold. [1–6] Single-stranded (ss) oligonucleotides on gold surfaces have been used, for example, as biosensors for the detection of DNA and RNA, [7,8] small-molecule detectors, [9] and modified oligonucleotides have been used to create switchable superhydrophobic surfaces. [10] In these systems the binding of a target strand of complementary ss-DNA/RNA causes a measurable change in the conductive, mechanical, or interfacial properties of the monolayer/substrate. Similarly, double stranded (ds) oligonuleotides have been utilized in diagnostics, [11] single-molecule studies, [12,13] electrochemical assays, [4,14] the detection of transcription factors [15,16] and restriction enzymes, [17] and in studies of charge-transfer processes in nucleic acids. [18] All of these applications rely only on the immobilization of oligonucleotides (ss or ds) on surfaces; density and packing are not critical parameters. SAMs of ds-DNA are particularly interesting for potential

---

† I performed this work in collaboration with Jan W. de Vries, Pavlo I. Gordiichuk, Deepak K. Prusty, and Xingfei Zhou, who prepare the ds-DNA and performed part of the AFM imaging. The manuscript is in preparation.

applications that exploit the tunable, nano-scale architecture of ds-DNA; specifically in defining the gap-size, *i.e.*, space between electrodes, in solid-state charge-transport junctions and in combining these applications with the tunable molecular-recognition that is inherent to DNA.
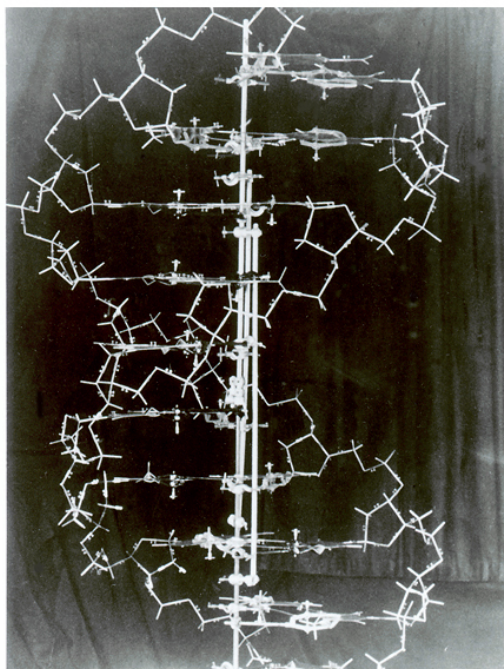
Courtesy of Cold Spring Harbor Archives. Noncommercial, educational use only.

Figure 5.1: The original DNA demonstration model, designed by James Watson and Francis Crick in 1953.

An important distinction is necessary between simply immobilizing DNA on surfaces, which relies on irreversible processes to link the DNA to the surface, and self-assembly, which allows the controlled formation of nanostructures that are defined by—and retain the unique structural properties of—DNA. Molecular monolayers formed via *self-organization* (*e.g.*, through irreversible bonding to SiO_2 substrates) and *self-assembly* (*e.g.*, through thiolates on gold to form SAMs), give rise to disparate properties. [19–21] For instance, self-organized monolayers cannot self-repair or undergo dynamic exchange with molecules from solution, but are not subject to thermal or electrochemical des-

orption. The phosphate backbones of DNA is charged, which leads to intermolecular repulsion and it is too bulky to form dense monolayers spontaneously. Thus monolayers of DNA are formed as mixed monolayers and require an additional step to passivate the regions of the surface that do not contain surface-bound DNA. This passivation step has a dramatic impact on the final structure of the monolayer, particularly in the case of SAMs because the DNA and the passivating molecules (*e.g.*, alkanethiols) are in equilibrium between the bound and unbound states. For example, Satjapipat et al.[22] used reductive desorption by Atomic Force Microscopy (AFM) to selectively create islands of bare gold in SAMs of alkanethiolates in which islands the ss-DNA is attached via directed self-assembly. An alternative strategy is to use carboxyl terminated SAMs at pH=8 in order to have negative charges on the surface and repulsion to the backbone of the DNAs forcing it to stand vertically.[23] Another approach is the one showed from Liu et al. who used "nanografting" to form islands with an AFM tip *in situ* in the presence of thiolated ss-DNA.[24] Once clean from the thiols the surface is then exposed to the DNA. These methods—particularly the latter—are superb for creating non-equilibrium mixed SAMs, but they are labor intensive and do not lend themselves to forming SAMs on large (*i.e.*, $> 1\ \mu m^2$) substrates and are therefore not suitable for constructing solid-state electronic devices. More recently Josephs et al. using electrochemical atomic force microscopy, have directly determined the nanoscale spatial distribution of thiolated DNAs that are attached to gold. The authors found that, similarly to what I describe further in this chapter, *pre-passivating* or "inserting" a short SAM of alkanethiolates before exposure to thiolated DNA lead to a more uniformly distributed layer of DNA. The fact that the DNA is homogeneously distributed and organized on the surfaces is an essential requirement for sensing.[23,25,26] Depending on the purposes and goals one can adopt different way to functionalized the surface with double or single strand DNA. Nevertheless it is inherently important to have a fine control of the density and accessibility of the functionalized DNA. In literature the typical procedure for forming a mixed SAM of DNA over arbitrarily large areas is to first expose a gold surface to a solution of thiolated DNA and then to post-passivate (back-filling) the surface with an alcohol-terminated thiolate, such as 1-mercaptohexane-6-ol (MCH).[8,27] This procedure relies on the surfactant properties of thiolates on gold to disrupt the non-specific interactions between DNA and gold (*i.e.*, competitive adsorption), leaving the DNA that is anchored through the thiol linker intact. Using fluorescence

microscopy to image monolayers of DNA on gold with micrometer resolution, Bizzotto et al. discovered direct evidence of significant heterogeneity in probe densities.[28] The backfilling procedure also implicitly assumes that gold-thiolate interactions are stronger than (nonspecific) DNA-gold interactions and that the gold-thiolate interaction of MCH will not compete with the gold-thiolate interaction of DNA; however, there is no thermodynamic reason that this should be the case.[29,30] In fact, the complete exchange of a SAM of one thiolate by a second thiol typically occurs in a few minutes.[31] Thus, the thermodynamic minimum created by post-passivation with MCH is a homogenous SAM of MCH. As few studies on DNA differentiate self-assembly and self-organization, the kinetics and thermodynamics of the self-assembly of thiolated oligonucleotides have not been thoroughly investigated. For the hybridization of surface-bound ss-DNA or electrochemical studies, the actual structure of the SAM of DNA or how the DNA is attached to the surface is inconsequential; provided a few strands of DNA are standing upright on the surface, their properties will dominate. In contrast to what has been described previously, studies of the charge-transport and tunneling behavior of DNA in SAMs using, for example, eutectic Ga-In (EGaIn)[32], hanging drops of mercury,[33] or large-area molecular junctions[34] will require well-defined, well-characterized SAMs of ds-DNA in which the nucleic acid molecules protrude from the surface to accurately define the tunneling gap and to avoid collecting erroneous data.[35] Moreover, when using ds-DNA, care must be taken to avoid de-hybridization during the post-passivation step. For applications in which it is important to form dense, high-quality SAMs of ds-DNA in a controllable fashion, I have reversed the typical procedure, instead pre-passivating a gold surface with an alkanethiolate that is the same length as the thiolate linker that is attached to the ds-DNA. This pre-passivation forms a hydrophobic SAM that has a lower energy of interaction with DNA, salts, and surfactants than MCH and a dramatically lower-energy interaction than bare gold. When the passivated substrate is immersed in a solution of thiolated ds-DNA, the ds-DNA exchanges through bi-molecular reactions with the existing SAM, beginning with the defects (*e.g.*, grain-boundaries, step-edges, impurities, etc.)[36] and then growing from these nucleation sites. This process is summarized schematically in Figure 5.2. A comparison between the two passivation methods is shown in 5.3.

Exchange with a passivating SAM is not significantly slower than the diffusion-controlled adsorption of DNA to a bare gold surface, but does afford a degree of control over the
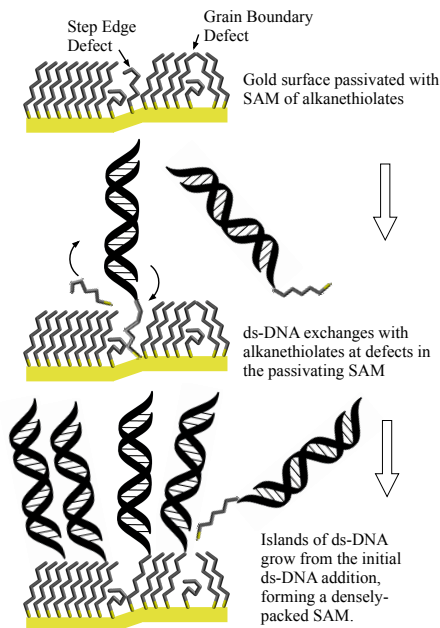
Figure 5.2: A schematic (not to scale) of the formation of a SAM of ds-DNA on a gold surface that is pre-passivated with a SAM of an alkanethiolate (HT). Top; the pre-passivating SAM contains defects—grain boundaries, step-edges, etc. Center; ds-DNA exchanges with alkanethiolates at defect sites, where the alkanethiolates are disordered, nucleating the formation of a SAM of ds-DNA. Bottom; the SAM of ds-DNA grows out from the initial ds-DNA forming islands of ds-DNA that eventually coalesce into a densely packed SAM (within minutes).
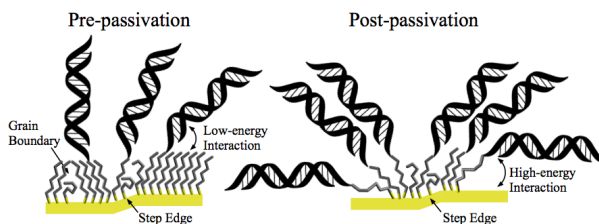
Figure 5.3: A schematic comparison of the pre- and post-passivation. The figure is derived from experimental evidences, such as AFM and QCM.

density of the DNA and, importantly, it ensures that the ds-DNA is bound to the surface exclusively via the thiolate linker (and not through nonspecific DNA/Au interactions). Moreover, due to the mechanism of growth—which is similar to that of any thiol that lacks competitive, non-specific surface interactions—none of the DNA is irreversibly oriented parallel to the surface (*i.e.*, lying down). The areas that are not covered by DNA remain passivated, both chemically and electrically, by the SAM formed during the pre-passivation. In this chapter I discuss the difference between pre and post-passivation and the first solid state tunneling junction comprising mixed monolayers of ds-DNA of varying lengths on gold substrates.

5.2 Results and Discussion

Using a combination of AFM, quartz crystal microbalance (QCM), and contact angle measurements, we investigated three ds-DNAs which differ in length, consisting of 14, 22 or 30 basepairs (bp), hereafter referred to as ds-DNA-14, ds-DNA-22, and ds-DNA-30, respectively. Throughout the chapter to refer to pre- and post-passivation, I use the prefixes "pre" and "post." For example, a SAM formed from ds-DNA of 14 bp by pre-passivation is denoted "pre-ds-DNA-14." Unless stated otherwise, pre-passivation always refers to a gold surface that is pre-passivated with hexanethiol (HT) and then exposed to ds-DNA and post-passivation always refers to a gold surface that is exposed to ds-DNA first, and then post-passivated with MCH.

5.2.1 Large-area Surface Studies

The principle difference between our pre-passivation method and the typical post passivation method is that, with pre-passivation the DNA is never exposed to bare gold. Instead, the DNA is only exposed to a SAM of a methyl-terminated alkanethiolate, which has a much lower energy of interaction with the DNA than bare gold. With post-passivation, the mixture of chemi- and physisorbed DNA formed from immersing a bare gold surface in a solution of thiolated DNA (ss or ds) is subsequently treated with an alcohol-terminated alkanethiol, typically MCH. Both methods involve forming a SAM and then exchanging that SAM with a free thiol from solution to form a mixed SAM, such that the entire surface of the substrate is covered. In general, one SAM

of thiolates will be replaced completely by a free thiol in a few minutes over a wide range of concentrations and regardless of the solvent(s). [31] Thus, when a SAM of HT is immersed in a solution of DNA, the DNA should almost completely replace the HT, stopping only when the DNA has reached the maximum surface density allowed by size and electrostatic repulsion. The final structure is therefore a mixed-monolayer that principally comprises DNA, but in which no bare gold remains. Conversely, when a SAM of DNA is immersed in a solution of MCH—even for a few minutes—the MCH should almost completely replace the DNA (MCH is an excellent surfactant for gold). The fact that any DNA is left behind implies that the remaining DNA was bound to the surface more strongly than MCH could bind, or that it was kinetically trapped (*e.g.*, by forming tight clusters). Because the DNA is initially exposed to bare gold, there is also a possibility that the strength of the non-specific DNA/Au interactions will vary with the length/charge/sequence of the DNA, affecting both the kinetics and thermodynamics of the replacement of the DNA by MCH and therefore the structure of the SAM. A potential consequence of pre-passivating with HT instead of MCH is that the interaction between the DNA and the surface of the HT, though relatively low in energy, will be more favorable than that of water and HT. This situation would create a driving force for the DNA to lay flat against the HT surface during the formation of the SAM of DNA, defeating the purpose of pre-passivating the gold, and introducing a similar dependence of the structure of the SAM on the length/charge/sequence of the DNA. To ensure that this was not the case I compared the contact angles of pure water, buffer, and ds-DNA/buffer with both the methyl-terminated SAM of HT, and the alcohol-terminated SAM of MCH. These data are summarized in Table 5.1 and show that the energies of interaction with the SAM of HT are, in all cases, lower than with the SAM of MCH and that the presence of ds-DNA decreases the contact angle of water by the same amount in all cases, indicating no extraordinary interactions with the SAM of HT—*i.e.*, that the ds-DNA does not prefer the liquid/solid interface. The contact angles for SAMs of HT are, in all cases, less than 100° because SAMs of alkanethiolates with fewer than eight carbons in length are somewhat disordered, *i.e.*, liquid like, at room temperature. This disorder is desirable as it should allow for the facile exchange of ds-DNA with the SAM while still passivating the gold substrate.

	Milli-Q water	Buffer	ds-DNA/buffer
HT SAM	95°	95°	94°
MCH SAM	59°	60°	57°

Table 5.1: Static contact angles measured for Milli-Q water, buffer, and ds-DNA-14 relative to a SAM of HT, and a SAM of MCH. These data indicate that neither the buffer nor the DNA interact with the surfaces more strongly than water because the contact angles do not change significantly for a given interface.

5.2.2 The Kinetics of Dynamic Exchange

To probe the kinetics of the self-assembly processes and the relative degrees of exchange between HT/MCH and ds-DNA on the pre-ds-DNA and post-ds-DNA surfaces I prepared several gold sensors for QCM analysis. These data are summarized in Figure 5.4 as the changes in frequency of the fifth overtone, Δf, as a function of time, in seconds. Two sensors were pre-passivated with a SAM of HT for 1 h (Q1 and Q2); the other two (Q3 and Q4) were clean gold. A solution of ds-DNA-14 was fed into Q1 and Q3 and ds-DNA-30 was fed into Q2 and Q4, all at a constant rate of 0.1 ml/min, exposing all four sensors to ds-DNA solution for 1 h. The arrow labeled "ds-DNA" in Figure 5.4 indicates the starting time of this injection. Within one minute after the injection of ds-DNA, Δf decreased (became more negative) for all four sensors, indicating an increase in mass. The changes in Δf in Figure 5.4 are ~ 70 for Q1, ~ 85 Hz for Q2, ~ 80 for Q3 and ~ 95 Hz for Q4, indicating that Q1 and Q2 (pre-ds-DNA) adsorbed $\sim 10\%$ less ds-DNA (see below) than Q3 and Q4 (bare gold). It is evident from Figure 5.4 that the sensors treated with ds-DNA-14 show a smaller drop in frequency compared to those exposed to ds-DNA-30. The absolute value of this change, $|\Delta\Delta f|$, can be correlated to the change in mass or thickness using the Sauerbrey equation, which is based on the viscoelastic properties of the monolayers[37]. If the film (monolayer) is sufficiently thin and rigid, the decrease in frequency will be proportional to the mass of the film. The SAMs of ds-DNA, however, do not fully meet these criteria, and therefore do not completely couple to the oscillation of the sensor, hence the Sauerbrey relation will underestimate the mass on the sensor. Thus, these measurements can give only a rough comparison of the relative changes in mass; however, the evolution of Δf in time provide valuable insight into the kinetics of the exchange processes. The other characterization methods presented in this paper only give information about the SAMs

at equilibrium–*i.e.*, they provides only thermodynamic information. At 4000 s ($\sim$ 1 h) I flushed each sensor with rinsing solutions (the arrow labeled "Rinse" in Figure 5.4); Q1 and Q2 were rinsed with mq-water to reestablish the starting condition whereas Q3 and Q4 were rinsed with buffer solution free of ds-DNA. After rinsing, Δf recovered to -17 Hz for Q1(pre-ds-DNA-14) and -37 Hz for Q2 (pre-ds-DNA-30). The difference in these values reflects the difference in molecular weight between ds-DNA-14 and ds-DNA-30; *i.e.*, the surface coverage is the same for both. The fact that Δf increases (becomes less negative) after the rinse demonstrates that the non-specifically-bound ds-DNA was readily removed from the passivated surface, while the fact that it remains less than zero indicates that a substantial amount of ds-DNA remains bound to the sensor, presumably through the thiol linker. The two post-passivated sensors, Q3 and Q4, showed considerably less (< 5 Hz) change in Δf, which indicates that most of the ds-DNA was bound too tightly to be removed by rinsing. The slight rise in the signals for Q1 and Q2 after the rinsing step is likely the result of de-hybridization of the surface-bound ds-DNA after prolonged exposure to mq-water. The fact that the Δf rise is smaller for Q2 may indicate that de-hybridization is slower for ds-DNA-30 than for ds-DNA-14. At 5000 s, I injected 1 mM aqueous solutions of MCH into sensors Q3 and Q4 (the arrow labeled "MCH" in Figure 5.4) leading to a rapid rise in Δf for both sensors over 120 s. We estimate a loss of about $70 - 85\%$ of the mass of the surface-bound ds-DNA, neglecting differences in the viscoelastic properties of buffer and mq-water. After the final wash with mq-water (the arrow labeled "mq-water" in Figure 5.4), Δf for Q3 (post-ds-DNA-14) and Q4 (post-ds-DNA-30) was -5 Hz and -20 Hz, respectively. This difference, as with sensors Q1 and Q2, reflects the difference in molecular weight between ds-DNA-30 and ds-DNA-14. The absolute values, however, are less negative for both Q2 and Q3 than for Q1 and Q2, meaning that less ds-DNA remains on the sensors exposed to the post-passivation (MCH) conditions than the pre-passivation (HT) conditions. As with Q1 and Q2, the slight rise in the signals for Q2 and Q3 is likely due to de-hybridization, but the difference is less pronounced. The results of the QCM experiments demonstrate three properties of the kinetics of the formation of mixed-monolayers of ds-DNA. i) There is no appreciable difference in the rates of adsorption of ds-DNA onto bare gold and gold that has been pre-passivated with HT. ii) Most of the ds-DNA that adsorbs onto the SAM of HT used for pre-passivation is bound weakly enough to be removed by rinsing while most of the ds-DNA that adsorbs onto bare gold is bound too tightly to

be removed. iii) Post-passivation with MCH removes more ds-DNA than does rinsing a pre-passivated surface that has been exposed to ds-DNA. These observations support the hypothesis that pre-passivation with HT eliminates strong, non-specific interactions between ds-DNA and the gold substrate and that it results in SAMs comprising more ds-DNA than does post-passivation with MCH.
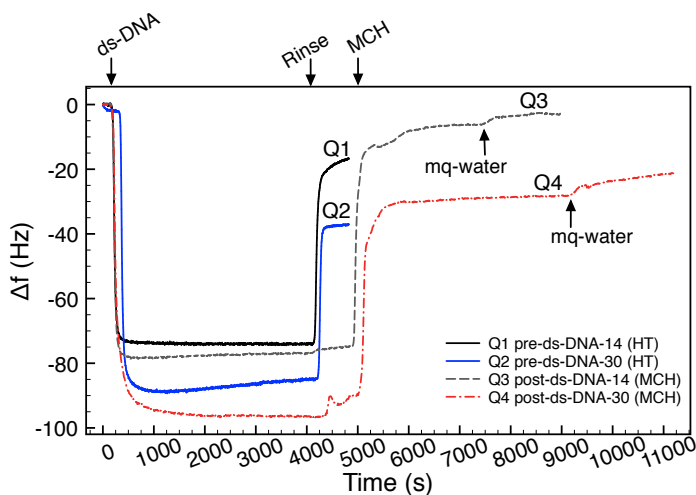
Figure 5.4: Plots of the change in frequency of the fifth overtone of quartz crystal microbalances. The black and blue solid lines, respectively Q1 (pre-ds-DNA-14) and Q2 (pre-ds-DNA-30), are QCM gold sensors supporting a SAM of HT. The black dashed line Q3 (post-ds-DNA-14) and the red dot-dash line Q4 (post-ds-DNA-30) are naked QCM gold sensors. At time indicated with an arrow labeled "ds-DNA," ds-DNA-14 and 30 were injected, causing a sudden drop in frequency. After one hour at the time indicated with the arrow labeled "Rinse," Q1 and Q2 are simply rinsed with mq-water whereas Q3 and Q4 were flush with buffer. The remaining two sensors, Q3 and Q4 are expose to MCH in water at the time indicated with an arrow labeled "MCH," causing the frequency to recover at a rate proportional to the replacement of the SAM of ds-DNA with the thiol.

5.2.3 Surface Topology

To investigate the structural features of the SAMs of ds-DNA directly, and to compare pre- and post-passivation with different lengths of ds-DNA, we performed a series of AFM measurements. Figure 5.5 compares AFM images of SAMs of pre- and post-ds-DNA on Au^{TS} surfaces (Template stripped Au film 200nm think, the process of TS is

described in more details, see Chapter 2). The images in the left column (A-C) show SAMs of pre-ds-DNA-14, 22, and 30 that were treated for 1 h with HT and then 1 h with ds-DNA. The images in the right column (D-F) show SAMs of post-ds-DNA-14, 22, and 30 that were treated for 1 h with ds-DNA and then 1 h with MCH, in accordance with previous reports using post-passivation with MCH. [27] Qualitatively, the images for ds-DNS-14 and ds-DNA-30 agree with the QCM data; there is approximately the same coverage in the images in the left and right columns for ds-DNA-30, but significantly less post-ds-DNA-14 (Figure 5.5D) than pre-ds-DNA-14 (Figure 5.5A). For the shorter double stranded chains like ds-DNA-14, the surfactant properties of MCH readily remove the ds-DNA molecules, leaving the surfaces almost free of ds-DNA-14; the overall change in Δf for post-ds-DNA-14 in Figure 5.4 was only 5 Hz, compared to 17 Hz for pre-ds-DNA-14. In principle, shorter immersion times would leave more post-ds-DNA on the surface, however, the QCM data indicate that the ds-DNA is lost in the first 5-10 minutes of immersion with MCH.

The AFM images of pre-ds-DNA-14 (Figure 5.5A) and 22 (Figure 5.5B) show a dense carpet of DNA, while the structure of the underlying features of the Au^{TS} surface is visible in post-ds-DNA-14 (Figure 5.5D) and 22 (Figure 5.5E). The density of ds-DNA (bright spots*) apparently increases going from post-ds-DNA-14 to post-ds-DNA-22, but is clearly far less dense than pre-ds-DNA-14 and 22. Unlike the SAMs formed from ds-DNA-14 and 22 (pre- or post-), both post-ds-DNA-30 (Figure 5.5F) and pre-ds-DNA-30 (Figure 5.5C) show fibrous structures. It is possible that, due to the length of ds-DNA-30, the surface/DNA interactions are significantly stronger than for ds-DNA-14 or 22, or that ds-DNA-30 (10 nm) is simply too long to stand upright and, at least partially, falls over onto the surface under ambient conditions (in which the AFM data were acquired). Another possible explanation is that the fibrous structures are an artifact of the AFM measurements. All of these measurements were performed in tapping mode, which is sensitive to the rigidity of the material on the substrate. If, for example, ds-DNA-30 is not as rigid as the shorter ds-DNAs, the influence of the tip interacting with the DNA may cause the images to smear, giving the appearance of fibrous structures. While I do not necessarily expect a one-to-one correlation of the clusters in the AFM images of ds-DNA-14 and 22 to individual ds-DNA molecules, the measured diameters of the

---

*The spots ascribed to DNA were uniform in size, but larger than the theoretical values, likely due to convulsion of the tip in tapping mode.

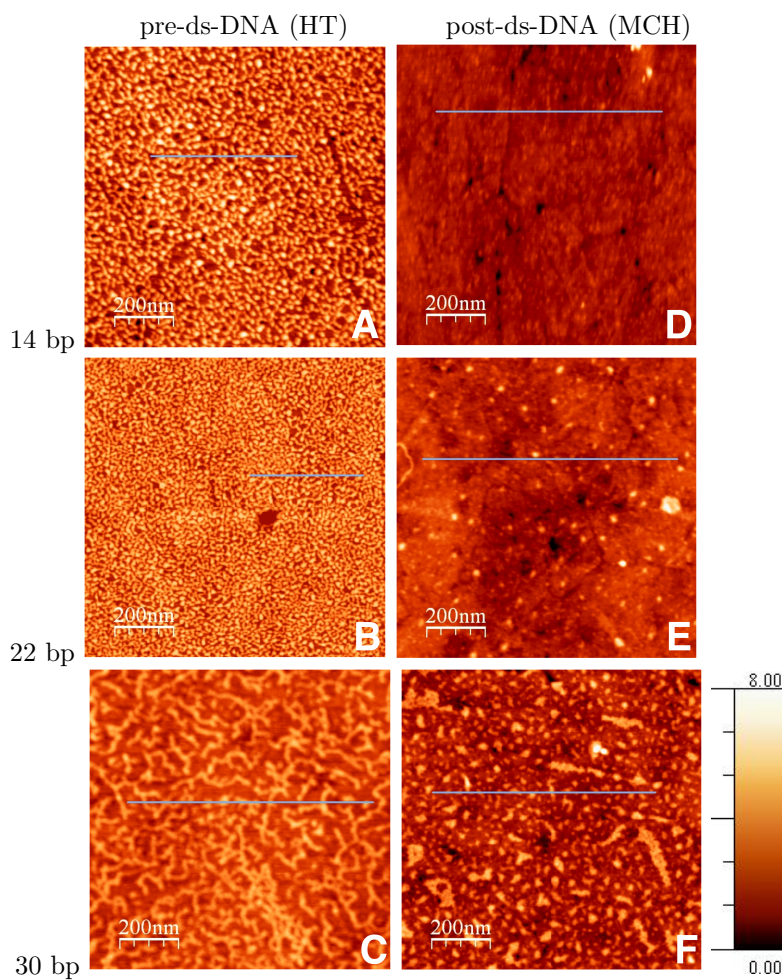Figure 5.5: From top to bottom; AFM images of $\mathrm{Au^{TS}}$ substrates treated for one hour with ds-DNA-14, ds-DNA-22, and ds-DNA-30 either after 1 h of pre-passivation with HT (A-C) or before 1 h of post-passivation with MCH (D-F). The scale bars are all 200 nm. The Z-scale (shown in the lower-right) is $0-8$ nm. The horizontal lines are the sections from which the height profiles shown in Figure S7 were derived.

clusters were fairly consistent. It is possible that these clusters are individual ds-DNA molecules and that the diameters we observe by AFM are the result of the convolution of the tip from surface charges and other repulsive interactions at the surface of the SAMs of ds-DNA. Regardless of these ambiguities, it is abundantly clear that SAMs formed by post-passivation do not contain enough ds-DNA to construct charge-transport junctions, which require SAMs that are sufficiently dense to support a top contact of EGaIn. I examined the height profiles and calculated RMS roughnesses of all of the SAMs pictured in Figure 5.5. These data are summarized in Table 5.2 and show quantitatively what we observe qualitatively; namely that the topology of the pre-ds-DNA surfaces is rougher than the post-ds-DNA surfaces. It is clear from from Table 5.2 that the RMS roughness of pre-ds-DNA decreases slightly with increasing length of the DNA, while post-ds-DNA shows the opposite trend. I interpret the roughness as a reflection of the topology of the SAMs of ds-DNA; the roughness of post-ds-DNA-14 (Figure 5.5D) is very close to that of bare Au^{TS} (or Au^{TS} supporting a homogeneous SAM of MCH). The roughness increases with the length of post-ds-DNA because the density of the ds-DNA increases. The density of the ds-DNA on the surface precludes the exact determination of height by AFM; however, from the heigh-profiles we can conclude that, for pre-ds-DNA-14 (Figure 5.5A) and 22 (Figure 5.5B), the double helices are oriented away from the surface, while for pre-ds-DNA-30 (Figure 5.5C), the helices are lying down on the surface of the SAM of HT. From the combination of the large-area studies and the AFM data, I conclude that the quality and density of the SAMs of post-ds-DNA depend on the length of the ds-DNA, but that the quality and density of SAMs of pre-ds-DNA do not (at least up to 22 bp and using a six-carbon thiol linker). We hypothesize that, when the bare gold surface is exposed to ds-DNA, the DNA first adsorbs non-specifically forming a lying-down phase, as is typically the first step in the growth of SAMs of thiolates on gold.[38] For alkanethiolates, the energy of this non-specific binding is very low compared to the specific gold-thiolate interaction, and the SAM transitions through an intermediate phase (*e.g.*, a "striped phase") and into the standing-up phase. Due to the size and functionality of DNA, however, this last step is not possible and, in the case of post-ds-DNA, the energy of the non-specific interaction scales with the length of the ds-DNA. When these SAMs of ds-DNA are exposed to MCH, the amount of DNA that is stripped from the surface is also proportional to this energy and therefore scales with length as well. Thus, post-ds-DNA-30 (Figure 5.5F) comprises mostly ds-DNA-30 that is lying

down on the surface, while pre-ds-DNA-30—although similar in appearance and mass—comprises ds-DNA-30 that is partially oriented away from the surface due to the low energy of interact between ds-DNA and the passivating SAM of HT *i.e.*, pre-ds-DNA-30 is simply too long to stand upright, but is not irreversibly bound to the surface through non-specific interactions. This hypothesis is supported by the larger values of RMS roughness for pre-ds-DNA-30 than post-ds-DNA-30, but direct evidence by AFM is precluded by the lack of well-defined edges that are, for example, present in SAMs prepared by nanografting.[24]

Table 5.2: RMS roughness of SAMs of pre- and post-ds-DNA calculated from AFM data.

Basepair	pre (nm)[a]	$post$ (nm)[a]
ds-DNA-14	1.17	0.26
ds-DNA-22	1.01	0.49
ds-DNA-30	0.88	0.68

[a] Calculated from the data shown in Figure 5.5

5.2.4 Immersion Time in Pre-Passivated SAMs.

The QCM data suggest that the bulk of the SAM of pre-ds-DNA forms within minutes and that only minor structural rearrangements occur over the following hours. These data do not, however, reveal anything about the structure or topology of the SAM, thus we acquired AFM images of SAMs of pre-ds-DNA-14 over a range of different immersion times, both of ds-DNA and of HT. These data are summarized in Figure 5.6. The left column shows images of SAMs of pre-ds-DNA-14 formed using a constant pre-passivation time of 1 h and varied immersion times with ds-DNA-14. The right column shows images of SAMs of pre-ds-DNA-14 formed by varying the pre-passivation time (*i.e.*, immersion time with HT) and keeping the immersion time with ds-DNA-14 constant at 1 h. I chose a minimum immersion time of ds-DNA of 1 h in the left column because it is well past the time regime in which the QCM data show a change in mass. I chose a smaller minimum time for the immersion with HT because, in principle, a SAM of HT formed from 10 min of exposure is significantly more disordered than a SAM formed from > 1 h of immersion time; this increased disorder may impact the final structure of the

SAM of pre-ds-DNA-14 because it will increase the rate and density of the nucleation of ds-DNA-14, which occurs at defects (*i.e.*, sites of relatively high disorder) in the SAM of HT. The first image in the left column and the second image in the right column were formed under the same conditions, 1 h with ds-DNA-14 and 1 h with HT, but were prepared on separate days. Qualitatively, there is very little difference between the images in Figure 5.6, which is not surprising given that they are all formed with ds-DNA-14 by pre-passivation with HT. An interesting—and expected—trend is that the RMS roughness (Table 5.3; from the AFM data in Figure 5.6) decreases from 1.18 to 0.61 nm as a function of immersion time with ds-DNA-14. A similar trend is seen for immersion time with HT, however, the numbers are larger and the relative change smaller, going from 1.39 to 1.00 nm. This result suggests that the density of packing in the SAM of ds-DNA-14 is proportional to the time it is exposed to solutions of free ds-DNA-14 (*i.e.*, how long the system is allowed to undergo self-assembly). This trend can be seen in the AFM data, though the sample at 24 h appears to have large islands (note: the RMS roughness were still calculated from the entire image). These islands are most likely due to phase segregation—the degree of which is highly time-dependent— or are vacancy islands, which is evidence that the pre-ds-DNA-14 is mobile enough to re-arrange on the Au surface, even in the presence of a pre-passivating SAM of HT. While these islands appear as HT (or bare Au) in the AFM image, it is likely that they are filled with ds-DNA (or HT), but are difficult to visualize.[39] Islands are also apparent in the AFM images of SAMs formed from 1 h of immersion of ds-DNA-14 after 24 h immersion with HT; however, the fact that they decrease in size after 48 h of immersion suggests that they are formed during the self-assembly of the SAM of HT and not ds-DNA-14. Taken together, the RMS roughness and AFM images suggest that, as a function of immersion time with ds-DNA-14, the density of pre-ds-DNA-14 increases only slightly (*i.e.*, the thickness does not change), but that the order increases (*i.e.*, the RMS roughness decreases) and that these changes are the result of the process of self-assembly (*e.g.*, we observe phase segregation/vacancy islands). This result also suggests that by altering either the exposure time to ds-DNA or HT, the density and order of the SAM can be controlled. For example, for charge-transport junctions, the highest possible packing-density is desirable, but for studies that require subsequent access to the ds-DNA in the SAM (*e.g.*, exchange, de/re-hybridization, intercalation, etc.), lower packing-density/ordering is desirable.
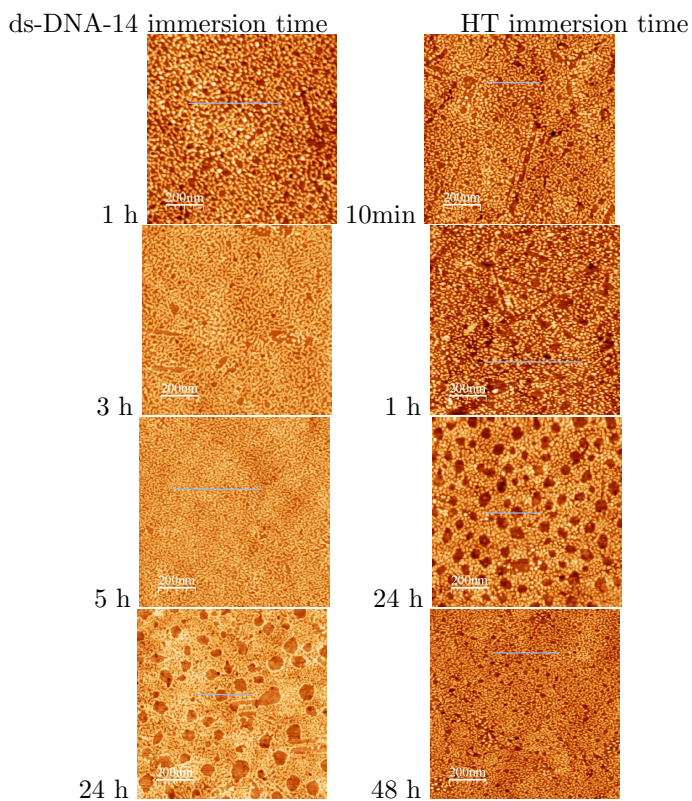
Figure 5.6: Left column; AFM images of $\mathrm{Au^{TS}}$ treated for increasing time with ds-DNA-14 after being pre-passivated one hour with HT. Right column; AFM images of gold substrates treated for increasing time with HT before exposure to ds-DNA-14 for 1 h. The scale bars are all 200 nm. The Z-scale ranges from $0-8$ nm for every image except for the third from the top in the right column, which ranges from $0-5$ nm.

Table 5.3: RMS roughness (in nm) determined by AFM, respectively, of SAMs of pre-ds-DNA-14 with different immersion times.

ds-DNA-14[†]	RMS Roughness[a]	HT[‡]	RMS Roughness[a]
1h	1.18^{b}	10 min	1.20
3h	0.86	1 h	1.39^{c}
5h	0.73	24 h	1.23
24h	0.61	48 h	1.00

[†] After 1 h of pre-passivation with HT.   [‡] Before 1 h of exposure to ds-DNA-14.

[a] Calculated from the data shown in Figure 5.6   [c] Second AFM image in right column of Figure 5.6

[b] First AFM image in the left column of Figure 5.6

5.2.5 Charge-Transport in DNA-Junctions

I performed conductance measurements of SAMs of HT, pre-ds-DNA-14, pre-ds-DNA-22, and pre-ds-DNA-30. After ds-DNA immobilization the samples were rinsed with Milli-Q. Conduction through DNA is far from straightforward and is more likely a superposition of different processes. Many reports and reviews have been reported, a few examples: ds-DNA charge transport over 34 nm with Nile Blue redox probe,[40] single DNA covalently attach to carbon nanotube,[41] hole transport in DNA over long distance by introducing synthetically modified oligonucleotides.[42] Charge transported through DNA systems is intrinsically difficult to understand but at the same time it is a very interesting process. Many mechanisms could play a role depending on the device structure and conditions.[43] Most of the systems investigated have the surfaces functionalized with thiolated DNA containing one or more modified nucleotides or redox probes which allows electrochemical measurements. In our case I performed charge transport studies on solid state, *i.e.*, without solvent, short ds-DNA junctions where the oligonucleotides drive the electrical properties of the entire devices. To form the molecular junction, MJ, I contacted the SAMs of ds-DNA on Au[TS] with tips of EGaIn. If the ds-DNA would be fully stretch, *i.e.*, maintain the full length, then we would expect a quasi-linear decrease of current density J with increasing number of base pair (bp). The resulting J/V for pre-ds-DNA 14, 22 and 30 are summarized in Figure 5.7, and each symbol is the mean of the Gaussian fit formed by the log-normal distribution of values of J. The J values of pre-ds-DNA 14 and 22 are within error of each other which is not surprising since they have rather similar morphologies, see AFM studies in Figure 5.5. The rather short length of DNA (14 and

22 base pair respectively) results in a uniform layer. In the case of these short mixed-DNA SAMs the current is most likely a result of a combination of defects, morphology and the pre-passivation layer length (in this case HT). Despite the short length of ds-DNA 14 and 22 the magnitude of J is still ~ 10 times lower than HT, thus the ds-DNA influences the current in these devices. Whereas pre-ds-DNA 14 and 22 have similar J, pre-ds-DNA 30 is nearly 3 order of magnitude less conductive. Although I did not expect such a difference, the former result could be explain by looking at the surface topology. The length of ds-DNA 30bp creates a network of DNA on the surface (at least in the solid state) homogeneously passivating the entire surface. Furthermore the yields of working junctions are much higher for SAMs containing ds-DNA as compared to HT only. As expected the yield of working junctions increases towards longer ds-DNA because of the ability of the thiolated oligonucleotide to fill the defect sites covering the surface uniformly.

In order to make sure that the DNA is driving the current in these molecular junctions and not the passivating layer or Ga_2O_3, I treated all three SAMs with 1M NaOH aqueous solution for 1 hour, which is known to hydrolyze the DNA backbone. After treatment with NaOH the samples were rinsed and conductance measurement with EGaIn were performed. The results are shown in Figure 5.8. Clearly, the length-morphology dependence is gone and all the three lengths give comparable magnitudes of J. As expected, the shorter double strands suffer only from a small change in J, clearly there is more to cleave in the ds-DNA 30 bp. In fact pre-ds-DNA 14 has nearly identical values of J in Figure 5.7 and 5.8. We do not intend to speculate on the charge transport mechanism in our junctions because of the complexity involved in process with mixed monolayers and nominally long molecule ($> 5nm$). However, to further prove the importance of pre-passivation in making solid state sensors, I measured ds-DNA immobilized directly on a bare Au^{TS} surface, *i.e.*, without pre-passivation of any kind. I expected the ds-DNA to interact strongly with the surface through the thiol linker and the phosphates groups along the helices. I immersed Au^{TS} into a fresh solution of ds-DNA with varying length overnight $\sim 20h$. After being in contact with DNA the samples were rinsed as described before and J/V traces were recorded in a similar manner. For clarity we name Nopre-ds-DNA to refer to the latter samples where ds-DNA is expose to Au^{TS} without a pre-passivation step. We also acquired AFM images for the Nopre-ds-DNA 14 and 30bp, see Figure 5.10. The resulting J/V curves are shown in Figure 5.9, all

three Nopre-ds-DNA 14, 22, and 30 showed rather low yields of working junction ~25%, which is accentuated in the shortest DNA length, *i.e.*, Nopre-ds-DNA 14. By looking at Figure 5.9 it is clear that since the ds-DNA has no specific binding modes, random multilayers of aggregates are formed, thus the length of the ds-DNA becomes irrelevant for the transport properties, *e.g.*, there are no substantial differences between Nopre-ds-DNA 14, 22, and 30. I hypothesize that most of the DNA lies flat on the surface, and the excess of negative charges repel some double strands away from the surface, see Figure 5.10. However it is clear that the DNA is not distributed homogeneously, resulting in high surface roughnesses. The former experiments further prove the importance of pre-passivating before exposure to ds-DNA, or in general to bio-molecules, in order to limit the non-specific interaction. Taken all together, the current measurements prove that the DNA is mediating the current in such devices, and only with our preparation method could we observe a length dependence and organization over large areas, organization that is the essential requirement for applications. Furthermore Dickey et al. demonstrated that EGaIn can be incorporated into microfluidic devices, for alkanethiolates and Ferrocene terminated SAMs.[32] Therefore I believe that EGaIn and microfluidics have great potential for excellent application in the near future.
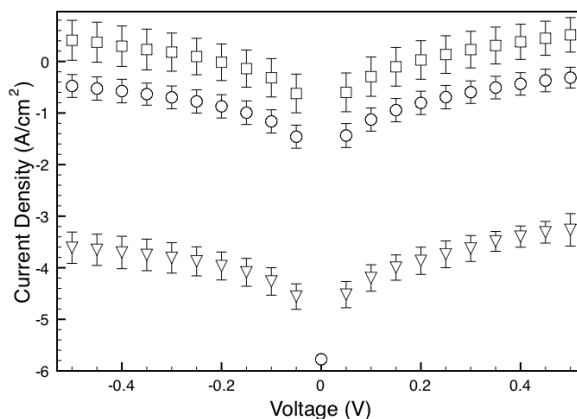
Figure 5.7: Plot showing J/V curves of pre-ds-DNA 14 (square), 22 (circle), and 30 (facedown-triangle) respectively.
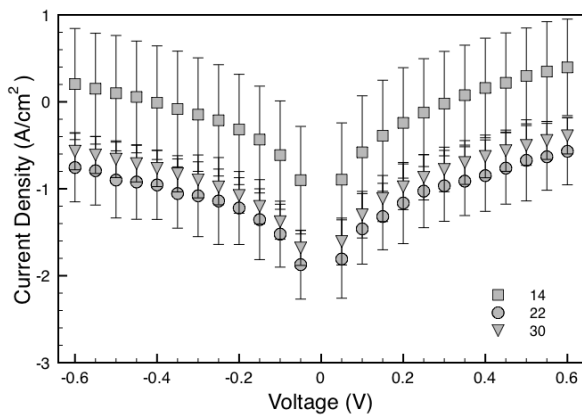
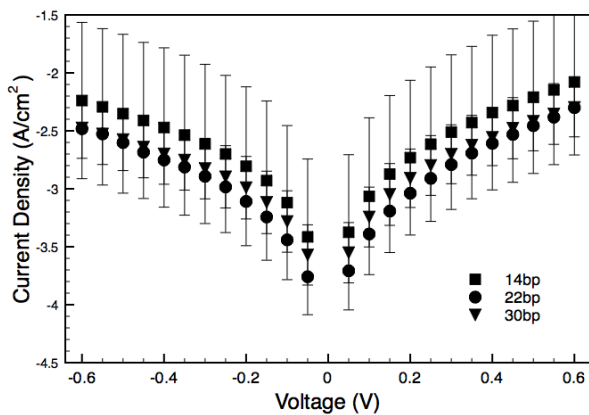Figure 5.8: Plot showing J/V curves of pre-ds-DNA 14, 22, and 30 after the SAMs has been treated with NaOH.

Figure 5.9: Plot showing J/V curves of thiolated Nopre-ds-DNA 14, 22, and 30 assembled on Au^{TS} without the pre-passivation step.
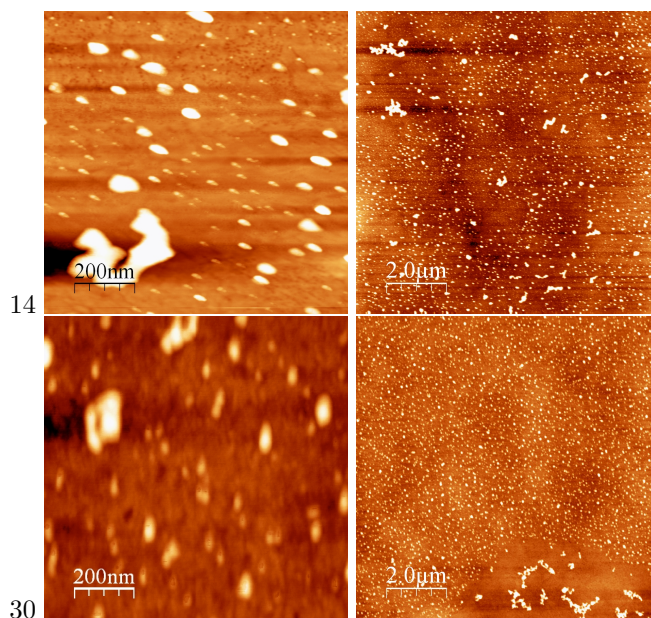
Figure 5.10: 1 μm^2 and 10 μm^2 AFM images of Nopre-ds-DNA 14 (Top) and 30 (Bottom), on Au$^{\mathrm{TS}}$ surface

5.3 Conclusions

We successfully prepared high density, well-control, mixed SAMs containing thiolated ds-DNA on Au^{TS}. We highlight the importance of characterizing the monolayers and investigating morphology and kinetics with AFM and QCM respectively. In order to use EGaIn to measure charge transport, we needed uniformly dense monolayers, thus I pre-passivated the Au^{TS} surfaces by exposing to a diluted solution of HT. The pre-passivated surfaces are then exposed to solution of ds-DNA solution, where the oligonucleotides exchange with few HT molecules onto defect sites. We demonstrated how pre-passivating results in a tight, dense SAM of ds-DNA, and that the length of the double strand dominated the charge transport properties of the final device. We do not intend to speculate on the actual mechanism of charge transport in such solid state junctions, however an understanding of the electrical properties and surface organization are essential requirements to use oligonucleotides in real applications like biosensors and detectors. In particular our work differs from the existing literature because we produced solid state junctions in which the DNA is playing an active role in the charge transport. Our solid state device architecture can be applied in microfluidics enabling to inject target solution, subsequently EGaIn and repeat the cycle over and over.

5.3.1 Relevant publications

While this manuscript was in preparation, Katsouras et al., who also collaborated with the graduate students of Prof. A. Herrmann, reported a charge transport study through DNA oligomers in large-area molecular junctions.[44] Katsouras et al., like us, pre-passivated their Au^{TS} bottom contact with HT prior exposure to ds-DNA of different lengths. Their Large-Area molecular junctions however require a buffer layer, PEDOT:PSS (poly(3,4-ethylenedioxythiophene) and poly(4-styrenesulphonic acid), which cover entirely the lithographically created hole where the DNA is anchored. The authors found that in the devices containing ds-DNA with one thiol linker there are very small difference in J, *i.e.*, comparable current density within one order of magnitude, whereas the devices containing ds-DNA with two thiol linkers (I believe their hypothesis was that the second thiol linker would make chemical contact with the PEDOT:PSS) are even indistinguishable. Our findings are instead different, but I ignore what would be the effect of a second thiol linker, which in my personal opinion would indeed facilitate the

lie-down conformation. Katsouras et al. claimed that the transport through the DNA goes in the traverse direction and not along the molecules based on a combination of ellipsometry, AFM and charge transport studies. I believe that the buffer layer is also averaging out the surface topology of the underneath mixed ds-DNA SAM hiding the length dependence that in our case we can see. Katsouras et al. compared the current densities of ds-DNA and hexadecanethiol SAMs, that happen to have the same lengths $\sim 2nm$ *i.e.*, the lateral dimensions of the double strand is approximately 2 nm. They found absolutely no difference between the two devices indicating no selectivity to DNA recognition, but it is only a matter of spacer in between the Au^{TS} and buffer layer. Furthermore in their device architecture the active molecules are buried under a thick layer of conductive polymer (PEDOT:PSS) which inhibit any sensing or recognition application related to DNA or other biomolecules.

Bibliography

[1] D. Klinov, K. Atlasov, A. Kotlyar, B. Dwir, and E. Kapon. DNA nanopositioning and alignment by electron-beam-induced surface chemical Patterning. *Nano Lett.*, 7(12):3583–3587, 2007.

[2] B. Gao, K. Sarveswaran, G. H. Bernstein, and M. Lieberman. Guided Deposition of Individual DNA Nanostructures on Silicon Substrates. *Langmuir*, 26(15):12680–12683, August 2010.

[3] A. Singh, S. Snyder, L. Lee, A. P. R. Johnston, F. Caruso, and Y. G. Yingling. Effect of Oligonucleotide Length on the Assembly of DNA Materials: Molecular Dynamics Simulations of Layer-by-Layer DNA Films. *Langmuir*, 26(22):17339–17347, 2010. Reference 25.

[4] A. A. Gorodetsky, A. K. Boal, and J. K. Barton. Direct Electrochemistry of Endonuclease III in the Presence and Absence of DNA. *J. Am. Chem. Soc.*, 128(37):12082–12083, September 2006.

[5] M. Kwiat, R. Elnathan, M. Kwak, J. W. de Vries, A. Pevzner, Y. Engel, L. Burstein, A. Khatchtourints, A. Lichtenstein, E. Flaxer, A. Herrmann, and F. Patolsky. Non-covalent monolayer-piercing anchoring of lipophilic nucleic acids: Preparation, characterization, and sensing applications. *J. Am. Chem. Soc.*, 134(1):280–292, 2012.

[6] G. R. Abel, E. A. Josephs, N. Luong, and T. Ye. A switchable surface enables visualization of single DNA hybridization events with atomic force microscopy. *J. Am. Chem. Soc.*, 135(17):6399–6402, April 2013.

[7] M. G. Hill, J. K. Barton, E. M. Boon, D. M. Ceres, and T. G. Drummond. Mutation detection by electrocatalysis at DNA-modified electrodes. *Nature Biotechnol.*, 18(10):1096–1100, October 2000.

[8] S. Husale, H. H. J. Persson, and O. Sahin. DNA nanomechanics allows direct digital detection of complementary DNA and microRNA targets. *Nature*, 462(7276):1075–1078, December 2009.

[9] A.-E. Radi, J. L. Acero Sánchez, E. Baldrich, and C. K. O'Sullivan. Reagentless, Reusable, Ultrasensitive Electrochemical Molecular Beacon Aptasensor. *J. Am. Chem. Soc.*, 128(1):117–124, January 2006.

[10] S. Wang, H. Liu, D. Liu, X. Ma, and X. Fang. Enthalpy-Driven Three-State Switching of a Superhydrophilic/Superhydrophobic Surface. *Angew. Chem. Int. Ed.*, 2007.

[11] C. C. Weber, N. Link, C. Fux, A. H. Zisch, W. Weber, and M. Fussenegger. Broad-spectrum protein biosensors for class-specific detection of antibiotics. *Biotechnol. Bioeng.*, 89(1):9–17, 2004.

[12] T. Cordes, J. Vogelsang, M. Anaya, C. Spagnuolo, A. Gietl, W. Summerer, A. Herrmann, K. Müllen, and P. Tinnefeld. Single-Molecule Redox Blinking of Perylene Diimide Derivatives in Water. *J. Am. Chem. Soc.*, 132(7):2404–2409, February 2010.

[13] A. Tafvizi, L. A. Mirny, and A. M. van Oijen. Dancing on DNA: Kinetic Aspects of Search Processes on DNA. *ChemPhysChem*, 12(8):1481–1489, May 2011.

[14] L. B. Lowe, S. H. Brewer, S. Krämer, R. R. Fuierer, G. Qian, C. O. Agbasi-Porter, S. Moses, S. Franzen, and D. L. Feldheim. Laser-Induced Temperature Jump Electrochemistry on Gold Nanoparticle-Coated Electrodes. *J. Am. Chem. Soc.*, 125(47):14258–14259, November 2003.

[15] A. A. Gorodetsky, L. E. P. Dietrich, P. E. Lee, B. Demple, D. K. Newman, and J. K. Barton. DNA binding shifts the redox potential of the transcription factor SoxR. *Proc. Natl. Acad. Sci. USA*, 105(10):3684–3689, March 2008.

[16] A. A. Gorodetsky, A. Ebrahim, and J. K. Barton. Electrical Detection of TATA Binding Protein at DNA-Modified Microelectrodes. *J. Am. Chem. Soc.*, 130(10):2924–2925, March 2008.

[17] E. M. Boon, J. E. Salas, and J. K. Barton. An electrical probe of protein–DNA interactions on DNA-modified surfaces. *Nature Biotechnol.*, 20(3):282–286, March 2002.

[18] S. O. Kelley, N. M. Jackson, M. G. Hill, and J. K. Barton. Long-range electron transfer through DNA films. *Angew. Chem. Int. Ed.*, 38(7):941–945, 1999.

[19] G. M. Whitesides and M. Boncheva. Beyond molecules: Self-assembly of mesoscopic and macroscopic components. *Proc. Nat. Acad. Sci. USA*, 99(8):4769–4774, 2002.

[20] J. C. Love, L. A. Estroff, J. K. Kriebel, R. G. Nuzzo, and G. M. Whitesides. Self-assembled monolayers of thiolates on metals as a form of nanotechnology. *Chem. Rev.*, 105(4):1103–1170, 2005.

[21] S. Zhang. Fabrication of novel biomaterials through molecular self-assembly. *Nature Biotechnol.*, 21(10):1171–1178, October 2003.

[22] M. Satjapipat, R. Sanedrin, and F. Zhou. Selective Desorption of Alkanethiols in Mixed Self-Assembled Monolayers for Subsequent Oligonucleotide Attachment and DNA Hybridization. *Langmuir*, 17(24):7637–7644, 2001.

[23] E. A. Josephs and T. Ye. A Single-Molecule View of Conformational Switching of DNA Tethered to a Gold Electrode. *J. Am. Chem. Soc.*, 134(24):10021–10030, June 2012.

[24] M. Liu, N. A. Amro, C. S. Chow, and G.-y. Liu. Production of Nanostructures of DNA on Surfaces. *Nano Lett.*, 2(8):863–867, August 2002.

[25] E. A. Josephs and T. Ye. Nanoscale Spatial Distribution of Thiolated DNA on Model Nucleic Acid Sensor Surfaces. *ACS Nano*, 7(4):3653–3660, April 2013.

[26] E. A. Josephs and T. Ye. Electric-Field Dependent Conformations of Single DNA Molecules on a Model Biosensor Surface. *Nano Letters*, 12(10):5255–5261, October 2012.

[27] T. M. Herne and M. J. Tarlov. Characterization of DNA Probes Immobilized on Gold Surfaces. *J. Am. Chem. Soc.*, 119(38):8916–8920, 1997.

[28] J. N. Murphy, A. K. H. Cheng, H.-Z. Yu, and D. Bizzotto. On the Nature of DNA Self-Assembled Monolayers on Au: Measuring Surface Heterogeneity with Electrochemical in Situ Fluorescence Microscopy. *J. Am. Chem. Soc.*, 131(11):4042–4050, March 2009.

[29] K. Prime and G. M. Whitesides. Self-assembled organic monolayers: model systems for studying adsorption of proteins at surfaces. *Science*, 252(5009):1164–1167, May 1991.

[30] C. D Bain and G. M. Whitesides. Formation of monolayers by the coadsorption of thiols on gold: variation in the head group, tail group, and solvent. *J. Am. Chem. Soc.*, 111(18):7155–7164, 1989.

[31] C. D. Bain, E. B. Troughton, Y. T. Tao, J. Evall, G. M. Whitesides, and R. G. Nuzzo. Formation of monolayer films by the spontaneous assembly of organic thiols from solution onto gold. *J. Am. Chem. Soc.*, 111(1):321–335, 1989.

[32] M. D. Dickey, R. C. Chiechi, R. J. Larsen, E. A. Weiss, D. A. Weitz, and G. M. Whitesides. Eutectic Gallium-Indium (EGaIn): A Liquid Metal Alloy for the Formation of Stable Structures in Microchannels at Room Temperature. *Adv. Funct. Mater.*, 18(7):1097–1104, April 2008.

[33] R. E. Holmlin, R. Haag, M. L. Chabinyc, R. F. Ismagilov, A. E. Cohen, A. Terfort, M. A. Rampi, and Whitesides G. M. Electron transport through thin organic films in Metal-Insulator-Metal junctions based on Self-Assembled monolayers. *J. Am. Chem. Soc.*, 123(21):5075–5085, 2001.

[34] H. B. Akkerman, P. W. M. Blom, Dago M. de Leeuw, and B. de Boer. Towards molecular electronics with large-area molecular junctions. *Nature*, 441(7089):69–72, May 2006.

[35] H. Valkenier, E. H. Huisman, P. A. van Hal, D. M. de Leeuw, R. C. Chiechi, and J. C. Hummelen. Formation of high-quality self-assembled monolayers of conjugated dithiols on gold: Base matters. *J. Am. Chem. Soc.*, 133(13):4930–4939, 2011.

[36] J. B. Schlenoff, M. Li, and H. Ly. Stability and self-exchange in alkanethiol monolayers. *J. Am. Chem. Soc.*, 117(50):12528–12536, 1995.

[37] D. Johannsmann. Viscoelastic, mechanical, and dielectric measurements on complex samples with the quartz crystal microbalance. *Phys. Chem. Chem. Phys.*, 10(31):4516, 2008.

[38] F. Schreiber. Structure and growth of self-assembling monolayers. *Prog. Surf. Sci.*, 65:151–256, 2000.

[39] C. Schoenenberger, J. A. M. Sondag-Huethorst, J. Jorritsma, and L. G. J. Fokkink. What Are the "Holes" in Self-Assembled Monolayers of Alkanethiols on Gold? *Langmuir*, 10(3):611–614, March 1994.

[40] J. D. Slinker, N. B. Muren, S. E. Renfrew, and J. K. Barton. DNA charge transport over 34 nm. *Nature Chem.*, 3(3):230–235, January 2011.

[41] X. Guo, A. A. Gorodetsky, J. Hone, J. K. Barton, and C. Nuckolls. Conductivity of a single DNA duplex bridging a carbon nanotube gap. *Nature Nanotech.*, 3(3):163–167, February 2008.

[42] J. C. Genereux, S. M. Wuerth, and J. K. Barton. Single-Step Charge Transport through DNA over Long Distances. *J. Am. Chem. Soc.*, 133(11):3863–3868, March 2011.

[43] J. C. Genereux and J. K. Barton. Mechanisms for DNA Charge Transport. *Chem. Rev.*, 110(3):1642–1662, March 2010.

[44] I. Katsouras, C. Piliego, P. W. M. Blom, and D. M. de Leeuw. Transverse charge transport through DNA oligomers in large-area molecular junctions. *Nanoscale*, 5:9882–9887, 2013.

Summary

In this thesis a broad overview of tunneling junctions comprising SAMs with eutectic Gallium Indium as top electrode is presented. I at first introduce the concepts of Molecular Electronics, SAMs, tunneling junctions, and compared two techniques to measure charge transport properties, Hg-drop and EGaIn, which have their state of matter in common: being liquid at room temperature. EGaIn, despite being a relatively new technique in the world of Molecular Electronics, rapidly caught the attention of several research laboratories. Controlling molecular conductance is an essential requirement on the road towards functional molecular electronic devices. The field of molecular electronics is generally interested in active molecular components and new functionalities. An important issue in molecular electronics is the understanding on how the molecules govern the device performance. The understanding of the electrical properties is often hidden behind the complexity of the devices architecture, in some cases the performances of the device are more important than the deeper understanding, *i.e.*, function trumps spectroscopy

I showed in this thesis how EGaIn can be used as conformal top electrode to uncover new molecular phenomena. The goal of my research was not to develop devices for industrial application, rather to characterize SAMs electrically and correlate chemical structures to functionalities.

In **Chapter 2** I described the first experimental evidence of quantum interference in SAMs. My collaborator, Hennie Valkenier, kindly synthesized a series of conjugated molecules during her PhD; in this pool of compounds there were also the three arylethynelenes studied in Chapter 2. At that time these were the first experiments with fully conjugated molecules using EGaIn. Molecules were design in order to determine the conductance influences of the conjugation pattern. We studied three SAMs with linear, cross, and broken-conjugated anthracene moieties and we observed a good agreement between the current in single molecule transport calculation and the current density in EGaIn junctions. We showed that quantum interference can be seen also in SAM based junctions, not only single molecules, and that EGaIn is sensitive enough to detect changes in conjugation patterns.

In **Chapter 3** I described the importance of molecular dipoles in tunneling junctions comprising SAMs. I showed that tunneling junctions incorporating EGaIn as a top contact are sensitive enough to differentiate SAMs that differ by the substitution of a single atom (C-H to N). Conductance data (J/V curves) and length dependence (β and J_0) are sufficient to differentiate the two series, Ph-SAM and Py-SAM, but the differences are subtle and require prior knowledge of the two series being measured. However V_{trans}, obtained by replotting the J/V traces, provides a clear distinction between the two series. We observed a clear shift in work function due to the collective effect of dipole moments in SAMs. Interestingly we found that both the calculated HOMO levels and $\Delta\Phi$ are linearly correlated to V_{trans}.

Alkanethiolates have been widely used because of their simplicity and versatility to functionalized metal surfaces. In **Chapter 4** I explored the self assembly properties of terminal alkynes as alternative to thiols in molecular electronics. I characterized spectroscopically and electrically a series of n-alkyl acetylenes with increasing numbers of carbon finding that the acetylene SAM formed dense, robust monolayers. The acetylene SAMs showed similar electrical properties to thiols making them a valid alternative. Acetylene chemistry is more straightforward than thiols, thus more complex molecules can be synthesize and assembled on surfaces without the need for in situ deprotection.

In **Chapter 5** we characterized a mixed SAM of double-strand DNA. We introduced and optimized a new method to form dense monolayer of DNA. We further characterized the monolayers with a combination of several techniques and in particular we looked into the charge transport properties of a series of double strand DNA using EGaIn as top electrode. We found that EGaIn also in this case is sensitive to distinguish assemblies of DNA with different double stranded number of pairs, *i.e.*, different length. We also unambiguously demonstrated that the sensitivity is completely lost if we don't treat the surface with a passivating layer prior DNA adsorption, indicating that pre-passivating is a required step in order to achieve any sensitivity in our devices.

Samenvatting

In deze thesis wordt een breed overzicht gepresenteerd van tunneling junctions uit SAMs met een top elektrode bestaande uit Eutectisch Gallium Indium. Ik begin met het introduceren van de enkele concepten van Moleculaire elektronica, SAMs en tunneling junctions. Hierbij vergelijk ik twee technieken voor het meten van lading transport eigenschappen; de kwik-druppel en EGaIn, welke beide in overeenkomst hebben vloeibaar te zijn bij kamer temperatuur. Ondanks dat EGaIn een relatief nieuwe techniek is in de wereld van de Moleculaire Elektronica heeft deze techniek een snelle opmars gemaakt bij meerdere onderzoeks- laboratoria. Het vermogen om moleculaire geleiding te beheersen heeft een essentile noodzaak voor functionele moleculaire elektronische devices. Over het algemeen is het veld van moleculaire elektronica genteresseerd in actieve moleculaire componenten en nieuwe functionaliteiten. Een belangrijke kwestie in moleculaire elektronica is het begrijpen hoe moleculen de device prestaties benvloeden. Het inzicht van de elektronische eigenschappen is vaak verscholen achter complexiteit van de architectuur van de device, in sommige gevallen zijn de prestaties van de device belangrijker dan het diepere achterliggende begrip.

In deze thesis liet ik zien hoe EGaIn gebruikt kan worden als conformele Top elektrode om nieuwe moleculaire fenomenen bloot te leggen. Het doel van mijn onderzoek was niet het ontwikkelen van devices voor industrile doeleinden, het doel was om SAMs elektronisch te karakteriseren en chemische structuren naar hun functionaliteiten te correleren.

In **hoofdstuk 2** beschreef ik de eerste experimentele bewijzen van quantum interferentie in SAMs. Hennie Valkenier, synthetiseerde een serie geconjugeerde moleculen tijdens haar PhD; in deze overvloed van organische moleculen bevonden zich drie aryl ethynelenen die in dit hoofdstuk zijn bestudeerd. Ten tijde van dit experiment was dit voor het eerst dat volledig geconjugeerde moleculen werden gemeten via EGaIn. De moleculen werden ontworpen ter bepaling van de invloed van het conjugatie patroon op de geleiding. We bestudeerden drie SAMs met lineaire, gekruiste, en gebroken- geconjugeerde functionele antraceen groepen en we observeerden een verband tussen de stroom in het transport berekeningen van enkelvoudige moleculen en de elektrische stroomdichtheid in EGaIn juncties. We toonden aan dat kwantum interferentie niet alleen in enkelvoudige moleculen maar ook in SAM gebaseerde juncties te zien zijn, daarnaast toonden we aan

dat EGaIn gevoelig genoeg is om veranderingen in conjugatie patronen waar te nemen.

In **hoofdstuk 3** beschreef ik wat het belang is van moleculaire dipolen in tunneling junctions bestaande uit SAMs. Ik toonde aan dat tunneling junctions waarbij EGaIn als topcontact werd gebruikt, gevoelig genoeg was voor de SAM om onderscheid te maken tussen de substitutie van een enkel atoom (C-H naar N). Geleiding data (J/V curven) en lengte afhankelijkheid (? en J0) waren voldoende om onderscheid te maken tussen de twee series, Ph-SAM en Py-SAM, maar de verschillen waren subtiel en vereisten enige voorkennis van de twee te meten series. Hoewel we Vtrans, verkregen middels het her plotten van J/V curves, was er een duidelijk onderscheid zichtbaar tussen de twee series. We observeerden een duidelijke shift in werk functie ten opzichte van het collectieve effect van de dipool momenten in SAMs. Opmerkelijk was dat we ondervonden dat zowel de uitgerekende HOMO levels en de ?? lineair gecorreleerd zijn met Vtrans.

Wegens hun enkelvoud en veelzijdigheid worden alkaan thiolaten veelvuldig gebruikt om metaal oppervlakten te functioneren. In **hoofdstuk 4** verkende ik de zelf assemblage eigenschappen van terminale alkynen als vervanging voor thiolen in moleculaire elektronica. Ik heb een serie van n-alkyl acetylenen met oplopende hoeveelheden koolstofatomen spectroscopisch en elektrisch gekarakteriseerd, hierbij constateerde ik dat de acetyleen SAMs een compacte robuuste monolaag vormden. De acetyleen SAMs vertoonden gelijkwaardige elektrische eigenschappen als de thiolen, wat de acetyleen een goed alternatief maakt voor SAMs. Acetyleen chemie is eenvoudigere chemie dan thiol chemie, waardoor meer complexe moleculen gesynthetiseerd kunnen worden en assemblage kan plaatsvinden op oppervlakten zonder dat er gebruik gemaakt hoeft te worden van in situ beschermgroepen.

In **hoofdstuk 5** karakteriseerden we gemengde SAMs bestaande uit dubbele-streng DNA. We introduceerden en optimaliseerden een nieuwe methode om dichte monolagen van DNA te vormen. Verder karakteriseerden we de monolagen via een combinatie van verscheidene technieken om in het bijzonder met behulp van EGaIn als topelektrode op zoek te gaan naar de lading transport eigenschappen van een serie dubbel streng DNA. We ondervonden dat EGaIn ook in dit geval gevoelig genoeg was om onderscheid te maken tussen assemblages DNA met verschillende dubbele streng paren (e.g. ver-

schillende lengten). We hebben tevens onbetwistbaar aangetoond dat de gevoeligheid verdwijnt wanneer we de oppervlakte van de SAM niet eerst behandelen met een passiverende laag voor de DNA adsorptie, wat aangeeft dat pre-passivatie een vereiste stap is voor het bereiken van gevoeligheid in onze devices.

Acknowledgements

At the end of this fatigue with great pleasure I would like to acknowledge, not only those who have contributed to this thesis, directly or indirectly, but all friends, colleagues, and acquaintances that interacted with me during my lovely stay in Groningen.

It seems only yesterday that I arrived in Groningen, a young city full of joy and festivals waiting for me. I would like to thank all of those who cannot find their name in the following acknowledgment, every little experience helped me to grow and improve as a person and scientist.

First and foremost, I would like to thank infinitely my supervisor Dr. Ryan C. Chiechi without whose guidance and active daily participation this thesis would not have been possible. Ryan for me was more than a "boss", he was a mentor, an example. I'm very honored to have accomplished my PhD under his supervision, I feel like he taught me a lot about science and much more, plus he always did it in a friendly way. A special thanks to him for his infinite support, patience and contribution to resolve all the important issues, from the project's inception to completion. I cannot stress enough how many little things he taught me, but I also would like to thank Ryan for something he did not teach me: playing disc (Frisbee)!! I had lots of fun to do some throws together. Ryan, I wish you all the best and I'm sure you will have a bright future because you've got the stubbornness and tenacity associated with an astonishing general knowledge all the way from Chemistry to Brewing!!
I would like to thank also Kees Hummelen for the useful discussions during group meetings and assistance through my PhD.

I believe that being the first PhD of a new Assistant Professor is not always easy, especially if both are new in the country. When I arrived the laboratory was practically empty, and my project could not start right away. However, this gave me the possibility to play around with an interesting microfluidics project, soft-lithography and more importantly see what the University of Groningen could offer me. I made close connections with several groups in and out the Zernike Institute in order to accomplish my research. A special thanks goes to the MEPOS group: Johan Brondijk, Auke Kronemeijer, Martijn Kuik, Gert-Jan Wetzelaer, Ilias Katsouras and their technician Jan Harkema. Thank you guys to let me work in your cleanroom, use your probe station, and for useful discussions. A special thanks goes to Prof. Wesley Browne and his group members. In particular to Hella Logtenberg and Oleksii Ivashenko for helping me with the Plasma cleaner and Raman measurement, respectively. Sincere thanks go to Maria J. Lopez who not only let me use their clean room in the UMCG, but moreover spent a big chunk of her time to help me with the master preparation.

I would like to gratefully acknowledge the support of my group members. Thanks to Hennie, Wenqiang, Cindy, Jelmer, Jeremio, Frank, Ricardo, Parisa, Thomas, Olga, Bouke, Thijs, Mehrnoosh, Jenny, Difei, Zhiyuan, Dan, Jim, and Piet. It was a very nice experience to work with you in the same group. Essential members of our group, sometimes forgotten, are Reinder, Renate, and Alfred able to look for our safety, fix our mistakes, and provide to the whole group great help, for this I sincerely thank you.

I would like to thank my collaborators Prof. Gemma Solomon, Dr. Mutlu I. Muglali, Prof. Michael Rohwerder, and Prof. Andreas Terfort for their contributions to this thesis. Special thanks to my collaborators from Prof. Andreas Herrmann's group: Jan Willem, Pavlo, and Deepak for their support and contribution to this thesis.

The life of a PhD is not only between the academic walls. I feel extremely lucky because during these four years I was surrounded by marvelous friends that were always truly nice to me. A special hug goes to Marianna, my beloved singer and flatmate for the patience of having me around the whole time! Stefano G. for great moments together in the house, you were always kind and patience, an excellent flatmate. The Romans, how much fun we had? Santos, Freddo, and Alessio thank you bros for the great time we spent together. Santos thank you for the guitar lessons, and Ale thank you for your help with the cover. Stefano M. and Martina thank you for the great dinners and the board games we played together. Kamil, Navid, Santi, and Igor, the buddies for the parties and the great time spent together. Igor thank you for the nice dinners and parties, I wish you all the best in your life. Pablito, my spanish friend, for being such a good friend to me, I won't forget our evenings in your old student house and the erasmus' nights. Davide B., since you arrived we start to hang out so much, you are one of those "good guys" that nowadays are so rare. You were always very generous and willing to help everybody, a real friend. Serena, "la tora", you are strong and stubborn as I hardly see in girls, but with a sweet heart that nobody has. I will bring with me the memories of our climbs. Raquel, thank you for the nice coffee breaks and your sincere friendship. Last, but certainly not the least is Toni, I don't know how would have been my stay in Groningen without you. I enjoyed so much the time together inside and outside the university. I could write an entire thesis about our stories. You introduced me to climbing (in Netherlands!!!) and I immediately liked it. I wish there would be more people like you in this world.
Grazie

A special thanks goes to Angela ♡, who took special care of me, especially in the last year of my PhD. I wish we could stay together for a long time. Grazie Mamma e Papa' per avermi voluto sempre bene e per avermi appoggiato in ogni mia scelta. Siete i migliori genitori che un figlio possa desiderare.

<div align="right">

January 17, 2014
Davide

</div>